2019

Sparsity Constrained Inverse Problems - Application to Vibration-based Structural Health Monitoring

Chandler B. Smith
University of Vermont

Follow this and additional works at: https://scholarworks.uvm.edu/graddis

Part of the Civil Engineering Commons

Sparsity Constrained Inverse Problems - Application to Vibration-based Structural Health Monitoring

A Dissertation Presented

by

Chandler Baldwin Smith

to

The Faculty of the Graduate College

of

The University of Vermont

In Partial Fulfillment of the Requirements
for the Degree of Doctor of Philosophy
in Civil and Environmental Engineering

August, 2019

Defense Date: July 1, 2019
Dissertation Examination Committee:

Eric Hernandez, Ph.D., Advisor
Paul Hines, Ph.D., Chairperson
Mads Almassahki, Ph.D.
Ting Tan, Ph.D.
Dryver Huston, Ph.D.
Cynthia J. Forehand, Ph.D., Dean of the Graduate College

ABSTRACT

Vibration-based structural health monitoring (SHM) seeks to detect, quantify, locate, and prognosticate damage by processing vibration signals measured while the structure is operational. The basic premise of vibration-based SHM is that damage will affect the stiffness, mass or energy dissipation properties of the structure and in turn alter its measured dynamic characteristics. In order to make SHM a practical technology it is necessary to perform damage assessment using only a minimum number of permanently installed sensors. Deducing damage at unmeasured regions of the structural domain requires solving an inverse problem that is underdetermined and(or) ill-conditioned. In addition, the effects of local damage on global vibration response may be overshadowed by the effects of modelling error, environmental changes, sensor noise, and unmeasured excitation. These theoretical and practical challenges render the damage identification inverse problem ill-posed, and in some cases unsolvable with conventional inverse methods.

This dissertation proposes and tests a novel interpretation of the damage identification inverse problem. Since damage is inherently local and strictly reduces stiffness and(or) mass, the underdetermined inverse problem can be made uniquely solvable by either imposing sparsity or non-negativity on the solution space. The goal of this research is to leverage this concept in order to prove that damage identification can be performed in practical applications using significantly less measurements than conventional inverse methods require. This dissertation investigates two sparsity inducing methods, l_1-norm optimization and the non-negative least squares, in their application to identifying damage from eigenvalues, a minimal sensor-based feature that results in an underdetermined inverse problem. This work presents necessary conditions for solution uniqueness and a method to quantify the bounds on the non-unique solution space. The proposed methods are investigated using a wide range of numerical simulations and validated using a four-story lab-scale frame and a full-scale 17 m long aluminum truss. The findings of this study suggest that leveraging the attributes of both l_1-norm optimization and non-negative constrained least squares can provide significant improvement over their standalone applications and over other existing methods of damage detection.

CITATIONS

Material from this dissertation has been published in the following form:

Smith, C.B. and Hernandez, E.M.. (2019)."Non-negative constrained inverse eigenvalue problems - application to damage identification." *Mechanical Systems and Signal Processing*, 129, 629-644.

Smith, C.B. and Hernandez, E.M.. (2018). "Detection of spatially sparse damage using impulse response sensitivity and LASSO regularization." *Inverse Problems in Science and Engineering*, 27(1), 1-16.

Material from this dissertation has been submitted for publication to the *Journal of Engineering Mechanics* on March 27, 2019 in the following form:

Smith C.B., Hernandez E.M.. (2019). "Identifying local reductions to mass and stiffness with incomplete modal information, sparsity, and non-negative constraints."

Material from this dissertation has been submitted for publication to the *Journal of Mechanical Systems and Signal Processing* on August 1, 2019 in the following form:

Smith C.B., Hernandez E.M.. (2019). "Non-negative and sparsity constrained inverse problems in damage identification - Application to a full-scale 3D truss."

ACKNOWLEDGEMENTS

TABLE OF CONTENTS

LIST OF FIGURES

ix

LIST OF TABLES

Chapter 1

Introduction

Vibration-based structural health monitoring (SHM) seeks to detect, quantify, locate, and prognosticate adverse changes to structural properties by processing vibration signals [Rytter, 1993]. The appeal in using vibration measurements is to avoid direct and potentially invasive damage evaluation methods so that the structure can be continuously monitored without impeding its intended function. Measured vibrations provide an avenue to identify damage because changes in physical properties manifest as changes in dynamic response characteristics such as vibration frequencies, modes shapes, and damping [Farrar et al., 2001, Brownjohn, 2007]. If the presence of damage is detected from measured dynamic response, the next step in SHM is to quantify and locate the detected damage. Quantifying and locating structural damage using measured vibrations requires solving an inverse problem. An inverse problem arises when the unknown and unobservable phenomenon, in this case damage, must be deduced from partial information obtained from indirect observations of the system, i.e. measured vibrations. There are many ways to pose and solve the vibration-based SHM inverse problem in terms of the measurement type, the model, and the

parameters [Doebling et al., 1996, Farrar and Worden, 2013].

The physics-based inverse problem seeks to reconstruct the change in physical properties appearing as parameters in a structural dynamics model from the changes in modal features. Since structural damage is typically a local phenomenon, solving the physics-based inverse problem requires finding changes in a small subset of parameters. This poses a fundamental challenge to SHM because the effects of local damage on global vibration response are weak and must be discerned from the effects of modelling error, environmental changes, and unmeasured excitation [Moser et al., 2011]. Furthermore, the parameter space must be large enough to account for local changes occurring anywhere along the structure [Friswell, 2007]. The convention in SHM is to estimate modal features from vibrations that provide direct spatial information such as mode shapes, mode shape curvature, or modal strain energy to ensure a high sensitivity to damage and enough measurements to uniquely solve the inverse problem. However, spatially distributed features are inherently inaccurate, difficult to extract, and require a substantial array of sensors to monitor full-scale structures for damage [Doebling et al., 1997, Pintelon et al., 2007, Reynders et al., 2008].

This research presents a novel optimization framework for uniquely solving the vibration-based SHM inverse problem using significantly less measurements than conventional inverse methods require. The concept is to leverage sparsity in the solution space using a combination of l_1-norm optimization and the non-negative least squares. Since damage tends to reduce a small subset of stiffness and mass parameters, the inverse problem can be reframed as a problem in finding the sparsest reduction in the parameter space, i.e. a non-negative change in parameters with the fewest nonzero elements. This research substantiates if the solution has sufficiently few nonzero ele-

ments with respect to its domain then imposing either sparsity or non-negativity as a constraint on the inverse problem can result in physically meaningful solutions to severely underdetermined inverse problems even when other forms of regularization or constrained optimization have failed.

1.1 MOTIVATION

One of the practical limitations of the physics-based inverse method is that ensuring a unique solution to the vibration-based SHM inverse problem requires more information than what is available from a few sensors [Berman, 1984]. Additional information necessitates spatially distributed features which are sensitive to system identification error and to the effects of unmeasured excitation. Some modal features are not spatially distributed, such as the eigenvalues (i.e natural frequencies). The eigenvalues are easier to extract, are less sensitive to noise, and only require measurements from a few optimally placed sensors. However, only a small subset of eigenvalues can be extracted from vibration measurements. Several comprehensive reviews on the subject conclude that without using spatially distributed modal features, there isn't enough modal information from eigenvalues to ensure a unique and physically meaningful solution to the inverse problem [Doebling et al., 1996, Salawu, 1997, Sohn et al., 2003].

Contrary to conventional inverse methods, early works on the sparsity concept have verified that local damage can be quantified and located from changes in eigenvalues using sparse vector recovery in the form of l_1-norm optimization [Zhou et al., 2013, Hernandez, 2014]. Questions still remain on the practical limitations of impos-

3

ing sparsity, the robustness of an eigenvalue-based damage identification method to irreducible model error, and how various sparse vector recovery methods compare. This research addresses these questions by proposing and investigating a variety of sparsity inducing optimization methods on several types of structures.

1.2   OBJECTIVE

The objective of this research is to investigate the merits of leveraging sparsity to quantify and locate structural damage while contributing new theory underlying the application of sparsity to physics-based inverse problems in vibration-based SHM. Three convex optimization methods are investigated. The first method, the l_1-norm optimization, is a direct and popular approach to sparse vector recovery. The second method, the non-negative least squares, indirectly imposes sparsity by targeting reductions in stiffness and mass using the non-negative constraint. The final framework combines the two methods into the non-negative constrained l_1-norm optimization method. A theory to determine uniqueness by estimating the bounds on the optimal set of points satisfying the non-negative constrained l_1-norm optimization is investigated.

1.3   CONTRIBUTIONS

This research develops a novel optimization framework for solving the vibration-based inverse problem based on the merits of leveraging sparsity. The various sparse vector recovery frameworks are validated and investigated for a wide range of structures

increasing in complexity with each chapter of the dissertation: a series of numerical simulations in ch.3, a four-story lab-scale steel frame in ch.4, and a 17 meter long full-scale truss in ch.5. This research contributes theoretical and practical observations on the relationship between sparsity, non-negativity and the eigenvalues. The contributions of each chapter are:

- Chapter 3 suggests the suitability of using the non-negative least squares to solve the underdetermined damage identification inverse problem. It is argued that the non-negative constraint induces unique solutions to the ill-posed inverse problem if the solution is sufficiently sparse. A measure for determining uniqueness is presented. The method is verified on the linear truncated inverse problem and its performance compared to l_1-norm optimization using three numerically simulated structures of increasing complexity. The findings of this study are then extrapolated to the nonlinear inverse problem.

- In chapter 4, damage defined by simultaneous changes in stiffness and mass is considered. This study suggests that the non-negative least squares and l_1-norm optimization are both inadequate as standalone programs. These findings motivate a novel method - the non-negative constrained l_1-norm optimization. The proposed inverse method leverages the monotonic relationship between the stiffness and mass parameters and the eigenvalues. The proposed inverse method is tested for robustness on a four-story lab-scale steel frame where the damage reduces the stiffness and mass.

- Chapter 5 presents the culmination of this research in terms of the proposed algorithms from previous chapters and the complexity of the structure tested.

This chapter introduces a novel concept of measuring solution space bounds to the underdetermined system in order to aid in interpreting the validity of the optimal solution. The standalone applications of the l_1-norm optimization and the non-negative constrained least squares are compared to the proposed method. This chapter verifies and tests the proposed methods using experimental data measured from a 17 m long aluminum three-dimensional truss subjected to three progressive damage cases.

Chapter 2 provides the fundamental theoretical background to inverse problems. Chapters 3,4, 5, and Appendix A are presented in a form prepared for journal submission (each chapter has a section for the abstract, introduction, methods, results, conclusions, and references). In addition to the primary scope of this work related to the eigenvalues, appendix A provides an investigation into the application of l_1-norm regularization on the ill-conditioned inverse problem associated with using the impulse response. Appendix A substantiates that l_1-norm regularization is effective at dealing with severely ill-conditioned over-constrained inverse problems.

CHAPTER 2

FUNDAMENTALS

The Fundamentals chapter provides an extended summary of the physics-based inverse problem in vibration-based structural health monitoring (SHM). This includes a theoretical background on the physics-based model and the eigenvalue problem. The relevant advances in solving the inverse problem in SHM are discussed and detailed through a literature review. This is followed by a section on solving the underdetermined inverse problem using convex optimization. The chapter concludes with an illustrative example.

2.1 PHYSICS-BASED INVERSE PROBLEM

The physics-based inverse problem in vibration-based SHM seeks to estimate changes in the physical properties of a structure, which appear as parameters in a model, using changes in the dynamic characteristics describing the measured vibrations. This inverse problem has two primary applications that are not mutually exclusive: damage identification and finite element (FE) model updating. In FE model updating, an ini-

7

tial model and its parameter space are constructed from a physical description of the structure. This model is inherently uncertain. The prior parameters are then updated to minimize the model uncertainty using measurements from the healthy structure. In damage identification, the prior model represents the healthy structure. Measurements taken from the potentially damaged structure are used to detect, quantify, and locate damage by estimating the change in parameters from the prior. Hence, FE model updating can improve the reliability of the model for damage identification. Although this work focuses on damage identification, FE model updating is used to improve the models that were constructed for the experiments of this dissertation. A significant body of research is devoted to FE model updating [Natke, 1988, Mottershead and Friswell, 1993, Friswell and Mottershead, 1995, Imregun et al., 1995, Gladwell and Ahmadian, 1995, Ahmadian et al., 1998, Mottershead et al., 2011, Jang and Smyth, 2017].

2.1.1   INVERSE METHOD

The pursuit of a solution to the inverse problem is called the inverse method (also referred to as the sensitivity method or model updating in later chapters). The objective in the inverse method is to estimate the parameters of the model needed to minimize the residual between the features identified from the measurements and the features derived from the model. In general, the inverse method seeks to solve the nonlinear least squares problem:

$$\theta^* = \min_{\theta \in D(\mathcal{F})} \quad ||\mathcal{F}(\theta) - \hat{z}||_2 \tag{2.1}$$

where $\mathcal{F} : \theta \to z$ is a nonlinear mapping between the parameters $\theta \in \Re^p$ and the features $z \in \Re^q$. $\hat{z} \in \Re^q$ are the features estimated from the experimental data. The inverse method is initialized with the parameters defining the prior. The following sections detail the nonlinear operator, the parameters, and the features.

2.1.2 MODEL AND PARAMETERS

The operator $\mathcal{F}$ and its parameters are derived from a model. In general, a model is a transformation between an input and an output where the characteristics of the transformation are defined by the model's parameter space. In structural dynamics, the vibration response in terms of displacement, velocity, or accelerations (outputs) of a structure subjected to a known excitation in terms of time-varying forces (input) can be modelled by any n^{th} order linear transformation (e.g. physics-based, state space, auto-regressive, auto-regressive moving average, machine-learned, etc.) as long as the order of the model is suitable and the structure physically exhibits linear and stationary behavior i.e.: infinitesimal vibrations, linear elastic stiffness, reciprocity, and time-invariant physical properties.

Any suitable transformation is useful for detecting damage if the model is calibrated to the healthy structure. For example, estimating the change in coefficients of an auto-regressive time series model to match the input-output behavior exhibited by the monitored structure can indicate the presence of damage [Figueiredo et al., 2011]. However, only a few models are useful for interpreting the physical characteristics of the damage (location, quantity and type). One is the physics-based model.

The nth order physics-based model is a transformation which satisfies the governing equations of motion derived from Newton's second law (force = mass * accel-

eration) regarding an n degree of freedom (DoF) dynamical structure. This model transforms a vector of forces $p_t \in \Re^n$ into displacement, velocity and acceleration responses $(x_t, \dot{x}_t, \ddot{x}_t \in \Re^n)$ by a coupled system of second order linear differential equation,

$$\mathbf{M}_\theta \{\ddot{x}_t\} + \mathbf{C}_\theta \{\dot{x}_t\} + \mathbf{K}_\theta \{x_t\} = \{p_t\} \tag{2.2}$$

where the mass $\mathbf{M} = \mathbf{M}^T \in \Re^{nxn}$, damping $\mathbf{C} = \mathbf{C}^T \in \Re^{nxn}$, and stiffness $\mathbf{K} = \mathbf{K}^T \in \Re^{nxn}$ matrices are functions of the parameter space $\theta \in \Re^p$. This model describes structures exhibiting linear behavior.

2.1.3 Modal features

Modal features are derived from a combination of basic modal properties. Basic modal properties (i.e. natural frequencies, mode shapes, and damping) can be estimated from measured vibrations using modal analysis techniques developed from system identification theory [Jeong, 2002]. Since the vibration measurements depend on the excitation forces and the parameter space is coupled with the velocity and displacement responses, the system of equations of motion is not a practical operator for eq. 2.1. A preferred alternative is to derive a direct mapping from the parameters to the modal properties using the fundamental orthogonality properties of the equations of motion. This approach is limited to lightly damped structures such that a classical damping model is appropriate. This mapping is the direct eigenvalue problem in structural dynamics.

In the case of classical damping, the response of a linear dynamic system can be reduced to the sum of n weighted responses in its characteristic modes of vi-

bration. In other words, there exists a coordinate transformation $x_t = \mathbf{\Phi}q$, where $\mathbf{\Phi} = [\phi_1, \phi_2, .., \phi_n]$ and $\phi_i \in \Re^n$ is orthogonal with respect to the stiffness and mass matrices ($\phi_i^T \mathbf{M} \phi_j = 0$ and $\phi_i^T \mathbf{K} \phi_j = 0$, $i \neq j$). By selecting ϕ_i such that $\phi_i^T \mathbf{M} \phi_i = 1$), the orthogonality condition uncouples the equations of motion, and each element q_i of the vector q becomes the solution to a linear second order differential equation of the form

$$\ddot{q}_i + 2\zeta_i \omega_i \dot{q}_i + \omega_i^2 q_i = \{\phi_i^T\}\{p_t\} \tag{2.3}$$

where for $i = 1...n$, ζ_i and $\phi_i \in \Re^n$ is the classical damping ratio and mode shape associated with the ith natural frequency ω_i.

Mode shapes, the set of vectors orthogonal with respect to $\mathbf{K}$ and $\mathbf{M}$, are obtained by considering the nontrivial solution $\{x_t\} = \{\phi_i\}sin(\omega_i t)$ to the coupled equations of free vibration of a conservative system,

$$\mathbf{M}_\theta\{\ddot{x}_t\} + \mathbf{K}_\theta\{x_t\} = 0 \tag{2.4}$$

Substituting $\{x_t\} = \{\phi_i\}sin(\omega_i t)$ gives the direct eigenvalue problem,

$$(\mathbf{K}_\theta - \mathbf{M}_\theta \omega_i^2)\{\phi_i\} = 0 \tag{2.5}$$

The eigenvalues and the eigenvectors of the direct eigenvalue problem correspond respectively to the natural frequencies and mode shapes of the structure.

Features derived from eigenproperties (modal properties) are appealing because a direct mapping to mass and stiffness exists independent of excitation. Hence, one practical framework for posing the damage identification inverse problem is to define: (i) the parameters in terms of mass and stiffness, (ii) the model using the direct

11

eigenvalue problem, and (iii) the features in terms of the eigenproperties.

2.2 INVERSE METHODS IN VIBRATION-BASED SHM

The residual $||\mathcal{F}(\theta) - \hat{z}||_2$ is a non-convex function because the relationship between the parameters and the features is in general nonlinear. Uncertainty quantification frameworks such as a probabilistic Bayesian method and deterministic frameworks such as the Gauss-Newton, trust-region method, and Levenburg-Marquardt have been suggested for solving the inverse method [Simoen et al., 2015, Ahmadian et al., 1998, Gorl and Link, 2003, Teughals et al., 2004]. This research uses a deterministic framework based on constrained optimization.

The general optimization algorithm incrementally minimizes the objective through a series of steps each defined by the suboptimal solution to a first or second order truncated form of the inverse problem. The characteristics of the nonlinear inverse problem are inferred by investigating the linearized Taylor series expansion of $\mathcal{F}(\theta) - \hat{z}$. The Taylor truncation results in a system of linear equations defined as the sensitivity equation,

$$\mathbf{S}\Delta\theta = \Delta z \tag{2.6}$$

where $\mathbf{S} \in \Re^{qxp}$ is the Jacobian of $\mathcal{F}$, $\Delta\theta \in \Re^p$ is the unknown change in parameters, and $\Delta z \in \Re^q$ is the difference between the features produced by the model evaluated at the initial parameters and those estimated from the measurements.

In SHM, the preferred selection of the parameters and features are those that

induce an over-constrained system of equations or specifically where $\mathbf{S}$ has full column rank [Mottershead et al., 2011]. The over-constrained condition ensures that a unique solution with respect to the ordinary least squares exists.

In practical applications of the inverse method, defining the feature space using natural frequencies and mode shapes is the preferred practice to ensure that the number of measurements exceeds the number of unknown parameters [Abdel Wahab et al., 1999, Teughels and De Roeck, 2004, Pothisiri and Hjelmstad, 2003, Gorl and Link, 2003, Weber et al., 2009, Chellini et al., 2010, Moaveni et al., 2013, Grip et al., 2017]. This poses multiple challenges. A spatially distributed network of sensors is needed since only a small subset of eigenvalues can be extracted from measured vibrations, and the coordinates of the mode shapes can only be estimated at sensor locations. Also, mode shapes are difficult to identify accurately [Doebling et al., 1997, Reynders et al., 2008]. Unmeasured excitation further complicates modal analysis since the mode shapes cannot be mass normalized and the uncertainty in their estimation becomes dependent on the normalizing coordinate [Dohler et al., 2013].

Time-domain features such as response measurements and the impulse-response have also been suggested since they guarantee many measurements [Law and Li, 2006, Lu and Law, 2007, Link and Weiland, 2009, Smith and Hernandez, 2018]. However, taking more measurements in the same frequency range does not necessarily result in more unique information [Shaverdi et al., 2009]. This results in severe ill-conditioning. In addition, the time domain residual is a complex nonlinear function described by many local minima. Hence, general optimization algorithms tend to converge to suboptimal solutions.

Even if enough measurements are taken, the sensitivity matrix tends to be ill-conditioned due to a near rank-deficiency. Ill-conditioning is prevalent in vibration-based SHM because of measurement correlation due to incomplete modal information and a large parameter space [Mottershead, 1993]. Regularization is often necessary to mitigate the solution's sensitivity to measurement error in ill-conditioned problems [Neubauer, 1989, Vogel, 2002]. Among the various forms of regularization in SHM (e.g. truncated singular value decomposition, QR- decomposition [Wu and Law, 2004, Titurus and Friswell, 2008, Fritzen et al., 1998]), placing a side constraint on the parameters is often preferred [Friswell et al., 2001, Gorl and Link, 2003, Weber et al., 2009]. This type of penalized regularization is often done with the l_2-norm in order to enforce small changes in the estimated parameters. This form of regularization is known as the Tikhonov regularization [Neubauer, 1989].

2.3 Convex optimization

In order to facilitate the following discussion on underdetermined inverse problems, this section provides a description of convex optimization along with a few essential terms and definitions.

In general, optimization seeks to find the global minimum of an objective function over a given set. Convex optimization is a special case of general optimization where the constraints and objective functions satisfy a set of conditions which guarantees that the local minimum is the global minimum. The convex optimization program is

expressed as

$$x^* = \min_{x \in \mathcal{D}} \quad f_o(x)$$

$$\text{subject to} \quad h_i(x) = 0, \ i = 1, ..., m \qquad (2.7)$$

$$f_i(x) \leq 0, \ i = 1, ..., l$$

where x is the optimization variable, $f_o(x)$ is the objective function to be minimized, $h_i(x) = 0$ is a set of m affine equations, and $f_i(x) \leq 0$ is a set of l inequalities. Eq. 2.7 is a convex optimization program only if $f_0(x)$ is a convex function, $h_i(x)$ is affine, $f_i(x)$ is a convex function, and there exists a feasible x.

The set of points for which the objective and the constraint functions are defined is called the domain $\mathcal{D}$ of the optimization problem. The feasible region is the set of all points $x \in \mathcal{D}$ that satisfies the constraints. The optimal solution $f_o(x^*)$ minimizes the objective function given the constraints. x^* is an optimal point if it solves the optimization problem. The set of all optimal points is the optimal set. The optimal set only has one optimal point if and only if the objective function is strictly convex (not to be confused with convex). For more details on convex sets and functions see [Boyd and Vandenberghe, 2004].

The advantage in formulating a convex optimization program as opposed to a general optimization program is (i) the optimal solution is globally optimal, (ii) methods which solve convex optimization are efficient and reliable, and (iii) the theory underlying convex optimization can be used to interpret solutions to the inverse method.

2.4 UNDERDETERMINED INVERSE PROBLEMS

Inverse methods in SHM are seldom defined by an underdetermined system of equations. If the number of parameters exceeds the number of measurements $p < q$, the null space of $\mathbf{S}$ is non-empty and the inverse problem lacks a unique solution. In model updating for the purposes of improving the accuracy of a model, an underdetermined inverse problem is undesirable since a physically meaningful solution is not obtainable even with regularization [Friswell et al., 2001, Mottershead et al., 2011].

2.4.1 PRIORS AND SPARSITY

Although damage identification and model updating are both performed with the inverse method, the solution spaces should be significantly different. While model updating aims to make small adjustments to many parameters, damage identification seeks to find a significant change in only a few spatially local stiffness and(or) mass parameters. In other words, damage identification seeks solutions having few non-zero elements, i.e. sparse vectors. Because the solution is potentially sparse, it is possible to obtain meaningful solutions to the underdetermined inverse problem using convex optimization [Zhou et al., 2013, Hernandez, 2014, Zhou et al., 2015].

Assume there exists one physically meaningful vector $\Delta\theta$ among the infinite possible vectors satisfying the underdetermined system of equations $\mathbf{S}\Delta\theta = \Delta z$. In order to find $\Delta\theta$ which best represents physical reality, we need to define a criterion that can be uniquely satisfied and results in physically meaningful solutions. For example,

16

one criterion is to find the solution with the smallest magnitude l_2-norm ($||.||_2$), where

$$||\Delta\theta||_2 = \sqrt{\sum_{i=1}^{p} \Delta\theta_i^2} \qquad (2.8)$$

This criterion is common in FE model updating since the uncertainty in the prior parameters is bounded and is expected to be spread among many parameters. Solving the convex optimization program,

$$\Delta\theta_{mp}^* = \min_{\Delta\theta \in \mathcal{D}} \quad ||\Delta\theta||_2$$
$$\text{subject to} \quad \mathbf{S}\Delta\theta = \Delta z \qquad (2.9)$$

results in the Moore-Penrose solution which has a closed form, $\Delta\theta_{mp}^* = \mathbf{S}^T(\mathbf{SS}^T)^{-1}\Delta z$. Note that $\Delta\theta_{mp}^*$ is unique since $\mathbf{SS}^T$ has full rank. Uniqueness can also be proven by verifying that $||\Delta\theta||_2$ is strictly convex.

Minimizing with respect to different norms results in different optimal sets. This can be leveraged to induce a more desirable solution. Since damage identification seeks sparse solutions, one potential criterion is to minimize the number of non-zero elements in order to determine the sparsest solution. One measure for counting the number of non-zero elements in a vector is the l_0 pseudo-norm. Hence minimizing the l_0-pseudo norm results in the sparsest solution. However, the l_0 pseudo-norm is a non-convex function and hence can be computationally expensive to minimize with a non-convex solver. The problem of minimizing non-zero elements can be relaxed to a convex form by replacing the pseudo-norm with the l_1-norm ($||.||_1$) where

$$||\Delta\theta||_1 = \sum_{i=1}^{p} |\Delta\theta_i| \qquad (2.10)$$

This convex optimization program, referred to as the basis pursuit [Donoho, 2006], is written as

$$\Delta\theta_{bp}^* = \min_{\Delta\theta \in \mathcal{D}} \quad ||\Delta\theta||_1$$

$$\text{subject to} \quad \mathbf{S}\Delta\theta = \Delta z \tag{2.11}$$

The optimal point $\Delta\theta_{bp}^*$ does not have a closed form since the derivative does not exist everywhere for the absolute value operator. $||\Delta\theta||_1$ is also not strictly convex and hence there is no guarantee that $\Delta\theta_{bp}^*$ is unique.

The differences in the optimal solution between norms can be explained geometrically. Fig. 2.1 presents a two-dimensional representation of a generic underdetermined system of linear equations and the projections of the l_2-norm, the l_1-norm, and the l_0 pseudo-norm. In each sub-figure, the optimal solution minimizing the specific norm-operator subject to the linear system is shown. The point(s) at which the projection of the norm-operator intersects with the linear system is the optimal point. From Fig. 2.1a, the projection of the l_2-norm is a circle, so its optimal point is unbiased. From Fig. 2.1b, the l_1-norm projection is a rhombus and biases the optimal point to the axes which by definition are sparse vectors. From Fig. 2.1c, the l_0 pseudo-norm guarantees the sparsest vector; however, the operator is non-convex.
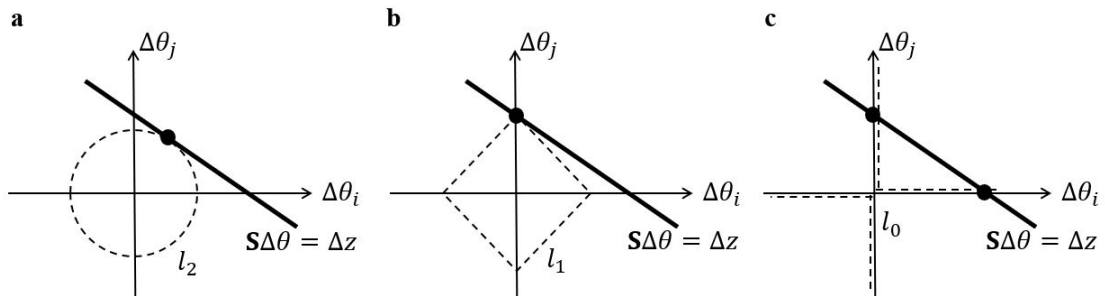
Figure 2.1: Optimal solutions to the underdetermined system of equations with respect to the a) l_2-norm, b) l_1-norm, c) l_0 pseudo-norm

The criterion for selecting a satisfactory solution to the underdetermined inverse problem is also manipulated by constraining the feasible region to reflect prior engineering experience. Local damage is often defined by a strict reduction in stiffness and(or) mass. Some authors have suggested using the non-negative constraint to impose the strict stiffness reduction prior on the solution space [Hassiostis and Jeong, 1995, Ren and De Roeck, 2002, Li and Law, 2010, Smith and Hernandez, 2019]. The non-negative constrained least squares solves the following convex optimization program,

$$\Delta\theta_{nn}^* = \min_{\Delta\theta \in \mathcal{D}} \quad ||\mathbf{S}\Delta\theta - \Delta z||_2$$
$$\text{subject to} \quad \Delta\theta \geq 0 \tag{2.12}$$

There is no guarantee in this problem that $\Delta\theta_{nn}^*$ is unique. Subsequent chapters address this problem in greater detail.

2.4.2 ILLUSTRATIVE EXAMPLE
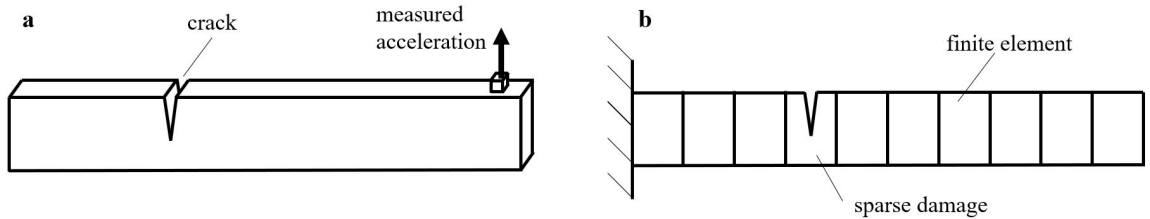
Figure 2.2: a) Damaged beam, b) discretized model with sparse damage

To illustrate how the choice of the optimization program affects the solution to the undetermined inverse problem consider the following example regarding the damaged beam in Fig. 2.2. 10 elements are monitored for damage using 3 identified eigenvalues. The sensitivity equation is defined by $\mathbf{S} \in \Re^{3x10}$, the unknown change in stiffness is

$\Delta\theta \in \Re^{10}$, and the change in eigenvalues between the damaged and undamaged structure is $\Delta z \in \Re^3$. The system of equations is clearly underdetermined. Damage induces a 10% stiffness reduction in element 4 and we wish to reconstruct the change in stiffness from the associated shift in eigenvalues. The estimated change in stiffness using $\Delta\theta^*_{mp}$, $\Delta\theta^*_{bp}$, and $\Delta\theta^*_{nn}$ are shown in Fig. 2.3. The Moore-Penrose solution (Fig. 2.3a) may be unique however it is physically meaningless. The solutions to the basis pursuit and the non-negative least squares on the other hand are physically meaningful as well as sparse.
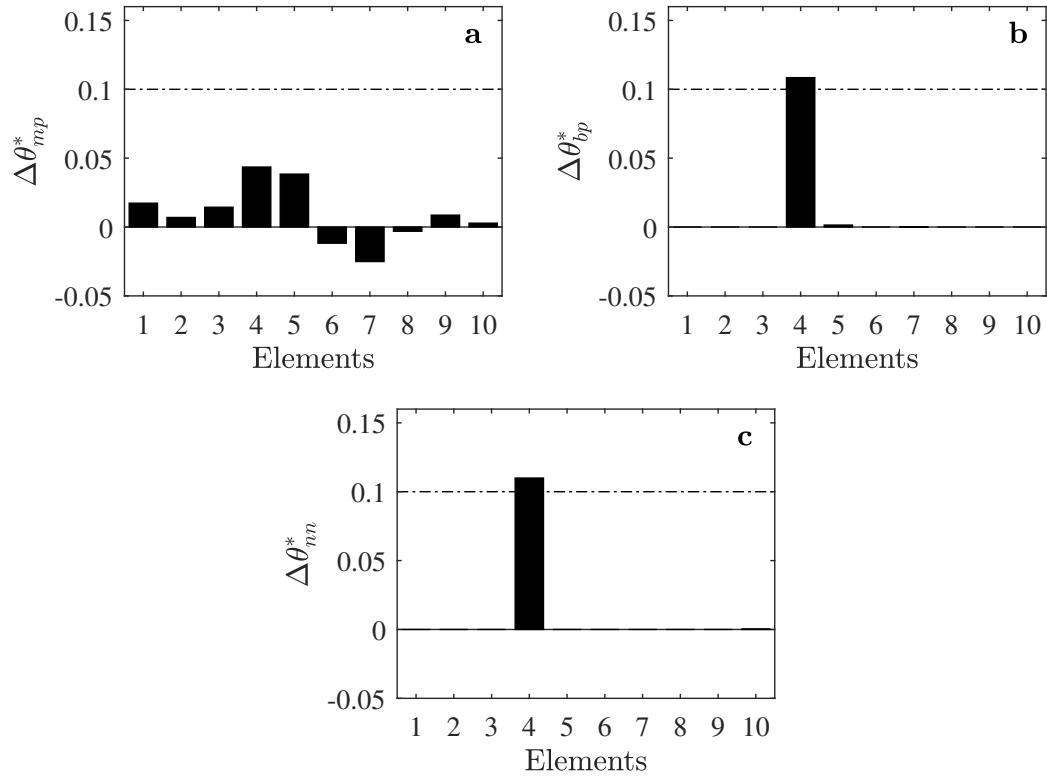
Figure 2.3: Optimal points using a) the Moore-Penrose, b) basis pursuit, and the c) non-negative constrained least squares

CHAPTER 3

NON-NEGATIVE CONSTRAINED INVERSE EIGENVALUE PROBLEMS - APPLICATION TO DAMAGE IDENTIFICATION

ABSTRACT

Damage identification using eigenvalue shifts is ill-posed because the number of identifiable eigenvalues is typically far less than the number of potential damage locations. This paper shows that if damage is defined by sparse and non-negative vectors, such as the case for local stiffness reductions, then the non-negative solution to the linearized inverse eigenvalue problem can be made unique with respect to a subset of eigenvalues significantly smaller than the number of potential damage locations. Theoretical evidence, numerical simulations, and performance comparisons to sparse vector recovery methods based on l_1-norm optimization are used to validate the find-

ings. These results are then extrapolated to the ill-posed nonlinear inverse eigenvalue problem in cases where damage is large, and linearization induces non-negligible truncation errors. In order to approximate the solution to the non-negative nonlinear least squares, a constrained finite element model updating approach is presented. The proposed method is verified using three simulated structures of increasing complexity: a one-dimensional shear beam, a planar truss, and a three-dimensional space structure. For multiple structures, this paper demonstrates that the proposed method finds sparse solutions in the presence of measurement noise.

3.1   INTRODUCTION

Given the mass $\mathbf{M}$, viscous damping $\mathbf{C}_d$, and stiffness $\mathbf{K}$ matrices of a structure, the direct eigenvalue problem seeks to solve

$$(\mathbf{M}\lambda_j^2 + \mathbf{C}_d\lambda_j + \mathbf{K})\phi_j = 0, \ j = 1...n$$

for the eigenvalues λ_j and eigenvectors ϕ_j.

The inverse eigenvalue problem consists in using the set of eigenvalues and eigenvectors to estimate $\mathbf{M}, \mathbf{C}_d,$ and $\mathbf{K}$. Solving the inverse eigenvalue problem for practical applications poses a challenge because only a subset of eigenvalues can be extracted from vibration data, and the corresponding eigenvector coordinates can only be estimated at sensor locations. This effectively reduces the number of independent parameters that can be used to define $\mathbf{M}, \mathbf{C}_d,$ and $\mathbf{K}$.

One application of the inverse eigenvalue problem is in damage identification using measured structural vibrations. The objective of damage identification is to:

22

(a) detect, (b) localize, (c) categorize, and (d) quantify changes in material or geometric properties which adversely impact the structure's performance [1]. Because structural vibrations emerge from the complex interaction between structural components, changes in local material properties tend to manifest themselves in the identified modal characteristics of the structure. Inverse eigenvalue analysis can be used to identify damage from identified changes in modal characteristics between the structure's undamaged and potentially damaged state [2]. In this paper, inverse eigenvalue analysis is specifically used to identify spatially localized damage such as cracks, perforations, reductions in thickness, etc., and to quantify these damages in terms of changes in material stiffness.

When defined in terms of stiffness, damage has an important property; non-negativity. Physically, non-negativity reflects the property that damage tends to strictly reduce the stiffness of the damaged element [3]. Therefore the resolution of damage identification can be significantly improved by strictly searching for stiffness reductions that are non-negative [4]. This characteristic differentiates damage identification from finite element model (FEM) updating, and can be used to restrict the feasible space of solutions.

A priori information, such as non-negativity and(or) sparsity, can be considered as a type of regularization. Recent application of regularization techniques can be found in [4–6, 8]. Weber adapted Kaltenbacher's iterative Tikhonov regularization and singular value decomposition to improve numerical stability [6, 7]. Li proposed an adaptive Tikhonov regularization that systematically eliminates free parameters that do not satisfy the strict stiffness reduction prior [4]. Grip applied total variation regularization in order to enforce sparsity on the solution space [8]. Other notable

alternatives not explicitly mentioned are reviewed in [3, 9]. Existing algorithms work well when the number of measurements is larger than the number of unknown parameters. However, obtaining more measurements than unknowns poses a practical dilemma; one must either increase the number of measurement devices and rely on less robust features such as eigenvectors, or reduce the number of unknown parameters by an a priori subset selection.

One potential alternative is to strictly monitor the structure's eigenvalues, which by virtue of their inherent robustness would simultaneously reduce uncertainty and the required number of measurement devices [10–12]. Of course, the use of eigenvalue-based methods would result in an underdetermined system of equations (given that only a subset of the smallest eigenvalues can be identified from structural vibrations). If the solution space is unconstrained, then the inverse eigenvalue problem is ill-posed [13]. As this paper will show, a solution space constrained by non-negative vectors may yield a unique solution if a sparse non-negative solution exists.

A sparse vector that satisfies an underdetermined system of linear equations is sometimes unique with respect to the smallest number of non-zero elements, i.e. the sparsest solution [14–16]. This finding has motivated sparse vector recovery; methods which seek to efficiently minimize the number of non-zero elements. In some applications, such as compressed sensing and localized damage identification, sparsity is a desirable characteristic. In structural health monitoring (SHM), sparse vector recovery methods have been successfully applied to the linear damage identification problem [17–23]. The noted works are largely based on minimizing with respect to the l_1-norm. The l_1-norm is a surrogate measure of the number of non-zero elements that is numerically convex, and can be minimized in a tractable manner [14–16].

Though successful, l_1-norm based damage identification methods require user biased regularization parameters. Furthermore, the l_1-norm forces sparse solutions even if the best solution is not sparse. However, methods that force sparsity are not necessary to the recovery of sparse, non-negative vectors. If a sparse non-negative solution exists, then non-negative constraints alone can recover a unique solution to the underdetermined linear system. If the solution is not sparse, then non-negativity alone will fail to deliver a sparse solution. This could prove to be a more robust and efficient approach.

The relationship between non-negativity and sparsity has only recently been explored [24–26, 28]. For systems of linear equations, the set $\{x|\ Ax = b,\ x \geq 0\}$ defines the non-negative feasible space. Applying a non-negative constraint to a highly underdetermined system of equations may at first seem trivial, but in the context of sparsity its far from it. It has been mathematically verified that if solutions to $Ax = b$ are sparse enough, and matrix **A** of a special structure, then the non-negative feasible space may only contain one solution, i.e. a singleton [25, 28]. If the feasible set is a singleton, then a unique solution exists and the constrained inverse problem becomes well-posed.

The objective of this paper is to show that sparse stiffness reductions can be located and quantified using only a subset of eigenvalue shifts by applying a non-negative constraint to the solution of the underdetermined nonlinear equations that result from the inverse eigenvalue problem. This paper can be broadly divided into two parts: the linearized inverse eigenvalue problem (section 3.3-3.5), and the non-linear inverse eigenvalue problem (section 3.6-3.7). This paper begins by introducing the parameter to eigenvalue operator (section 3.2). Section 3.3 presents the lin-

25

earized eigen-sensitivity inverse problem for small magnitude damage identification. Section 3.3.1 explains the theoretical evidence for obtaining unique solutions with the non-negative constraint and the role of sparsity. Section 3.3.2 presents the proposed method to obtain non-negative solutions, the non-negative least squares, and the uniqueness verification from [26]. In order to compare existing sparse recovery methods, section 3.3.3 reviews l_1-norm optimization. In sections 3.4 and 3.5, the proposed method is verified, and compared to sparse recovery techniques that use l_1-norm optimization using a simulated shear beam from [19], a simulated planar truss from [4], and a simulated 3D truss from [27]. Section 3.6 introduces the nonlinear inverse problem for locating and quantifying large damage. Motivated by the success of the non-negative constrained linearized inverse problem, section 3.6.1 presents the non-negative nonlinear least squares; a program that enforces the strict stiffness reduction prior on solutions to the nonlinear inverse problem. The proposed method uses sequential convex programming, substituting the preferred Gauss-Newton approach to FEM updating. Section 3.7 verifies the methodology with an investigation on the effect of measurement noise using the simulated planar truss and 3D truss. Section 3.8 concludes the paper with a discussion on the main findings, and suggests possible directions for future research on the topic.

3.2 PARAMETER TO EIGENVALUE OPERATOR

For lightly damped structures, the eigenvalue problem can be approximated by solving:

$$(\mathbf{K} - \lambda_j \mathbf{M})\phi_j = 0, \; j = 1...n \tag{3.1}$$

where the eigenvalues $\lambda = \lambda_1, \lambda_2, ..., \lambda_n$ are the roots of the polynomial resulting from

$$\det (\mathbf{K} - \lambda_j \mathbf{M}) = 0 \tag{3.2}$$

When damage can be defined by independent parameters that induce additive changes in the stiffness matrix, the stiffness matrix can be parameterized as

$$\mathbf{K}_\theta = \sum_{i=1}^{p} \mathbf{E}_i f_i (\theta_i) \tag{3.3}$$

where $f_i (\cdot)$ is a function, θ_i is the ith parameter that contributes to the stiffness matrix, and $\mathbf{E}_i$ is the elementary influence matrix corresponding to the ith parameter [13]. θ_i is often defined as the element's elastic modulus, shear modulus, cross sectional-area, or moment of inertia. In these cases, $f_i(\theta_i)$ is a positive monotonic function.

The parameter-to-eigenvalue map is denoted by

$$\mathcal{F}(\theta) = \lambda \tag{3.4}$$

where $\mathcal{F}$ is a nonlinear operator between the vector spaces $\theta \in \mathfrak{R}^{px1}$ and $\lambda \in \mathfrak{R}^{nx1}$. In practice, the number of eigenvalues that can be identified from global vibrations, denoted as m, is far less than the number of possible damage elements. In this paper, $m < n$ and $m < p$.

3.3   Linear inverse problem

If changes in stiffness due to damage are small enough such that neglecting higher order terms in the nonlinear operator induces only minor linear truncation errors, and the change in stiffness can be approximated by

$$\frac{\partial \mathbf{K}}{\partial \theta_i} \approx \frac{\Delta \mathbf{K}}{\Delta \theta_i} = \mathbf{E}_i \frac{\Delta f_i}{\Delta \theta_i} \tag{3.5}$$

then the relationship between the changes in parameters $\Delta \theta \in \Re^p$ and the changes in the identified eigenvalues between the undamaged and damaged structure $\Delta \lambda \in \Re^m$ can be approximately defined by

$$\mathbf{S}_{\theta_u} \Delta \theta \approx \Delta \lambda \tag{3.6}$$

where $\mathbf{S}_{\theta_u} \in \Re^{mxp}$ is the gradient of the nonlinear operator $\mathcal{F}(\cdot)$, also known as the sensitivity matrix or the Jacobian, evaluated at the parameters of the undamaged structure denoted $\theta_u \in \Re^n$. For clarity, the subscript θ_u is dropped for the rest of the sections on the linear inverse problem. Based on the sensitivity method to structural dynamics proposed in [13] and the gradient of the eigenvalues [29], the sensitivity matrix can be written as

$$\mathbf{S}_{j,i} = \frac{\partial \lambda_j}{\partial \theta_i} = \phi_j^T \frac{\partial \mathbf{K}}{\partial \theta_i} \phi_j \approx \frac{\Delta f_i}{\Delta \theta_i} \phi_j^T \mathbf{E}_i \phi_j \tag{3.7}$$

where $i = 1...p$ and $j = 1...m$ denote the row and column entry of the sensitivity matrix.

In this paper, the objective in small magnitude damage identification is to determine the change in parameters due to damage given the identified changes in eigenvalues such that

$$\mathbf{S}\Delta\theta = \Delta\lambda + \epsilon_0 \tag{3.8}$$

where ϵ_0 defines some measure of fit to the linear approximation. Since $m < p$, eq. 3.8 constitutes an underdetermined system of linear equations. Without additional equations or constraints, a solution $\Delta\theta$ is non-unique. However, additional constraints specific to damage identification can be considered, and may help reduce the indeterminacy of the problem.

3.3.1 Non-negative constraints and sparsity

The change in the vector of parameters that describes localized stiffness reductions can be represented by a non-negative, k-sparse vector, where k represents the number of nonzero elements, and $k << p$. Given the sparse stiffness reduction prior, one appropriately constrained set of solutions to the linear inverse problem is

$$S_{NN} = \{\Delta\theta|\ \mathbf{S}\Delta\theta = \Delta\lambda + \epsilon_0,\ \Delta\theta \geq 0\} \tag{3.9}$$

The feasible region, S_{NN}, is comprised of non-negative vectors $\Delta\theta$ that satisfy the system of equations. Note that S_{NN} is not an explicit constraint on sparsity. In fact, sparse constraints are not explicitly used in any of the methods proposed in this paper.

If there exists a $\Delta\theta \geq 0$ containing few non-zero elements that satisfies the system of equations, then that vector may be the only non-negative vector to satisfy the

system of equations. In other words, if a sparse and non-negative solution exists then the set S_{NN} may contain only only one vector. A highly underdetermined system that is satisfied by strictly one non-negative vector may seem unlikely, but consider the following lines of reason from [26]. There are m equations and p unknowns. If $p - m$ constraints are active and act as equalities, then the solution will be unique. For a non-negative constraint to become an equality constraint, the associated constrained element must be zero. Therefore, a sparse solution, having at least $p-m$ zero elements, may result in a single feasible point [26]. If the feasible region contains only one point, referred to as a singleton, then that point is the unique solution to the constrained inverse problem. To emphasize, the non-negative constraint promotes uniqueness to the underdetermined linear system because there exists a sparse solution.

The singleton property is not a general property of all non-negative constrained linear inverse problems; specific conditions must be satisfied. As proven in [28], the mapping matrix, in this case $\mathbf{S}$, must belong to the class of matrices having a row-span intersecting the positive orthant in order for the singleton phenomenon to occur, and will not occur otherwise. As defined in [25], a matrix $\mathbf{A}$ has a row span intersecting the positive orthant if there exists a strictly positive vector w that can be obtained as a linear combination of rows of $\mathbf{A}$, that is

$$\exists\, h \text{ s.t. } h^T \mathbf{A} = w^T > 0 \tag{3.10}$$

The eigenvalue sensitivity matrix belongs to this matrix class because by definition its rows are always non-negative. This occurs because the influence matrices (eq. 3.3) represent stiffness matrices of substructures and hence must be positive semi-definite. By the definition of a positive semi-definite matrix, $\phi_j^T \mathbf{E}_i \phi_j \geq 0$ for all j and

i. Since $f_i(\theta_i)$ from eq. 3.3 is a positive monotonic function, then by definition of the sensitivity matrix

$$\mathbf{S}_{j,i} \approx \frac{\Delta f_i}{\Delta \theta_i} \phi_j^T \mathbf{E}_i \phi_j \geq 0$$

The positive sensitivity matrix property is reflected physically because a reduction in stiffness always increases the natural period of the structure.

Although the sensitivity matrix satisfies the strict property needed to tighten S_{NN} to a single point, it is unknown whether this singleton phenomenon is guaranteed to occur. In current literature, the proofs that guarantee the singleton phenomenon require large minimum subspace angles between columns of the mapping matrix, and depend on the maximum number of nonzero elements of the solution [25]. The next section presents work from [26] that quantifies the size of S_{NN}, and determines if the set only contains one point (unique solution).

3.3.2   UNIQUE SOLUTIONS TO THE NON-NEGATIVE

LEAST SQUARES

In addition to truncation error, the estimated eigenvalues are functions of measurement noise and system identification errors. The model also does not perfectly represent the structure of interest. One measure of solution quality is the Euclidean magnitude of the residual between the measured and modelled change in eigenvalues. The authors propose to use the Non-negative Least Squares (NNLS) to minimize the residual and impose the non-negative constraint. The NNLS is a constrained convex

optimization program, and can be written simply as

$$
\begin{aligned}
\min_{\Delta\theta,\epsilon_0} \quad & ||\epsilon_0||_2 \\
\text{subject to} \quad & \mathbf{S}\Delta\theta = \Delta\lambda + \epsilon_0 \\
& \Delta\theta \geq 0
\end{aligned}
\tag{3.11}
$$

where $\epsilon_0 \in \Re^{mx1}$ is an optimization variable that represents the closest possible fit to the affine constraint such that the non-negative constraint holds. The NNLS is strictly convex with respect to ϵ_0 implying there exists only one optimal point ϵ_0^* that minimizes the objective function [30]. However, an infinite number of vectors $\Delta\theta^*$ may exist that satisfy the affine constraint given ϵ_0^*. Given the characteristics of the damage identification inverse problem: sparsity, the class of the sensitivity matrix, and the non-negative constraint, the authors expect only one $\Delta\theta^*$ to satisfy $\{\Delta\theta^*| \ \mathbf{S}\Delta\theta^* = \Delta\lambda + \epsilon_0^*, \ \Delta\theta^* \geq 0\}$. The $*$ notation indicates the optimal solution to the optimization.

The optimal solution can be checked for uniqueness by the following measure posed in [26]. Dillon proves that the non-negative feasible region contains only one point if and only if the optimal solution to the following convex optimization program results in $||d^*||_1 = 0$:

$$
\begin{aligned}
\min_{\mathbf{Y},\mathbf{Y}',d} \quad & ||d||_1 \\
\text{subject to} \quad & (\mathbf{Y} - \mathbf{Y}')^T(\Delta\lambda + \epsilon_0^*) = d \\
& \mathbf{Y}^T\mathbf{S} \geq \mathbf{I} \\
& \mathbf{Y}'^T\mathbf{S} \leq \mathbf{I}
\end{aligned}
\tag{3.12}
$$

where $\mathbf{Y}, \mathbf{Y}' \in \Re^{pxm}$. The details of the proof are based on duality in convex optimization theory and can be found in [26]. The optimal solution $||d^*||_1$ is not only an indicator of uniqueness, but can be interpreted as a measure of uniqueness, where smaller values indicate smaller feasible regions.

The uniqueness measure can be used to determine if the optimal solution to the NNLS correctly represents the change in parameters due to damage. Consider an ideal situation, one without truncation or measurement error. In the ideal case, there exists a feasible set of parameters $\Delta\theta \geq 0$ such that $||\epsilon_0^*||_2 = 0$. If $||d^*||_1 = 0$, then the feasible set is a singleton and the optimal point $\Delta\theta^*$ is the only solution that fits $\mathbf{S}\Delta\theta^* = \Delta\lambda$. Thus the uniqueness measure implies that the optimal point must be the correct damage location. In the case where the feasible set is not a singleton, then additional constraints/equations may be needed to induce a unique solution. A check on uniqueness provides a means of verifying the accuracy of the solution without knowing the solution prior; a distinct advantage over using l_1-norm methods where an equivalent uniqueness measure has not been established.

3.3.3 LEAST l_1-NORM OPTIMIZATION

This paper compares the NNLS to a method that is synonymous with sparse recovery. The basis pursuit, also known as the least l_1-norm optimization, is the preferred method for solving the underdetermined system of linear equations for the sparsest solution [14–16]. The basis pursuit is defined as

$$
\begin{aligned}
&\min_{\Delta\theta} && ||\Delta\theta||_1 \\
&\text{subject to} && \mathbf{S}\Delta\theta = \Delta\lambda
\end{aligned}
\tag{3.13}
$$

Note that the sparsest feasible solution will not be strictly sparse because the sparsest solutions must be adjusted to fit the equality. The zero elements of the sparsest solution are only approximately zero. If the level of measurement error is significant, or the linear approximation error large, the least l_1-norm can be modified to accommodate noise. This is known as basis pursuit denoising. Basis pursuit denoising can be programmed as

$$
\begin{aligned}
\min_{\Delta\theta} \quad & ||\Delta\theta||_1 \\
\text{subject to} \quad & ||\mathbf{S}\Delta\theta - \Delta\lambda||_2 \leq \alpha
\end{aligned}
\tag{3.14}
$$

where α is the user specified regularization parameter. These two convex optimization programs have broad applications in signal processing fields. In SHM, they have been successfully applied to the ill-posed eigen-sensitivity inverse problem in simulation and experiment, hence a reputable reference for comparison [19, 22].

3.4   SIMULATED EXPERIMENTS

AND IMPLEMENTATION

The performance of the basis pursuit and non-negative least squares is dependent on the structure of the sensitivity matrix and the number of identified eigenvalues. A variety of damage scenarios and structures are simulated in order to verify the methodology. Three structures, each increasing in complexity, are considered: i) a 21 element non-uniform shear beam simulated in [19], ii) a 31 element planar bar truss simulated in [4], and iii) a 144 element three-dimensional truss simulated in [27].

The shear beam has 21 degrees of freedom with elements enumerated from 1, the first mass closest to the support, to 21, the free end. The spring stiffness are as follows: $k_1 = ... = k_7 = 1000$, $k_8 = ... = k_{14} = 750$, and $k_{15} = ... = k_{21} = 500$, and the masses: $m_1 = ... = m_7 = 1$, $m_8 = ... = m_{14} = 0.75$, and $m_{15} = ... = m_{21} = 0.5$. The fundamental frequency is 0.436 Hz. The planar truss, as shown in Fig. 3.1, is comprised of 25 translation degrees of freedom and 31 elements. The truss was used in [4] to successfully demonstrate damage identification by changes in vibration response using the adaptive Tikhonov Gauss-Newton method; a method that also applies non-negative constraints. That method used vibration response as the damage sensitive feature, which resulted in a greater number of equations than unknowns. The truss is composed of ideal pinned bars, each with a modulus of elasticity of 70 GPa, cross sectional area of 0.0025 m^2, and density 2770 kg/m^3. The first three natural frequencies of the structure as simulated in this paper are 25.12 Hz, 53.20 Hz, and 87.76 Hz.

The simulated 3D truss is a beam element model based on the physical description of the 17.24 m long aluminum truss tested in [27]. Fig. 3.2 presents the physical characteristics of the truss. The truss is comprised of aluminum tubes each having modulus of elasticity of 69.64 GPa, density of 2714.5 kg/m^3, and Poisson's ratio equal to 0.33. Fig. 5.2a presents the beam element model demarcated by 11 bays. The model is comprised of 144 beam elements each having 12 degrees of freedom. The boundary conditions were fixed at the end of bay 1, and pinned in the y and z coordinates at the end of bay 11. The first three natural frequencies of the structure as simulated in this paper are 12.04 Hz, 13.14 Hz, and 16.93 Hz. Fig. 5.2b-e presents the naming convention for each cluster of elements defining a section of the truss.

Note that MCh_i denotes the 11 main chord segments along the indicated length, and Str_i denotes all 12 parallel struts sharing the indicated plane. The element groups are intended to help convey the results of the simulations to the reader.

The simulations are ideal because the model used to generate the simulated data is also the one used to implement the algorithm. The ideal simulations verify that the underdetermined system of equations possess unique non-negative sparse solutions, and that the measure of uniqueness can improve the robustness of the method with respect to incomplete modal information.

$$E = 70GPa \quad \rho = 2770kg/m^3$$
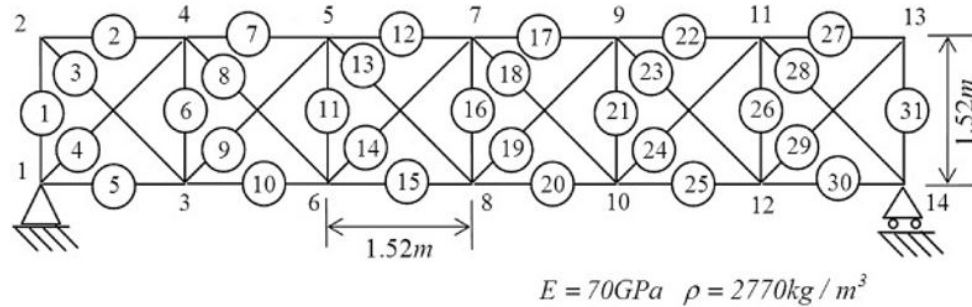
Figure 3.1: Statically indeterminate planar bar truss used for simulations (adopted from [4])
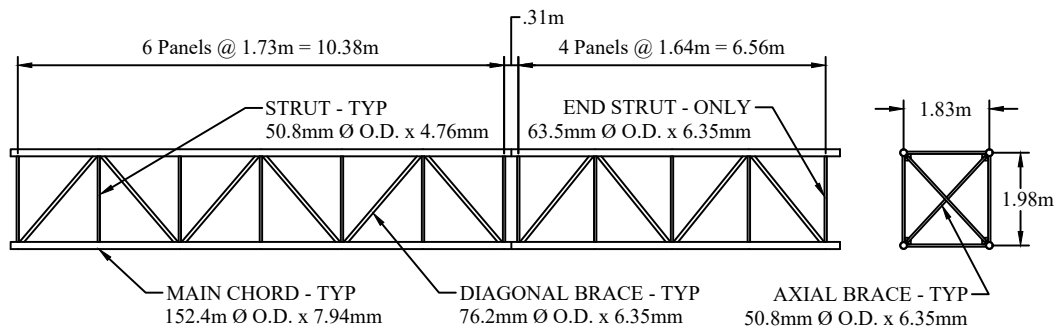
Figure 3.2: Plan view of 3D truss with dimensions and cross-section details

The CVX platform on Matlab was used to implement the convex optimization

36
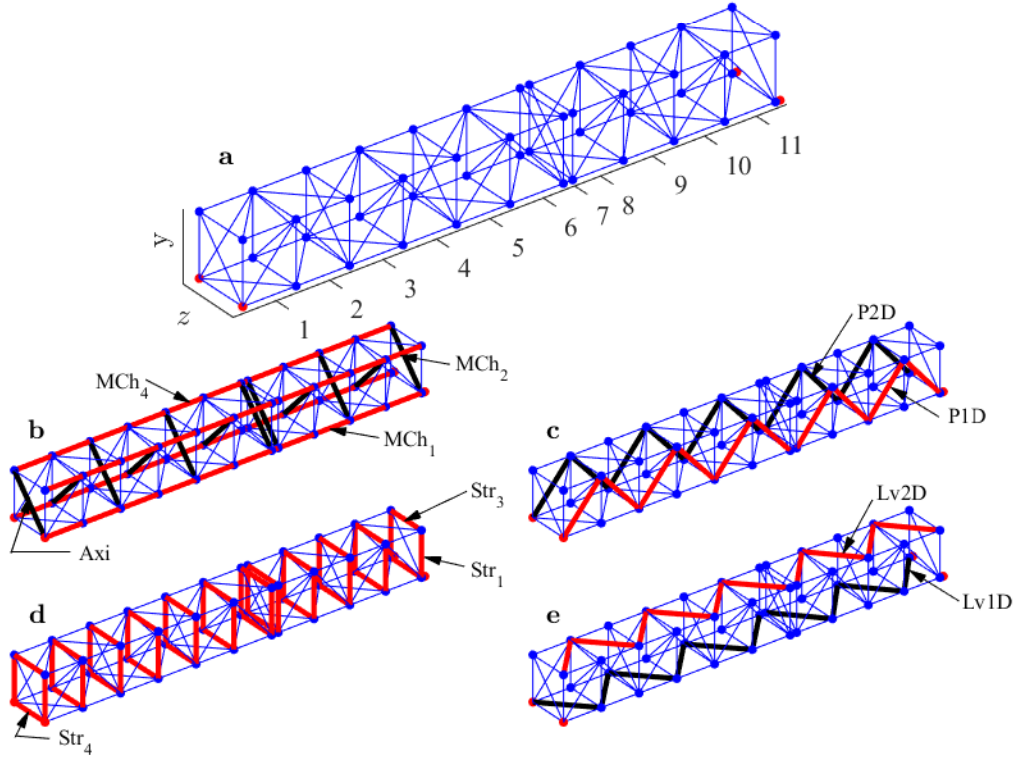
Figure 3.3: a) 3D truss model used to implement algorithms. Bays numbered 1-11. Red nodes indicate locations of boundary conditions: fixed condition at bay 1, and pinned in the y and z direction at bay 11. Clusters of elements defining the truss sections use the following naming conventions: b) main chords in red ($MCh_{1,2,3,4}$) and axial diagonals (Axi) in black, c) diagonal braces at plane 1 (P1D) in red and diagonal braces in plane 2 (P2D) in black, d) struts ($Str_{1,2,3,4}$) in red, and e) diagonal braces at level 1 (Lv1D) in black and diagonal braces at level 2 (Lv2D) in red

programs. This platform used the Gurobi solver at the best numerical precision to solve the optimization problems [33]. Throughout this paper, any value less than $1e - 7$ is denoted as zero, otherwise the value was noted as is.

3.5 NUMERICAL SIMULATIONS TO LINEAR METHODS: VERIFICATION AND COMPARISON

The NNLS (eq. 3.11) and uniqueness measure (eq. 3.12) are applied to simulated damage cases for both the shear beam and the truss structures described in the previous section. The results are compared to those obtained from the basis pursuit (eq. 3.13).

For the shear beam, the following four damage cases are considered: i) 5% stiffness reduction at El.6, ii) 5% and 10% stiffness reductions at El.6 and El.15 respectively, iii) 5%, 10%, and 5% reductions at El.6, El.15, and El.19, and iv) 5%, 10%, and 5% stiffness reductions at El.6, El.15, and El.17. Six eigenvalues are identified thus $\mathbf{S} \in \Re^{6x21}$. The results of the NNLS and the basis pursuit are shown in Fig. 3.4. For damage cases i-iii, Fig. 3.4a-c, the desired sparse solution is recovered with both the basis pursuit (blue) and the NNLS (yellow). In damage case iv, presented in Fig. 3.4d, both algorithms misidentified the damage.

The optimal solution to the NNLS ($||\epsilon_0^*||_2$) and the measure of uniqueness ($||d^*||_1$) are computed for each damage case. In damage cases i-iii, the measure of uniqueness is $||d^*||_1 = 0$. This result implies only one feasible vector, $\Delta\theta^*$, satisfies $\mathbf{S}\Delta\theta^* = \Delta\lambda + \epsilon_0^*$. $||\epsilon_0^*||_2 > 0$ due to the small truncation error. The uniqueness measure provides strong evidence that the estimated stiffness reduction is correct. In damage case iv, $||\epsilon_0^*||_2 = 0$ and $||d^*||_1 = 1$. The measure of uniqueness is large (relative to the user's experience), thus indicating that the obtained estimated stiffness reduction is not unique and

therefore the accuracy of the solution should be doubted. The solution is also over-fitting the data as indicated by $||\epsilon_0^*||_2 = 0$. The two measures provide evidence that additional constraints or equations may be needed to produce a unique solution.

Now consider a damage case where the solution should not be sparse, such as structural deterioration that spans a large portion of the shear beam. In this example, the deterioration reduces the stiffness of the first fifteen elements by 5%. Fig. 3.5a depicts the solutions for the basis pursuit denoising as a function of the regularization parameter α (eq. 3.14), and Fig. 3.5b depicts the results for the NNLS. For all choices of the regularization parameter, the solution indicates incorrectly that the damage is sparse. The NNLS, however, does not yield a sparse solution albeit incorrect. Note that the measure of uniqueness indicates a non-unique solution.

Next, the performance of the NNLS and the basis pursuit in detecting a 1% stiffness reduction at any single element (taken separately, one at a time) is investigated. Eigenvalues are selected sequentially from the lowest in increments of one until either a proper identification is obtained or a threshold of 20 eigenvalues is reached. The tests are performed on the shear beam, the planar truss, and the 3D truss. For each structure, the average estimated stiffness reduction corresponding to the smallest number of eigenvalues needed for proper identification was equal to 0.01 with a variance less than 10^{-5}. Fig. 3.6 presents the minimum number of eigenvalues required to properly identify damage in each element for a) the shear beam, b) the planar truss, and c) the 3D truss. If minimum number of eigenvalues is the criteria for performance, then the basis pursuit (dashed line) slightly outperforms the NNLS (solid line) for the shear beam. However, a different trend can be observed for the same procedure on both trusses. The average minimum number of eigenvalues re-
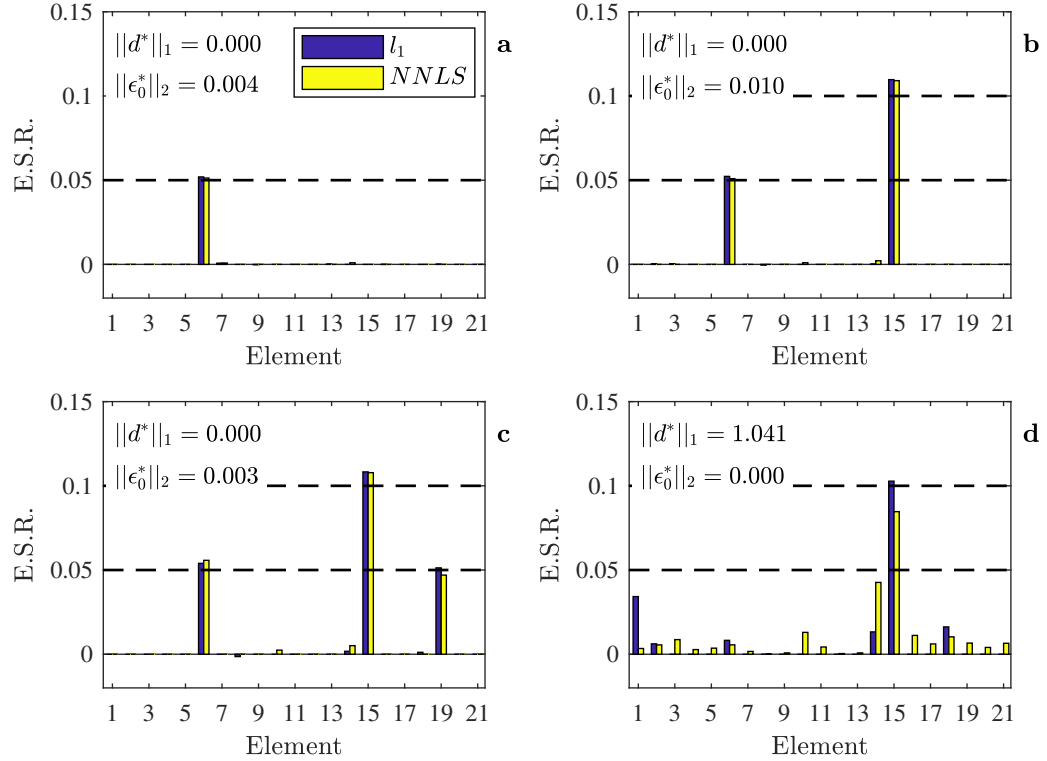
Figure 3.4: The estimated stiffness reduction (E.S.R.) of each element using the NNLS (yellow) and the basis pursuit (blue) given six identified eigenvalues for the following damage cases: a) 5% reduction at El.6, b) 5% and 10% reductions respectively at El. 6 and El. 15, c) 5%, 10%, and 5% reductions at El.6, El. 15, and El. 19., and d) 5%, 10%, and 5% reductions at El.6, El. 15, and El. 17.

quired for successful damage identification on the planar truss using the NNLS was 4.4 eigenvalues, while l_1-norm optimization averaged 7.0 eigenvalues. Regarding the 3D truss, only 65% of the damage cases were identified using the basis pursuit within the specified range of 20 eigenvalues. The unidentified elements were omitted from Fig. 3.6c; hence the discontinuities of the dashed line. The results indicate that the NNLS outperforms the basis pursuit for both truss structures. The results of this simulation also indicate that the average minimum number of eigenvalues needed for unique identification increases with the size of the structural domain. The 3D truss
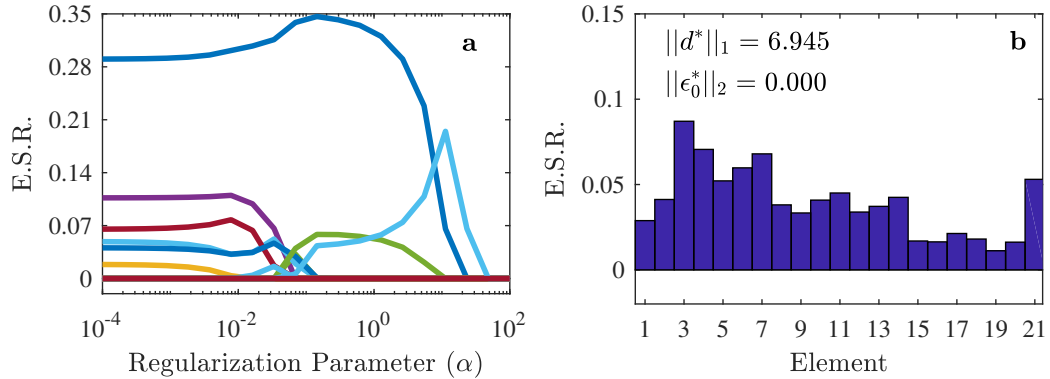
Figure 3.5: Estimated stiffness reduction (E.S.R.) using: a) basis pursuit denoising as a function of the regularization parameter, and b) the NNLS, for the case where the stiffness of the first 15 elements of the shear beam are reduced by 5%

required on average the most number of identified eigenvalues, 7.8 total, to properly identify a single damaged element using the NNLS.

The NNLS's success in recovering sparse solutions is correlated to a unique non-negative feasible set. In order to demonstrate this correlation, the minimum number of eigenvalues required to obtain a unique solution to the NNLS ($||d^*||_1 = 0$) is compared to the minimum eigenvalue recovery results for the NNLS. The results for the shear beam are shown in Fig. 3.7a, the planar truss in Fig. 3.7b, and the 3D truss in Fig. 3.7c. The minimum number of eigenvalues for uniqueness (dashed line) is never less than the minimum number of eigenvalues for sparse recovery (solid line). The intuition is that the singleton property of the non-negative constraint most often dictates the sparse recovery in the NNLS, but not always. Sometimes a sparse recovery can occur, although it may not necessarily be the only feasible solution as indicated in Fig. 3.7 where the dashed and solid points at a given element are not equal.

41
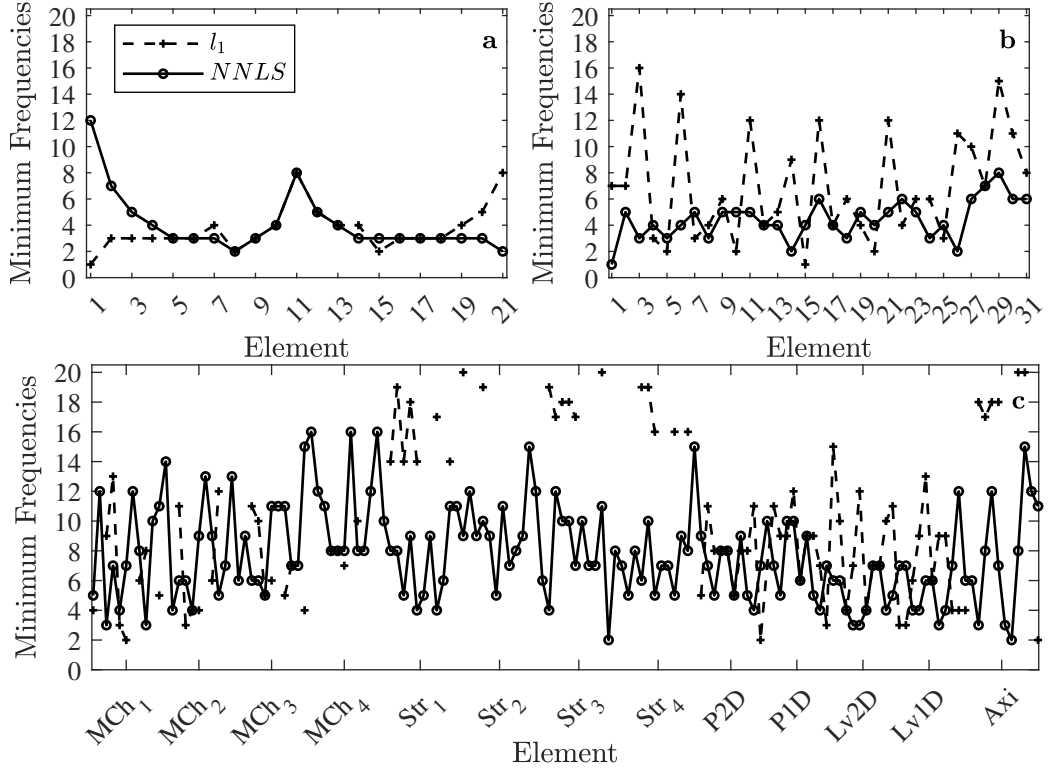
Figure 3.6: Minimum number of eigenvalues required to properly identify a 1% stiffness reduction at each element on a) the shear beam, b) the planar truss, and c) the 3D truss using the NNLS (solid) and the basis pursuit (dashed). The eigenvalues are selected lowest to highest until a proper identification is obtained or a maximum of 20 eigenvalues is reached. The basis pursuit only identified damage at 65% of the elements on the 3D truss

3.6 Nonlinear inverse problem

The linear model and method can be applied to small damage cases, but is insufficient to quantify and locate larger damages, where the linear truncation error is non-negligible. This section addresses the problem of substantial linear truncation errors due to large stiffness reductions. The objective is to solve the nonlinear system of equations defined in eq. 3.4 for θ, the parameters now representing the damaged structure, given λ, the associated eigenvalues of the damaged structure.
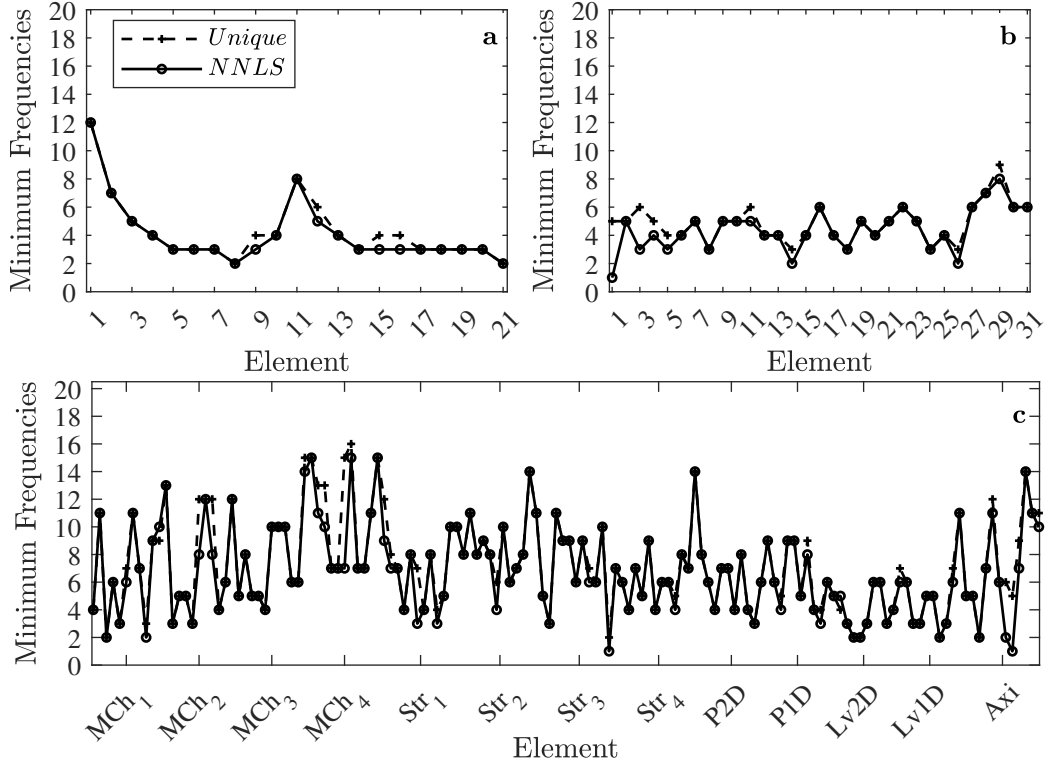
Figure 3.7: The minimum number of eigenvalues that satisfies the uniqueness condition $||d^*||_1 = 0$ (dashed), and the minimum number needed to successfully identify damage using the NNLS (solid), given a 1% stiffness reduction at any one element. Results shown for all elements comprising a) the shear beam, b) the planar truss, and c) the 3D truss

The inverse eigenvalue problem is typically formulated as an unconstrained nonlinear least squares (NLS) program:

$$\min_{\theta \in D(F)} \quad \frac{1}{2}||\mathcal{F}(\theta) - \lambda^\delta||_2^2 \tag{3.15}$$

where $\lambda^\delta = \lambda + \epsilon$, and ϵ represents the modelling, system identification error, and measurement noise. The preferred method to approximate the global minimum to the NLS is by iteratively solving a series of linear approximated least square type problems, typically referred to as finite element model updating. Without constraints,

FEM updating is a Gauss-Newton iterative method.

The Gauss-Newton method can be derived from first order conditions for a local minimum of the unconstrained NLS:

$$\mathbf{S}_{\theta*}^T(\mathcal{F}(\theta^*) - \lambda^\delta) = 0 \tag{3.16}$$

where $\mathcal{F}(\theta^*)$ and $\mathbf{S}_{\theta*}$ are respectively the nonlinear operator and the sensitivity matrix evaluated at the parameters satisfying local optimality. There are two primary concerns with the optimal conditions for a system having more nonlinear equations than unknowns. One, $\mathbf{S}_{\theta*}$ generally has full row rank for highly underdetermined problems, hence the null space of $\mathbf{S}_{\theta*}^T$ is empty. In order to satisfy the local optimum, $\mathcal{F}(\theta^*) = \lambda^\delta$, which implies that noise will be over-fit. Two, the optimal condition has more unknowns than equations; therefore there exists an infinite number of solutions that satisfy the local optimum.

3.6.1 NON-NEGATIVE NONLINEAR LEAST SQUARES

Like the linear inverse problem, only the feasible set that defines non-negative changes in the structure's parameters is of interest. Again, sparsity is not explicitly used as a constraint. The objective is not to approximate the global minimum to the unconstrained NLS, but instead approximate the minimum to the following constrained NLS:

$$\min_{\theta \in D(F)} \quad \frac{1}{2}||\mathcal{F}(\theta) - \lambda^\delta||_2^2$$
$$\Delta\theta = \theta_u - \theta \geq 0 \tag{3.17}$$

The first order optimality conditions for the non-negative NLS are defined as

$$\{\mathbf{S}_{\theta*}^{T}(\mathcal{F}(\theta^{*}) - \lambda^{\delta})\}_{i} = 0 \text{ if } \Delta\theta_{i}^{*} \geq 0$$
$$\{\mathbf{S}_{\theta*}^{T}(\mathcal{F}(\theta^{*}) - \lambda^{\delta})\}_{i} > 0 \text{ if } \Delta\theta_{i}^{*} = 0$$

(3.18)

for $i = 1...p$ [31]. Unlike the optimal conditions to the unconstrained NLS, the non-negative constraint can prevent over-fitting in the presence of noise.

In order to approximate local optimality to the non-negative NLS, a heuristic known as sequential convex programming (SCP) is applied. In the SCP method, a sequence θ_{k} is generated by setting

$$\theta_{k+1} = \theta_{k} + \Delta\theta_{k} \text{ for } k = 0, 1, 2...$$

(3.19)

where $\Delta\theta_{k}$ is the solution to a linearized convex sub-problem

$$\min_{\Delta\theta \in D(F)} \quad ||\mathbf{S}_{\theta_{k}}\Delta\theta_{k} - \Delta\lambda_{k}||_{2} + \alpha_{k}\Phi(\Delta\theta_{k})$$
$$\text{subject to} \quad f_{i}(\Delta\theta_{k}) \leq 0 \ i = 1, 2, 3...$$

(3.20)

$f_{i}(\Delta\theta_{k})$ are convex constraint equations often defining a trust region, $\alpha_{k} \in \Re$ is an iterated regularization parameter, and $\Phi : \Delta\theta \to \Re^{+} \cup 0$ is a proper convex penalty functional that can bound the step size and (or) impose known prior characteristics on the optimal solution. $\mathbf{S}_{\theta_{k}}$ is the sensitivity matrix evaluated at the updated parameter defined at the kth iteration, and $\Delta\lambda_{k} = \mathcal{F}(\theta_{k}) - \lambda^{\delta}$. For clarity, note that the index k is not the same as the degree of sparsity, k-sparse. SCP's can be related to the Gauss-Newton methods by manipulating the above constraints. For example, the classic Gauss-Newton method applies eq. 3.20 at each iteration with $\Phi(\Delta\theta_{k}) = 0$,

45

and the constraints removed. If $\Phi = ||.||_2$, then the routine is equivalent to the Levenberg-Marquardt method [7].

In this paper, the author proposes to solve the following convex sub-problem at each iteration:

$$\min_{\Delta\theta_k \in D(F)} \quad ||\mathbf{S}_{\theta_k}\Delta\theta_k - \Delta\lambda_k||_2$$

$$\theta_u - (\Delta\theta_k + \theta_k) \geq 0 \tag{3.21}$$

$$lb \leq \Delta\theta_k \leq ub$$

where $\theta_u - (\Delta\theta_k + \theta_k) \geq 0$ ensures that the final estimated change in parameters is non-negative, and $lb = ub = 0.05$ defines a lower and upper bound on the trust region for each step. For clarity, note that the first iteration solves the non-negative least squares problem with an upper bound, but any subsequent changes in the updated parameters do not have to be strictly non-negative.

The SCP is initialized at the parameter representing the undamaged structure, $\theta_u = \mathbf{1}$, a vector of ones, and its associated identified eigenvalues (λ_u). The iterations are terminated when the residual

$$||\mathcal{F}(\theta_k) - \mathcal{F}(\theta_{k+1})||_2 \leq c \tag{3.22}$$

becomes sufficiently small, where $c = 10^{-5}$ for this paper. The estimated changes in parameters due to damage are calculated as

$$\Delta\theta^* = \theta_u - \theta^* = \sum_{k=1} \Delta\theta_k^* \tag{3.23}$$

where θ^* are the parameters at the terminated iteration that are desired to match the true parameters of the damaged structure.

The graphic in Fig. 3.8 presents an example of a successfully implemented generic SCP process juxtaposed with the linear inverse problem. Beginning at the undamaged parameter (green marker), each local optimal solution $\Delta\theta_k^*$ moves the operator point one step closer to the damaged parameter (blue star) until convergence. In Fig. 3.8b, it is clear that without an updated solution, the damage magnitude approximated from the linear inverse problem is overestimated. Note that because SCP is a heuristic, like Newton type methods, it can fail to find the optimal or even a feasible point.
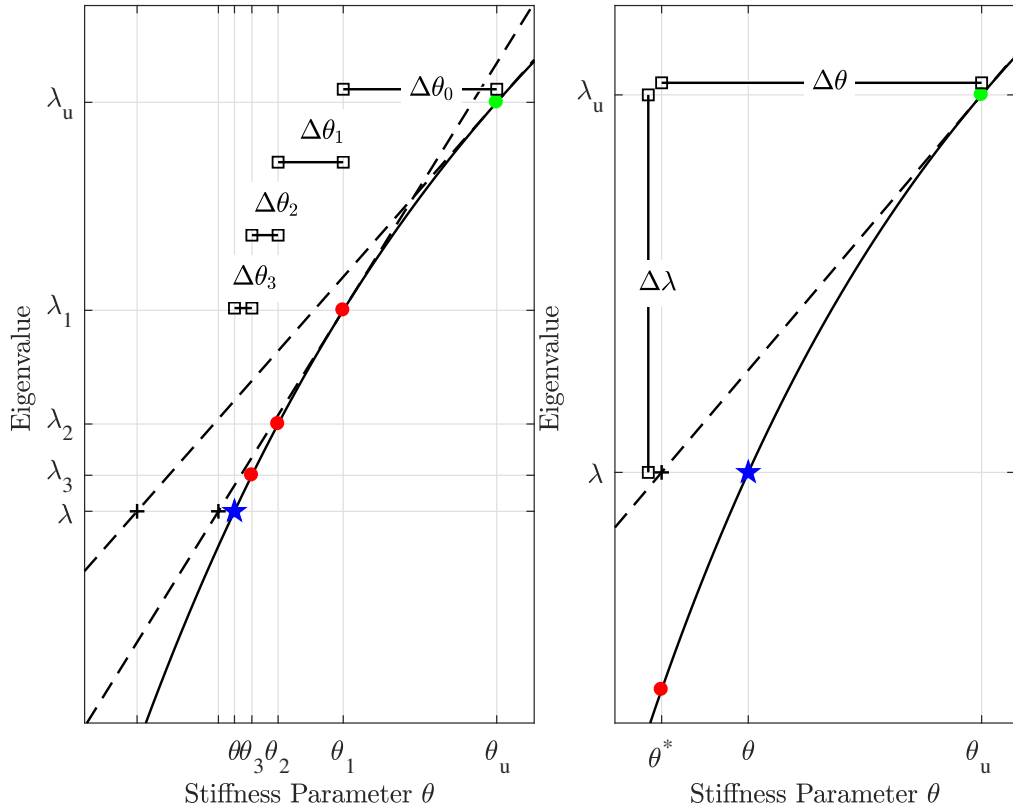
Figure 3.8: The nonlinear relationship (solid) and linearized relationship (dashed) between a given stiffness parameter and a given eigenvalue. a) The nonlinear method incrementally approaches the damage location, linearizing about the (red) operating points θ_k, and minimizing $\Delta\lambda_k$. b) The linear approximated inverse problem without iterations

3.7 VERIFICATION AND NUMERICAL SIMULATIONS

In this section, the efficacy of the proposed constrained NLS is verified. First, improvement over the linear NNLS is demonstrated. Consider the damage case where the stiffness at El.7 and El.8 of the shear beam are reduced by 85% and 50% respectively. Six eigenvalues are identified, which results in 6 nonlinear equations and 21 unknown parameters. The estimated stiffness reductions using the NNLS for the linear approximated problem are shown in Fig. 3.9a. The damages at El.7 and El.8 are greatly overestimated (nearly a 250% stiffness reduction at El.7), and the false indications of damage that occur at El.10 and El.18 are too large to distinguish from numerical error. In Fig. 3.9b, the final converged solution to the non-negative NLS is presented. The overestimation is corrected, and the false positives are completely removed. For visualization, Fig. 3.9c presents the estimated stiffness reduction of the constrained NLS at each iteration. The solution converges after 24 iterations. Note that the uniqueness measure calculated for the NNLS indicates a singleton set. Although the solution to the linear approximated NNLS incorrectly represents the damage, the uniqueness measure implies that the best fit feasible solution to the linear problem is unique. Perhaps the uniqueness measure could be used as a guide to determine the uniqueness of the solution to the nonlinear method, however the authors have not rigorously verified this.

The proposed non-negative constrained NLS is also verified on the 3D truss. In this example, the elastic modulus of the plane 2 diagonal (P2D) element in bay 9 is

48
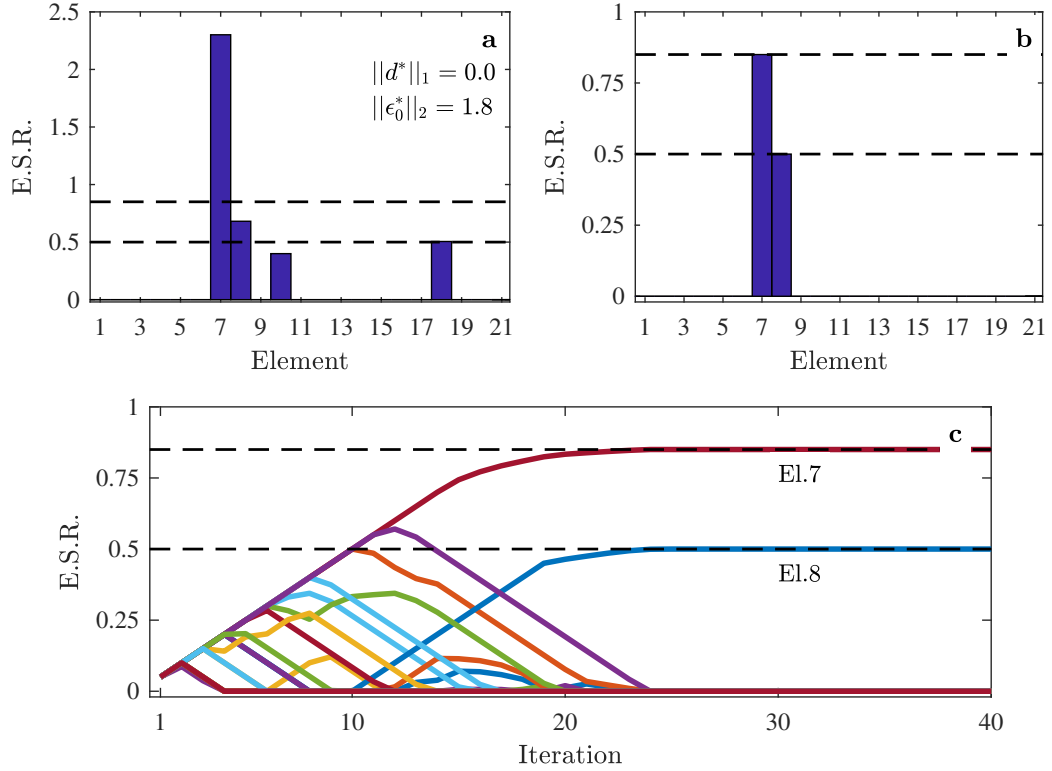
Figure 3.9: Given 85% and 50% stiffness reductions at El.7 and El.8 of the shear beam, a) the estimated stiffness reduction (E.S.R.) to the non-negative least squares applied to the linearized inverse problem, b) the final estimated stiffness reduction to the non-negative nonlinear least squares (NLS), and c) the estimated stiffness reduction at each iteration for the non-negative NLS

reduced by 30%, and the diagonal at level 1 (Lv1D) in bay 5 is reduced by 70%. 10 natural frequencies are identified resulting in an inverse problem with 10 equations and 144 unknowns. Fig. 3.10a presents the estimated stiffness reduction using the NNLS. The true damage locations are superimposed over the model using a thick green line, and any significant damages predicted by the algorithm are superimposed in the color red. Note that a correct identification is indicated by a green line highlighted in red. Based on Fig. 3.10a, the correct damage locations are contained in the non-zero subset of the optimal solution to the NNLS, however the results indicate a significant

false positive at one of the struts in bay 3. Fig. 3.10b presents the converged solution to the proposed non-negative constrained NLS. The method correctly quantifies and locates both of the damaged elements.
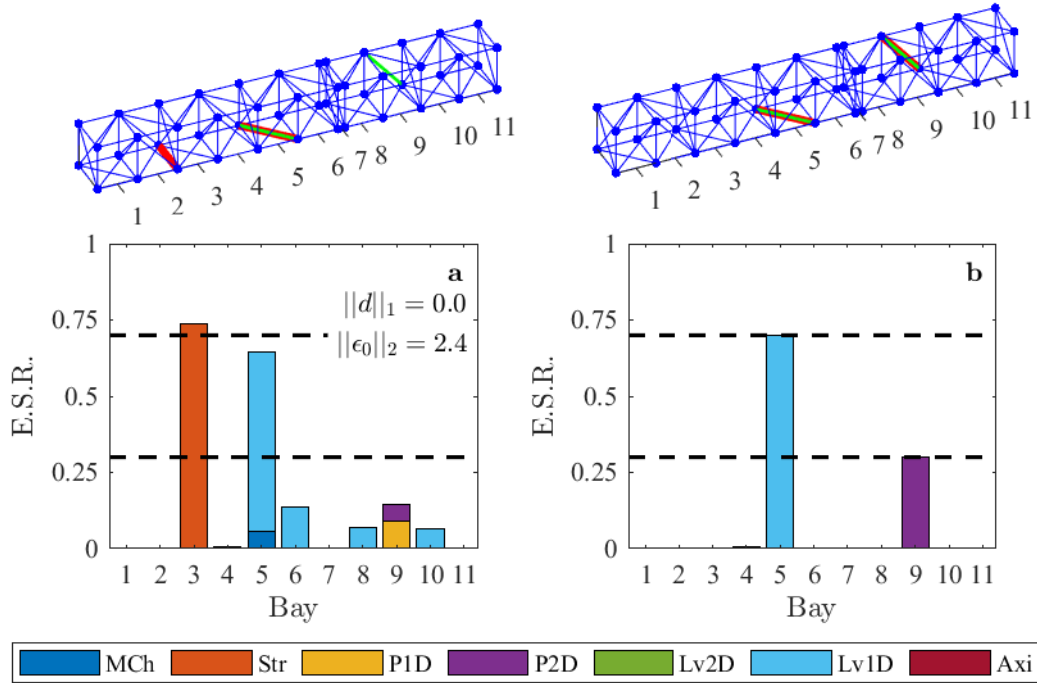
Figure 3.10: Estimated stiffness reduction using a) the non-negative least squares, and b) the non-negative nonlinear least squares for a 70% stiffness reduction at Lv1D bay 5 and a 30% stiffness reduction at P2D bay 9 on the 3D truss

3.7.1 MEASUREMENT ERROR INVESTIGATION

This section investigates the effect of measurement noise on the proposed methodology. The measurement error contained in ϵ is defined as a realization of a p-dimensional Gaussian random vector with zero mean and standard deviation of component ϵ_i proportional to the specified coefficient of variation. The vector of noise is

added to eigenvalues of the damaged structure.

The noise simulations are first considered for the planar truss. The damage cases simulated in [4] are replicated. The damage scenario is defined by 10% axial stiffness reductions at El.18, El.19, and El.22, and a 15% stiffness reduction at El.20. The number of possible damage locations is 31 rendering $\mathbf{S} \in \Re^{mx31}$. Without measurement noise the exact location and magnitude of the damage is determined using the proposed methodology when nine (or more) eigenvalues are identified. The results of the method with eight and nine identified eigenvalues are presented in Fig. 3.11. Note that the uniqueness measure applied to the linear approximated NNLS is significantly smaller with nine identified eigenvalues than with eight. Furthermore, at eight eigenvalues, the NNLS overestimates the truncation error as indicated by $||\epsilon^*||_2 = 0$. Again linear truncation error is large, and one cannot infer that the uniqueness measure indicates anything about the quality of the final solution to the nonlinear method.
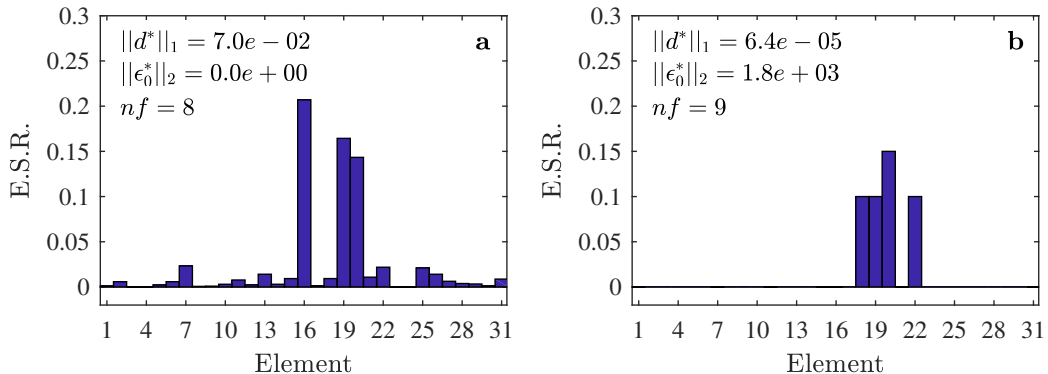
Figure 3.11: Estimated stiffness reduction (E.S.R.) using the non-negative nonlinear least squares given 10% stiffness reductions at El.18, El.19, and El.22, and a 15% stiffness reduction at El.20 on the planar truss. Results based on a) eight identified eigenvalues and b) nine eigenvalues

Four tests with coefficients of variation (CoV) equal to 0.0005, 0.001, 0.0015, and

0.002 were performed. The range of values selected for the CoV were obtained from uncertainty quantification studies on system identification of real structures [34]. The non-negative NLS was performed using $1,000$ realizations of ϵ with the specified CoV for each test totaling four thousand simulations. Results for the proposed method using nine identified eigenvalues are presented in Fig. 3.12. The results are compiled into box plots, where the central hash denotes the median, and the bottom and top edges of the box denote the 25th, and 75th percentiles. The whiskers extend to the most extreme data points not considered outliers. An outlier is at least 1.5 times greater than the edges of the box. For all noise cases, the damage locations are all identified with varying degrees of accuracy. It is unclear that the magnitude of damage at El.20 is larger than the other identified damage locations. The margin of error about the estimated stiffness reduction and the number of false positive outliers increase with increased level of noise. In all cases, El.15 and El.16 are falsely identified. The large range between the 25th and 75th percentile about El.15 and El.16 indicate a significant level of uncertainty.

Now consider the same damage locations and same CoV, except with increased stiffness reductions. The damage scenario is represented by 30% axial stiffness reductions at El.18, El.19, and El.22, and a 45% stiffness reduction at El.20. Fig. 3.13 presents the results in box plots using nine eigenvalues. It is now possible to observe the damage location and magnitude more clearly due to the decreased ratio between the noise and change in eigenvalues. The margin of estimation error about the locations is tighter than the previous damage scenario. It is apparent in this example that El.20 is more severely damaged. The false positives at El.15 and El.16 still remain, again showing significant levels of uncertainty. It is worth noting that these false pos-

itives are detected in elements which are close to the actual damage elements, which from a practical point of view is not as detrimental as cases where false positives are completely disconnected from the true positives.
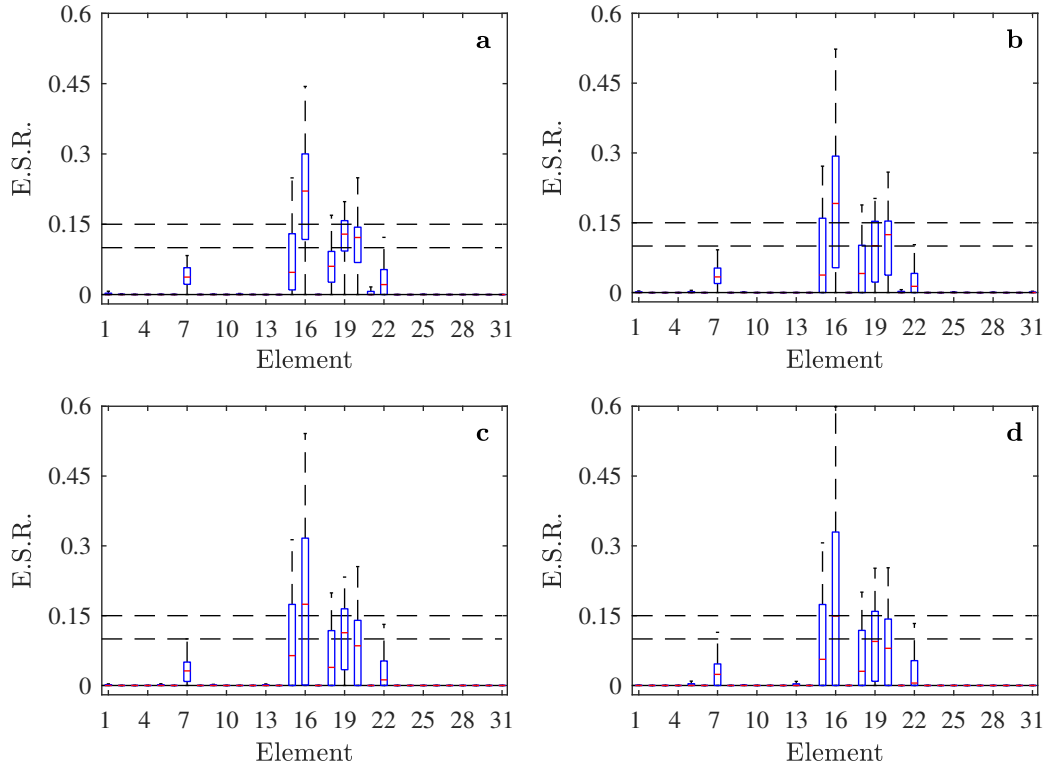
Figure 3.12: Estimated stiffness reduction (E.S.R.) using non-negative nonlinear least squares given 10% stiffness reductions at El.18, El.19, El.22, and a 15% reduction at El.20 on the planar truss using nine eigenvalues corrupted by Gaussian white noise with coefficients of variation of a) 0.0005, b) 0.001, c) 0.0015, and d) 0.002

In this final simulation, the investigation into measurement error is extended to the 3D truss. The same damage case presented in Fig. 3.10, that is 70% and 30% stiffness reductions respectively at Lv1D bay 5 and P2D bay 9, are tested in the presence of measurement error. Fig. 3.14 presents the results for the non-negative constrained NLS using 10 eigenvalues containing measurement noise. The coefficient of variation of the random noise vector corresponding to Fig. 3.14a is 0.0005, and
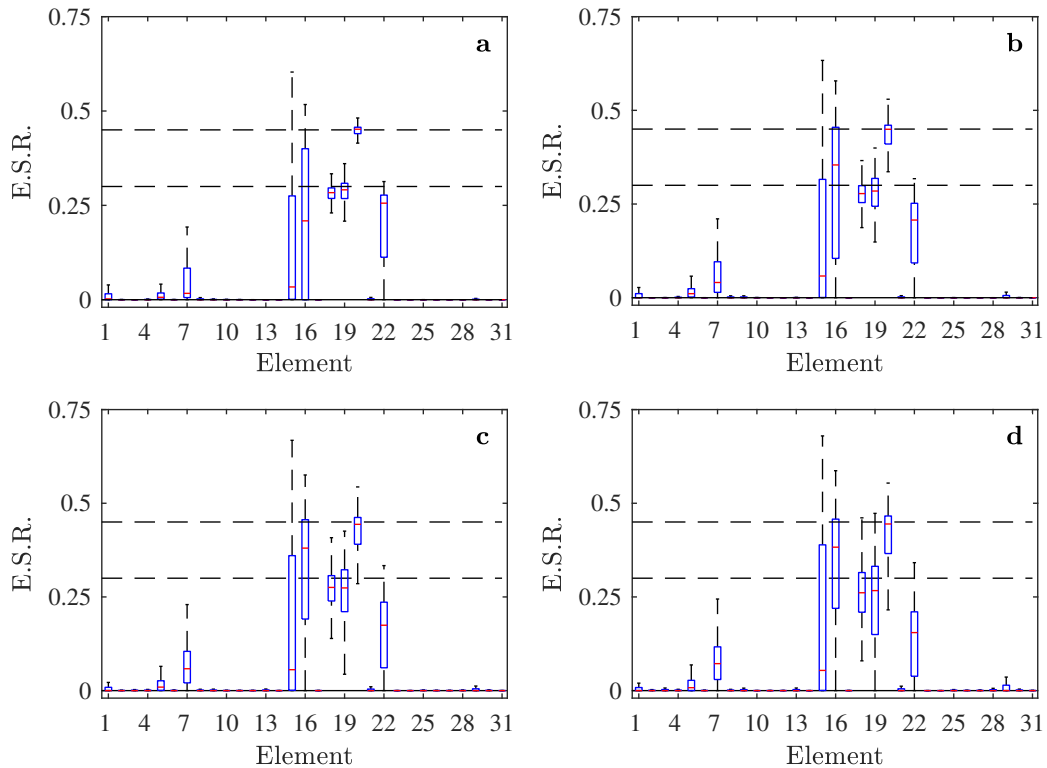
Figure 3.13: Estimated stiffness reduction (E.S.R.) using the non-negative nonlinear least squares given 30% stiffness reductions at El.18, El.19, El.22, and a 45% reduction at El.20 on the planar truss using nine eigenvalues corrupted by Gaussian white noise with coefficients of variation of a) 0.0005, b) 0.001, c) 0.0015, and d) 0.002

Fig. 3.14b is 0.002. Those values correspond to the minimum and maximum coefficients of variation previously tested on the planar truss. The solution to each of the 1000 realizations are presented in box plots. For the tested noise levels, the two groups of elements that dominate the solution are the struts (shown in blue) and the level 1 diagonals (shown in red). The locations of the dominant estimated stiffness reductions are superimposed over the structure as red lines (dominant implying a median estimated stiffness reduction of at least 10%). In the presence of measurement error, large false positive occur at the bay 4 strut and the bay 9 strut. The significant spread between the 25th and 75th percentiles at the struts occurs because the solution

54

tends to alternate back and forth predicting damage at the bay 5 or bay 9 struts, but very rarely at both locations simultaneously. The relatively small stiffness reduction at P2D bay 9 is missed by the algorithm. Despite the large false positives and the missed identification, the most significant damage at bay 5 is apparent among the noise even for CoV = 0.002. The correctly identified damaged element also has a tighter bound on its variance than its neighboring false positives. A tighter variance at the correctly identified damaged element relative to the large spread at the spurious damage locations is a reoccurring feature of the proposed method substantiated by both the planar and 3D trusses.

3.8 CONCLUSION

Inverse eigenvalue problems are typically ill-posed. This fact has hindered the use of eigenvalue shifts to detect local damages using standard finite element model updating methods. This paper presents an exception. If it is physically reasonable to constrain the solution set to only contain non-negative vectors and the solution is sparse then the inverse problem can become well-posed, and physically meaningful solutions to finite element model updating can be obtained. This situation occurs when damage is spatially localized and strictly reduces the stiffness. Part one of this paper presents theoretical evidence that justifies the use of the non-negative constrained least squares method to induce unique solutions to the underdetermined system of linearized eigenvalue equations. In order to check if the solution is unique, a means of measuring the uniqueness of the feasible solution set is presented. Numerically simulated damages performed on three structures, namely a shear beam, a planar truss, and a three-
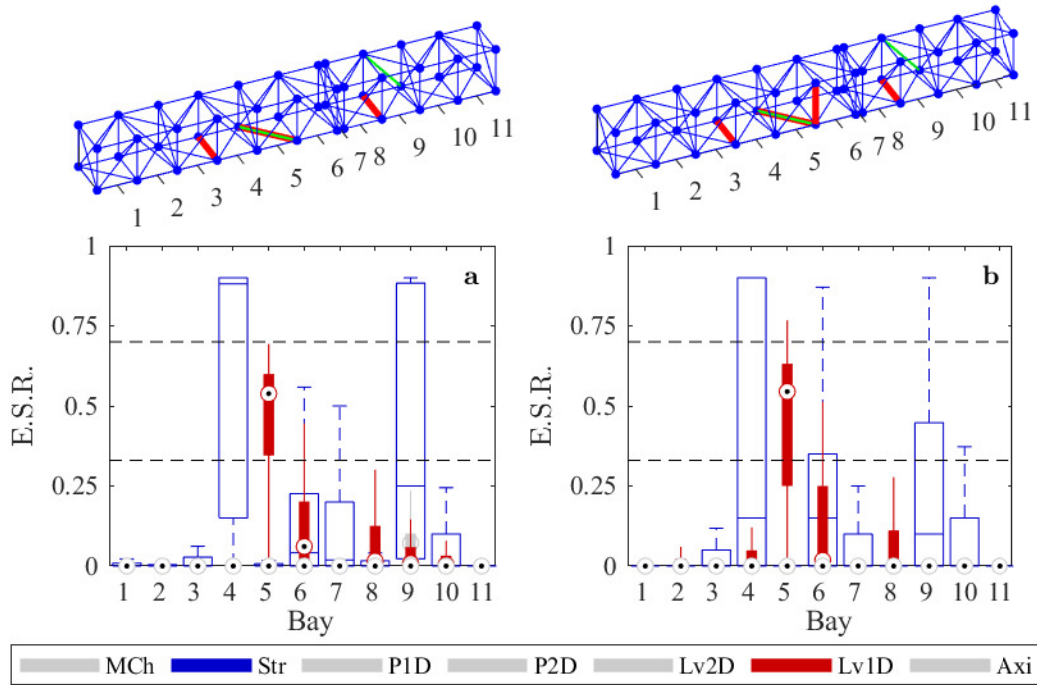
Figure 3.14: Estimated stiffness reduction (E.S.R.) using the non-negative nonlinear least squares for a 70% stiffness reduction at the level 1 diagonal (Lv1D) at bay 5 and a 30% stiffness reduction at the plane 2 diagonal (P2D) at bay 9 on the 3D truss using 10 eigenvalues corrupted by Gaussian white noise with coefficients of variation of a) 0.0005 and b) 0.002

dimensional truss, support the hypothesis. The non-negative least squares is shown to perform as well or better than the l_1-norm sparse recovery methods.

Part two adapts the non-negative constraint to the nonlinear inverse eigenvalue problem associated with large magnitude damages. A constrained FEM updating approach is constructed in order to solve the nonlinear least squares problem where the solution space represents only reductions in stiffness. The proposed non-negative nonlinear least squares accurately recovers the sparse non-negative vectors that best represents large magnitude damages. The proposed method is shown to perform

adequately in the presence of measurement noise, with the exception that small magnitude damages are disguised by noise. The authors expect that future work on the subject will focus on the effect of modelling errors (bias) on the proposed methodology and on quantifying the uncertainty in the damage estimates.

Acknowledgements

Bibliography

[1] K. Worden, C. Farrar, G. Manson, G. Park, The fundamental axioms of structural health monitoring, Proc. R. Soc. A, 463 (2007) 1639-1664.

[2] E. Görl, M. Link, Damage identification using changes of eigenfrequencies and mode shapes, J. Mech. Syst. Signal Pr. 17(1)(2003) 103-110.

[3] C. Farrar, K. Worden, Structural health monitoring: a machine learning perspective, Wiley, 2012.

[4] X.Y. Li, S.S. Law, Adaptive Tikhonov regularization for damage detection based on nonlinear model updating, J. Mech. Syst. Signal Pr. 24(6)(2010) 1646-1664.

[5] B. Titurus, M.I. Friswell, Regularization in model updating, International Journal for Numerical Methods in Engineering, 75(4)(2008) 440-478.

[6] B. Weber, P. Paultre, J. Proulx, Consistent regularization of nonlinear model updating for damage identification, J. Mech. Syst. Signal Pr. 23(6)(2009) 1965-1985.

[7] B. Kaltenbacher, Some Newton-type methods for the regularization of nonlinear ill-posed problems, Inverse Probl. 13(1997) 729-753.

[8] N. Grip, N. Sabourova, Y. Tu, Sensitivity-based model updating for structural damage identification using total variation regularization, J. Mech. Syst. Signal Pr. 84(A)(2017) 365-383.

[9] H. Sohn, C. Farrar, F. Hemez, D. Shunk, A Review of Structural Health Monitoring Literature: 1996-2001, Los Alamos National Laboratory Report, LA-13976-MS, 2003.

[10] M. Döhler, X-B. Lam, L. Mevel, Uncertainty quantification for modal parameters from stochastic subspace identification on multi-setup measurements, J. Mech. Syst. Signal Pr. 36(2)(2013) 562-581.

[11] S. Doebling, C. Farrar, Estimation of statistical distributions for modal parameters identified from averaged frequency response function data, Journal of Vibration and Control, 7(4)(2001) 603-624.

[12] C. Farrar, D. Jauregui, Damage detection algorithms applied to experimental and numerical modal data From the I-40 bridge, Los Alamos National Laboratory Report LA-13074-MS, Los Alamos, NM (1996).

[13] J.E. Mottershead, M. Link, M. Friswell, The sensitivity method in finite element model updating: a tutorial, J. Mech. Syst. Signal Pr. 25(7)(2011) 2275-2296.

[14] E. Candes, J. Romberg, Sparsity and incoherence in compressive sampling, Inverse Probl. 23(1)(2007) 969-985.

[15] D. Donoho, M. Elad, Optimally sparse representation in general (nonorthogonal) dictionaries via l1 minimization, Proc. Natl. Acad. Sci. 100(2003) 2197-2202.

[16] J. Tropp, Greed is good: algorithmic results for sparse approximation, I.E.E.E. Trans. Inf. Theory. 50(10)(2004) 2231-2242.

[17] M. Kaouk, D.C. Zimmerman, Structural damage assessment using a generalized minimum rank perturbation theory, A.I.A.A. J. 32(4)(1994) 836-842.

[18] S. Zhou, Y. Bao, H. Li, Structural damage identification based on substructure sensitivity and l1 sparse regularization, Proceedings of the SPIE 8692 Sensors and Smart Structures Technologies for Civil, Mechanical and Aerospace Systems (2013).

[19] E.M. Hernandez, Identification of isolated structural damage from incomplete spectrum information using l1-norm minimization, J. Mech. Syst. Signal Pr. 46(1)(2014) 59-69.

[20] M. Link, J. Ryan, D.C. Zimmerman, Structural damage diagnosis using frequency response functions and orthogonal matching pursuit: theoretical development. Struct. Control Health Monit. 22(2015) 889-902.

[21] X.Q. Zhou, X. Yong, S. Weng, L1 regularization approach to structural damage detection using frequency data, J. Struct. Health Monit. 14(6)(2015) 571-582.

[22] E.M. Hernandez, Identification of localized structural damage from highly incomplete modal information: theory and experiments. J. Eng. Mech. A.S.C.E. 142(2)(2016).

[23] C.B. Smith, E.M. Hernandez, Detection of spatially sparse damage using impulse response sensitivity and LASSO regularization, Inverse Problems in Science and Engineering 27(1)(2018) 1-16.

[24] D. Donoho. J. Tanner, Sparse nonnegative solution of underdetermined linear equations by linear programming. Proc. Natl. Acad. Sci. 102(27)(2005) 9446-9451.

[25] A. Bruckstein, M. Elad, M. Zibulevsky, On the uniqueness of non-negative sparse solutions to underdetermined systems of equations, I.E.E.E. Trans. Inf. Theory, 54(11)(2008) 4813-4820.

[26] K. Dillon, Y.P. Wang, Imposing uniqueness to achieve sparsity, Signal Processing, 123(2016) 1-8.

[27] G. Yan, S. J. Dyke, A. Irfanoglu, Experimental validation of a damage detection approach on a full-scale highway sign support truss, Mech. Syst. Signal Pr. 28(2012) 195-211.

[28] M. Wang, W. Xu, A. Tang, Conditions for a unique non-negative solution to an underdetermined system: from vectors to matrices, I.E.E.E. Trans. Signal Process., 59(3)(2011) 1007-1016.

[29] R. Fox, M. Kapoor, Rates of change of eigenvalues and eigenvectors, AIAA J. 6 (12)(1968) 2426-2429.

[30] S. Boyd, L. Vandenberghe, Convex Optimization, Cambridge University Press, 2009.

[31] C. Vogel, Computational Methods for Inverse Problems, S.I.A.M., 2002.

[32] H.W. Engl, M. Hanke, A. Neubauer, Regularization of Inverse Problems, Kluwer Academic Publishers, The Netherlands, 2000.

[33] M. Grant, S. Boyd, CVX: Matlab software for disciplined convex programming, version 2.0 beta, http://cvxr.com/cvx, (2013).

[34] E. Reynders, R. Pintelon, G. De Roeck, Uncertainty bounds on modal parameters from stochastic subspace identification, Mech. Syst. Signal Process. 22(4) (2008) 948-969.

Chapter 4

Identifying Local Reductions to Mass and Stiffness with Incomplete Modal Information, Sparsity, and Non-negative Constraints

Abstract

l_1-norm regularized inverse methods have been suggested as a means to quantify and localize spatially sparse damage from a set of identified natural frequencies. Thus far, damage has been interpreted as changes in stiffness without any appreciable associated changes in mass. In seeking to generalize l_1-norm based inverse methods

61

to encompass damage that produces significant changes in both mass and stiffness, this paper finds that sparsity is too weak a prior to uniquely solve the associated underdetermined inverse problem. However, when damage is defined by local reductions to stiffness and mass then the addition of a non-negative constraint when combined with sparsity can yield physically meaningful solutions. This work proposes a two-step model updating method to obtain sparse and non-negative solutions. The findings and proposed method are verified using two numerical models: a shear beam and a four-level plane frame. The proposed methodology is experimentally validated using vibration data taken from a four-level bolted steel frame subjected to multiple damage scenarios.

4.1 INTRODUCTION

Sparse vector recovery algorithms based on l_1-norm optimization have been suggested as a means to solve the inverse eigenvalue problem (IEP) for the purposes of quantifying and locating local structural damage [1, 2]. The IEP seeks to determine the parameters defining the stiffness and mass matrices such that the associated eigenvalue problem has the eigenvalues identified from the global vibrations [3,4]. Although the number of identifiable natural frequencies is typically insufficient to determine a unique solution to the general IEP [5–7], it was found that if the sought damage only affects a small subset of stiffness parameters then the IEP can be solved uniquely with sparse vector recovery. In many damage cases it is reasonable to consider stiffness only and neglect changes in mass, but in certain situations both mass and stiffness parameters may need to be identified. This paper investigates the unanswered ques-

tion of whether sparsity is a strong enough prior to uniquely determine both changes in mass and stiffness from a subset of natural frequencies.

Sparsity can be a desirable solution characteristic whenever damage is expected to be localized in small regions of the structural domain. Recently, methods that target sparse solutions have been mathematically formalized based on the concept of minimizing the number of nonzero elements of the possible solution [8,9]. However, operators that count nonzero elements are non-convex and hence a combinatorial search algorithm is needed to solve the problem. The l_1-norm has been suggested as a relaxed surrogate to counting nonzero elements because the function is geometrically similar to the nonzero counting operator, yet is conveniently convex [8,10]. Implementation of the l_1-norm in combination with traditional least squares tends to produce sparse solutions [10] and in some cases even produce the unique solution with the least nonzero elements for underdetermined systems of linear equations [8,11].

Application of sparse recovery methods can also be found in the structural health monitoring (SHM) literature, specifically combined with the inverse approach to damage identification as described in [12,13]. Hernandez proposed l_1-norm optimization to quantify and locate small changes in stiffness from natural frequencies [1], and validated the method on a cantilever beam [14]. The authors in [2] presented a nonlinear l_1-norm regularized least squares approach to the IEP. The application of sparse vector recovery has been extended to other damage features as well such as: the combination of natural frequencies and mode shapes using l_1-norm regularization [15,16] or using total variation regularization [17], frequency response functions using orthogonal matching pursuit [18], the time domain impulse response using l_1-norm regularization [19], and methods using measured response signals [20].

Another convex constraint that induces sparse solutions is non-negativity. Non-negativity is particularly appropriate for the purposes of damage identification given that damage tends to strictly reduce the local stiffness and/or mass of a damaged element [21]. Non-negativity and sparsity are not only physically inherent to the damage identification solution space, but can have complementary effects in regards to solving underdetermined inverse problems. If the solution is sparse enough and the structure of the inverse problem satisfies certain conditions, the non-negative constraint can recover the sparsest solution to an underdetermined system of algebraic equations [22, 23]. In SHM, Hassiotis and Jeong were the first to show that the damage identification IEP could be solved using just non-negative constraints [24]. Later Smith and Hernandez proposed a similar method and found that the damage identification IEP satisfies the characteristics needed for unique sparse recovery. Other methods have also suggested the application of non-negative constraints for damage identification [25, 26].

Among the mentioned inverse-based damage identification methods none have considered the more general case of identifying both the mass and stiffness parameters. The problem is of particular importance to the IEP since damage that reduces both stiffness and mass inversely affect the natural frequencies and further inhibit the existence of a unique solution. In this paper, the authors suggest that sparsity may be too weak a prior to quantify and locate changes in mass and stiffness simultaneously, but if the non-negative constraint is also imposed then the probability of unique identification significantly improves.

The objective of this paper is to investigate this claim by testing the performance of the most popular $l1$-norm based inverse methods in identifying changes to stiffness

and mass parameters on two numerical models: a uniform stiffness shear beam and a four-level frame. In addition, this paper proposes a two-step model updating method which combines the non-negative constraint and l_1-norm optimization to resolve the non-uniqueness issue. In step one, the nonlinear mapping is linearized and a non-negative constrained l_1-norm optimization program is used to solve the system of linear equations. In step two, the parameters associated with the nonzero elements of the sparse solution from step one are updated. The proposed method is verified on the numerical simulations and experimentally validated using vibration data measured from a one meter tall bolted steel frame. Each tested damage case is conducted by removing bolted connections; the intention being to significantly reduce both mass and stiffness.

The outline of the paper is as follows. The following section develops the inverse eigenvalue problem using the sensitivity method in structural dynamics. The method of approach section then details the l_1-norm optimization methods investigated, and the proposed non-negative and sparsity-based inverse approach. The methods are then investigated on the shear beam in the numerical verification section. Afterwards the experimental validation is detailed along with the challenges associated with non-unique solutions. The results of the frame experiment and the frame numerical simulations are summarized, followed by concluding remarks.

4.2 SENSITIVITY-BASED INVERSE METHOD

The sensitivity-based inverse approach to damage identification seeks to update a parameterized model such that the difference between the identified modal features from

65

the potentially damaged structure and those predicted by the model are minimized. In this paper, the feature residual is defined by the following system of algebraic equations

$$r_j(\theta) = \hat{\lambda}_j - \lambda_j(\theta) \ , \ j = 1, \cdots, q \tag{4.1}$$

where $\hat{\lambda}_j \in \Re$ is the jth eigenvalue identified from the physical system. $\lambda_j(\theta)$ is its matched j^{th} eigenvalue derived from the model using the undamped eigenvalue equation,

$$\mathbf{K}\phi_j = \mathbf{M}\phi_j\lambda_j \tag{4.2}$$

where $\phi_j \in \Re^n$ is the eigenvector corresponding to the jth eigenvalue. In practice, the total number of identified eigenvalues q is typically far less than the number of degrees of freedom n.

This paper is restricted to cases where the mass matrix $\mathbf{M} = \mathbf{M}^T \in \Re^{nxn}$ and the stiffness matrix $\mathbf{K} = \mathbf{K}^T \in \Re^{nxn}$ can be written as a linear combination of the updating parameters, that is

$$\begin{aligned}
\mathbf{K} &= \mathbf{K}_0 - \sum_{i=1}^{p_k} \mathbf{K}_i \delta k_i \\
\mathbf{M} &= \mathbf{M}_0 - \sum_{i=1}^{p_m} \mathbf{M}_i \delta m_i
\end{aligned} \tag{4.3}$$

where $\delta k_i \in \Re$ is the ith parameter contributing to the stiffness matrix, $\delta m_i \in \Re$ is the ith parameter contributing to the mass matrix, and $\mathbf{K}_i$ and $\mathbf{M}_i$ are respectively the stiffness and mass elementary influence matrices. $\mathbf{K}_0$ and $\mathbf{M}_0$ are the stiffness and mass matrices of the initial reference structure. Let $\theta \in \Re^p$ define the concatenated stiffness and mass parameters ($\theta = [\delta k \in \Re^{p_k}, \delta m \in \Re^{p_m}]$) where $p = p_k + p_m$. The

linear decomposition is valid when the physical changes to the damaged system affect material properties such as elastic modulus, shear modulus, cross-sectional area, and other linear multipliers of stiffness or mass.

Since the residual $r(\theta)$ lacks a closed form and is nonlinear, estimating θ requires iteratively solving a linearized form of eq. 4.1 until convergence. From the sensitivity approach in structural dynamics [27], the residual when approximated by a first order Taylor series expansion about a point $\theta_0 \in \Re^p$ results in the following linear relationship

$$r_j(\theta) \approx r_j(\theta_0) + \mathbf{S}(\theta_0)(\theta - \theta_0) \tag{4.4}$$

where $\mathbf{S} \in \Re^{qxp}$ is the sensitivity matrix and a function of θ. The θ notation is dropped for convenience.

In order to determine damage relative to a healthy baseline, updating is initialized at $\theta_0 = \mathbf{0}$. Rewriting eq. 4.4 and evaluating at $\theta_0 = \mathbf{0}$ gives the sensitivity equation, that is

$$\mathbf{S}\theta = \Delta\hat{\lambda} + \epsilon \tag{4.5}$$

where the jth component $\Delta\hat{\lambda}_j = \hat{\lambda}_j - \lambda_j(\theta_0)$, and ϵ comprises the truncation error and any measurement noise or system identification error that may exist. Note for clarity that $\theta > 0$ indicates a reduction in the stiffness or mass from the reference structure.

In this paper, the number of identifiable eigenvalues is always less than the total number of stiffness and mass parameters $(q < p)$ rendering eq. 4.5 an underdetermined system of linear equations.

4.2.1 SENSITIVITY MATRIX

The columns of the sensitivity matrix associated with the stiffness parameters are always negative, while columns associated with the mass parameters are always positive. This can be deduced from the definition of the sensitivity matrix. From the rate of change of the eigenvalues [28], the sensitivity matrix is

$$\mathbf{S}_{j,i} = \frac{\partial \lambda_j}{\partial \theta_i} = \phi_j^T \left(\frac{\partial \mathbf{K}}{\partial \theta_i} - \lambda_j \frac{\partial \mathbf{M}}{\partial \theta_i} \right) \phi_j \qquad (4.6)$$

where $i = 1, \cdots, p$. Combining eq. 4.3 and eq. 4.6 and treating δm and δk as independent variables gives

$$\mathbf{S}_{j,i} = [-\phi_j^T \mathbf{K}_i \phi_j \ , \ \lambda_j \phi_j^T \mathbf{M}_i \phi_j] \qquad (4.7)$$

This paper uses the terms stiffness sensitivity matrix to refer to $-\phi_j^T \mathbf{K}_i \phi_j$ and mass sensitivity matrix to refer to $\lambda_j \phi_j^T \mathbf{M}_i \phi_j$.

The stiffness and mass influence matrices represent stiffness and mass matrices of substructures, and hence must abide the positive semi-definite condition. By definition of a positive semi-definite matrix $-\phi_j^T \mathbf{K}_i \phi_j \leq 0$ and $\lambda_j \phi_j^T \mathbf{M}_i \phi_j \geq 0$ for all j and i since the eigenvalues are always non-negative. The monotonic property is physically validated by the observation that a reduction in stiffness always reduces the natural frequencies of the structure while a reduction in mass always increases the frequencies.

4.3 Method of approach

4.3.1 l_1-norm optimization methods

The intuition behind sparse vector recovery is to minimize the number of nonzero elements of the solution while finding a satisfactory fit to the system of equations. The l_1-norm has been suggested as a relaxed convex surrogate to counting nonzero elements and is among the most popular sparse recovery methods. This paper investigates three closely related l_1-norm optimization programs that have been applied in related damage identification research.

In the case where the changes in parameters due to damage are small such that the truncation error is negligible, the linear sensitivity equation eq. 4.5 is a satisfactory model. The underdetermined linear inverse problem can be solved for a sparse solution using the following convex optimization program known as the basis pursuit denoising,

$$
\begin{aligned}
\min_{\theta} \quad & ||\theta||_1 \\
\text{s.t.} \quad & ||\mathbf{S}\theta - (\Delta\hat{\lambda} + \epsilon)||_2 \leq \alpha
\end{aligned}
\tag{4.8}
$$

where $\{\alpha \in \Re \mid \alpha \geq 0\}$ is the regularization parameter; a predefined scalar acting as a weight between the solution fit measured by the Euclidean norm ($||.||_2$) and sparsity in terms of the vector l_1-norm ($||.||_1$). As $\alpha \rightarrow ||\Delta\hat{\lambda} + \epsilon||_2$, one obtains the sparsest solution, i.e. the solution with the fewest nonzero elements, $\theta^* = \mathbf{0}$. As $\alpha \rightarrow 0$, one most often obtains a vector comprised of at most q nonzero elements provided $\mathbf{S}$ has full row rank [29]. Again q is the number of rows of the sensitivity matrix.

Taking $\alpha = 0$, the optimization program is equivalent to the basis pursuit, the

second l_1-norm based method investigated in this paper. Replacing the least squares term with an affine constraint, the basis pursuit is written as

$$\min_{\theta} \quad ||\theta||_1$$
$$\text{s.t.} \quad \mathbf{S}\theta = \Delta\hat{\lambda} + \epsilon \tag{4.9}$$

In cases where the damage magnitude is large enough such that the linear truncation error in eq. 4.5 is non-negligible, a nonlinear approach to the problem is needed. This paper briefly compares the proposed method to the nonlinear LASSO. The nonlinear LASSO directly minimizes the following nonlinear optimization program using an iterative nonlinear solver,

$$\min_{\theta} \quad ||r(\theta)||_2 + \alpha||\theta||_1 \tag{4.10}$$

where again α is a regularization parameter defining the trade off between solution fit and solution sparsity.

4.3.2 PROPOSED INVERSE METHOD FOR NON-NEGATIVE SPARSE VECTOR RECOVERY

This paper suggests that the non-negative constraint is a necessary condition to quantify and locate damage in terms of stiffness and mass. By constraining the solution space to the non-negative orthant, not only is the expected physical damage properties imposed, but the structure of the sensitivity matrix leveraged such that the inverse problem provides physically meaningful results. Since the stiffness sensitiv-

ity matrix is always negative, and the mass sensitivity matrix always positive, the non-negative constraint forces the solution of the inverse problem to compensate any eigenvalue increase from the undamaged to damaged structure with a reduction in mass as opposed to a spurious increase in stiffness or vice versa. This claim becomes apparent in the subsequent numerical verification and validation sections.

The proposed method is implemented in two steps. Step one, the non-negative basis pursuit eq. 4.11 is solved, and a reduced system of algebraic equations is formed comprised of the parameters associated with the nonzero elements of step one's solution. In step two, the reduced nonlinear system is then solved using the non-negative nonlinear least squares eq. 4.12. The non-negative basis pursuit proposed for step one is defined as

$$
\begin{aligned}
\min_{\theta} \quad & ||\theta||_1 \\
\text{s.t.} \quad & \mathbf{S}\theta = \Delta\hat{\lambda} + \epsilon \\
& \theta \geq 0
\end{aligned}
\tag{4.11}
$$

The non-negative constrained nonlinear least squares is then applied to the reduced nonlinear system associated with the nonzero elements, that is,

$$
\begin{aligned}
\min_{\tilde{\theta} \in D(\tilde{r})} \quad & \frac{1}{2}||\tilde{r}(\tilde{\theta})||_2^2 \\
& \tilde{\theta} \geq 0
\end{aligned}
\tag{4.12}
$$

where $\tilde{r}$ is the reduced residual comprised of the sparse subset of parameters $\tilde{\theta} \in \Re^{\tilde{p}}$ where $\tilde{p} << p$.

Some details on the feasibility of the basis pursuit and the non-negative basis pursuit are briefly noted. As long as the sensitivity matrix is full row rank then

the basis pursuit is always feasible. In other words, there always exists a solution θ which satisfies the linear system of equations. The non-negative basis pursuit however can be infeasible if there does not exist a vector that satisfies the linear system of equations and the non-negative constraint. Infeasibility is often rare, at least to the point that it was not observed in any simulation or experiment, primarily because the stiffness sensitivity matrix is always positive and the mass sensitivity matrix is always negative. If in the case, the optimization program was infeasible, one could relax the affine constraint in eq. 4.11 to a more flexible form, that is $||\mathbf{S}\theta - \Delta\hat{\lambda}||_2 <= \alpha$. The smallest feasible value of α would be the optimal solution to the non-negative least squares ($\min_{\theta} ||\mathbf{S}\theta - \hat{\lambda}||_2$ s.t. $\theta \geq 0$).

The linear convex optimization programs were implemented using the CVX package in MATLAB [30]. This platform used the Gurobi solver at the best numerical precision to solve the optimization programs. The non-negative nonlinear squares was implemented using MATLAB's constrained nonlinear least squares *fmincon* with the interior-point optimization option [31]. The gradient of the objective function was provided to the solver. The nonlinear LASSO was solved using MATLAB's unconstrained nonlinear least squares *fminunc* function. The gradient of the objective function was numerically approximated.

4.4 Numerical verification: Shear beam

This section presents ideal numerical simulations used to demonstrate the basis pursuit's performance in identifying changes in mass and stiffness on a basic structure.

This follows with a demonstration highlighting the improvement to the inverse method when including a non-negative constraint. The simulations are ideal because the model used to derive the algorithm is also the one used to generate the data. For this proof of concept, a shear beam model with ten degrees of freedom is investigated. Each element (El.) is enumerated from one the first mass closest to the support to number ten, the free end. The shear beam has stiffness $k_1 = ... = k_{10} = 1500$ and alternating masses along the beam's length: $m_1 = 1$, $m_2 = 2$, $m_3 = 1$, ... , $m_{10} = 2$. The structure is undamped and its fundamental natural frequency is .740 Hz.
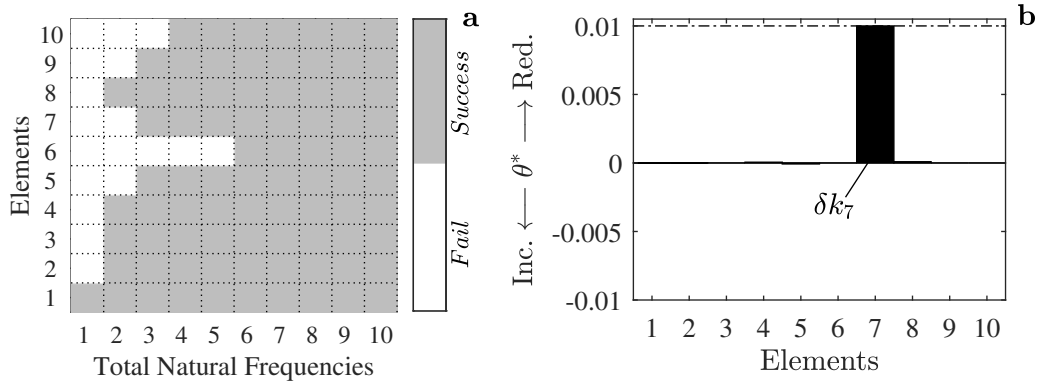
Figure 4.1: a) The successful detection of a 1% stiffness reduction on the shear beam as a function of damage location and number of identified natural frequencies using the basis pursuit. b) Estimated change in stiffness δk for a 1% stiffness reduction at El.7 on the shear beam using 6 natural frequencies

Prior to investigating problems involving stiffness and mass, this simulation first verifies that the basis pursuit successfully identifies changes in only stiffness on the shear beam. In this set of simulations, each damage case consists of a 1% reduction in stiffness at each element, taken one at a time. The basis pursuit was tested on each of the ten damage cases using 1, 2, 3,..., 10 natural frequencies totalling 100 tests. The sensitivity matrix contains 10 columns each corresponding to an element's stiffness. Fig. 4.1 presents which damage cases were correctly identified, alongside the solution

to one example in which 6 frequencies were used to identify a 1% stiffness reduction at El.7. The authors considered successful identification when i) the solution identified the correct stiffness location, ii) when the magnitude of the estimated damage was within 20% the true magnitude, and iii) when the estimated magnitudes at all other elements were less than 20% the true damage magnitude. From Fig. 4.1a, the basis pursuit solves the inverse problem for 82% of the cases, thus verifying the success of the l_1-norm approach.
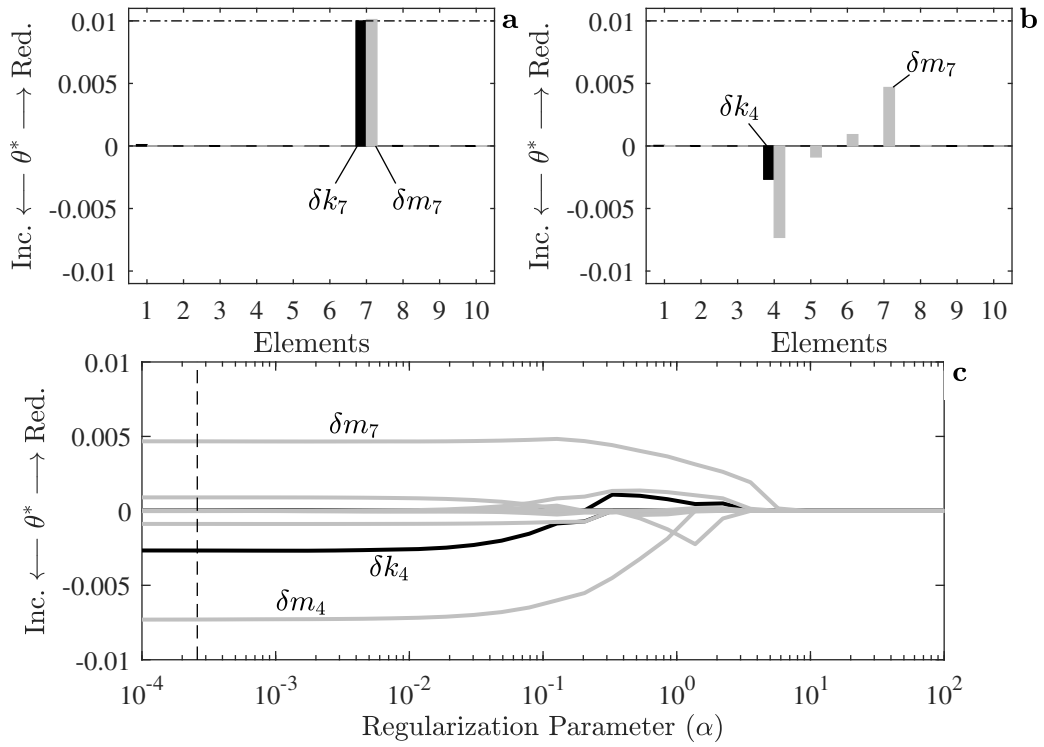
Figure 4.2: The estimated change in stiffness δk (black) and in mass δm (grey) for a 1% reduction in mass and stiffness at El.7 on the shear beam using 10 frequencies. Optimal solution shown using a) the non-negative basis pursuit, b) the basis pursuit, and c) the basis pursuit denoising as a function of regularization parameter. Dashed line in (c) is same solution shown in (b)

In contrast, the performance of the basis pursuit drastically reduces when at-

tempting to identify reductions in stiffness and mass at a single element. In this simulation, the stiffness and mass at El.7 were reduced by 1% their original values. The maximum number of natural frequencies, in total ten, were used to identify the damage. The sensitivity matrix is comprised of the stiffness and mass parameters rendering $\mathbf{S} \in \Re^{10x20}$. Fig. 4.2 presents the optimal solution θ^* of a) the non-negative basis pursuit (eq. 4.11), b) the basis pursuit (eq. 4.9), and c) the basis pursuit de-noising (eq. 4.8) as a function of the regularization parameter α. By observing Fig. 4.2, it is clear that the non-negative constraint is a necessary condition to estimate the correct reduction in mass and stiffness; otherwise the solution is dominated by physically meaningless changes in mass.
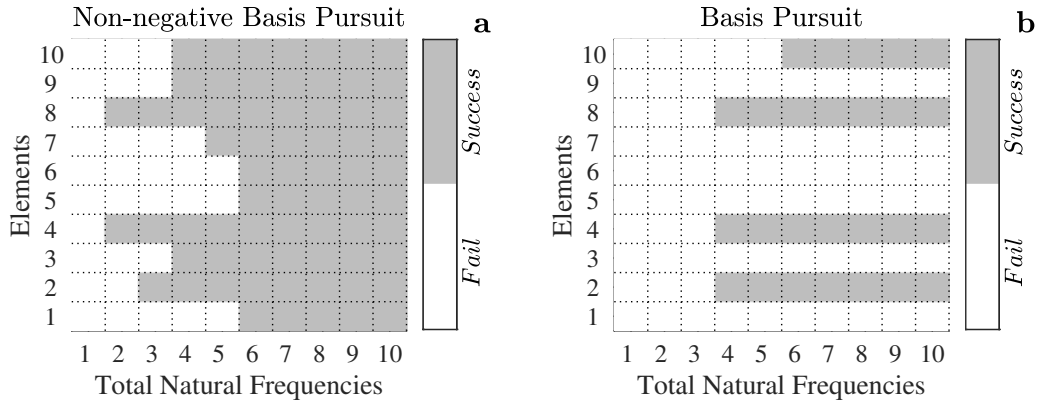
Figure 4.3: The successful detection of a 1% stiffness and mass reduction on the uniform shear beam as a function of damage location and number of identified natural frequencies using a) the non-negative basis pursuit, and b) the basis pursuit

In order to verify that the previous observation is a reoccurring phenomenon, the methods are tested on each possible damage location for the entire range of natural frequencies using the same approach that appeared in the first simulation. In this simulation, each ith damage case consists in a reduction in the stiffness k_i and the mass m_i by 1% their respective baseline. Fig. 4.3 presents which damage cases

were correctly identified. Successful identification required that the method correctly estimated both the change in stiffness and in mass. Fig. 4.3a indicates that the non-negative basis pursuit successfully identifies 68% of the damage cases, while Fig. 4.3b indicates that the basis pursuit only succeeded in 26% of the cases. Since the maximum number of eigenvalues were considered, Fig. 4.3b also indicates that it is likely impossible to estimate mass and stiffness simultaneously for damage occurring at El.1, 3, 5, 6, 7 and El.9 using natural frequencies and a sparsity prior.

4.5 FRAME STRUCTURE EXPERIMENT

A clear trend indicating that the non-negative constraint enhances the performance of the inverse eigenvalue approach was found using the simulated shear beam. In order to substantiate these observations, irreducible model error must be considered. For the purpose of validation, the authors tested the methods and observations on vibration data measured from the bolted fixed-moment steel frame shown in Fig. 4.4a.

The 1.22 m tall frame was comprised of 3.18 mm thick steel plates and steel angles, and assembled as shown in the elevation drawing Fig. 4.5. At each connection, the plate parallel to the floor is fastened to an orthogonal plate by two angles and six bolts as presented in detail drawing C-C'. Two damage scenarios were tested. In damage case 1 (DC1) a single steel angle connecting the fourth level post to the third level beam was removed (Fig. 4.4b), and in damage case 2 (DC2) the steel angle at the first level was removed. The damage introduced was intended to significantly impact local mass and stiffness. The modelled beam elements affected by the damages are
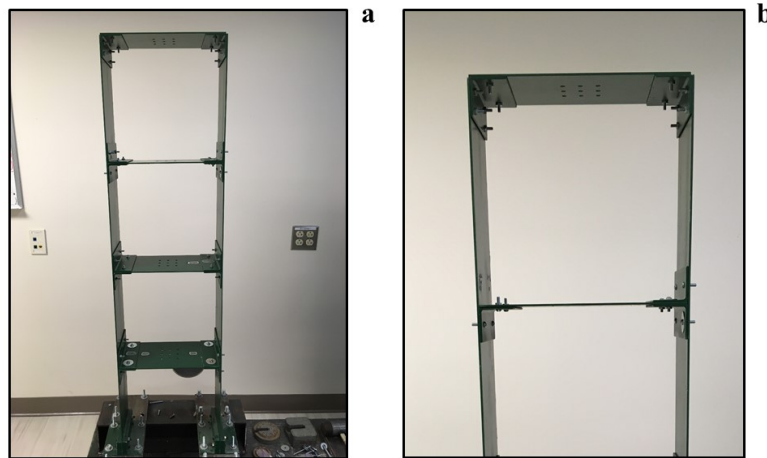
Figure 4.4: a) Photo of the bolted steel frame experiment before damage. b) Photo of damage case 1 where the third level steel angle was removed
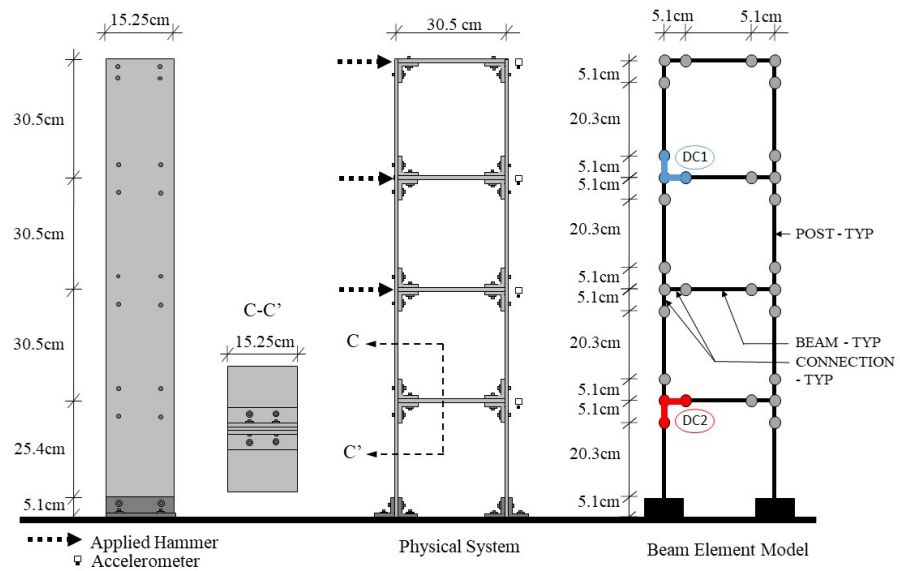
Figure 4.5: Diagram of the physical system with dimensions. Locations of the hammer strikes and accelerometers used for system identification are shown. On the far right is the structural model and the locations damage case 1 (DC1) and damage case 2 (DC2)

shown in Fig. 4.5 along side an element naming convention that is adhered to in this paper.

The frame was instrumented with four uniaxial accelerometers (PCB 333B30) located at each level. To excite the structure's modes, five hammer strikes from a modal impact hammer (PCB 086C03) were delivered at levels two, three, and four totaling 15 tests for the undamaged and damaged configurations. The sampling frequency was 400 Hz collecting 8192 points for each test. The ERA-OKID was used to extract modal information using the input measurements from the force transducer at the tip of the hammer and the outputted accelerations measured at the four degrees of freedom. The lowest four identified frequencies were selected. The average of the frequencies identified from the undamaged frame and the damaged frame are listed in Table 1. The coefficient of variation of the identified frequencies on average was below 0.001 due to the controlled lab space where the experiments were conducted. Because the variance was low, only the average of the identified frequencies were used to implement the algorithms.

Table 4.1: Comparison of Average Modal Frequencies

Mode	Model-undamaged (Hz)	Undamaged structure (Hz)	Damage case one (Hz)	Damage case two (Hz)
1	6.10	6.02	6.10	5.90
2	19.38	19.30	18.68	19.08
3	34.37	34.41	33.87	34.38
4	47.35	47.34	47.29	47.45

The finite element model used to derive the eigenvalue sensitivities (eq. 4.7) is comprised of 34 discrete beam elements and 30 translation degrees of freedom oriented parallel to the floor. The modulus of elasticity was 200 *GPa*. Coincident nodes were

fixed. At first, the derived natural frequencies were significantly larger than those identified from the undamaged frame indicating a need to update the model. The discrepancy between the model and the physical system was presumably dominated by an inadequate assumption on the rigidity of the connections. In order to match the model's frequencies to those identified, two design parameters were selected for updating: the moment of inertia of all vertically oriented and all horizontally oriented beam elements at the connections. The natural frequencies derived from the updated model are listed under Model in Table 5.1.

Each stiffness parameter (δk_i, eq. 4.3) corresponds to the elasticity of a single beam element. Among the 34 total stiffness parameters, 11 are identical in terms of their influence on the identified eigenvalues due to the frame's symmetry about its vertical axis. Hence, it is impossible to distinguish parameters on the left hand side of the frame from the right hand side. In order to clearly present the following analysis, the parameters of the sensitivity matrix are restricted to the 19 stiffness parameters demarcated in Fig. 4.6a. For the same reasons, the mass parameters (δm_i) are restricted to the subset associated with the nodes demarcated in Fig. 4.6c.

Despite removing the frame's global symmetry, the presence of local quasi-dependencies between stiffness parameters would complicate successful application of the inverse method. This challenge is ubiquitous to the damage identification IEP because the number of unique measurements is so limited. In order to locate local colinearity, the cosine angles between all 19 stiffness parameter sensitivities were calculated. Fig. 4.7a presents the cosine angles between each column of the stiffness sensitivity matrix
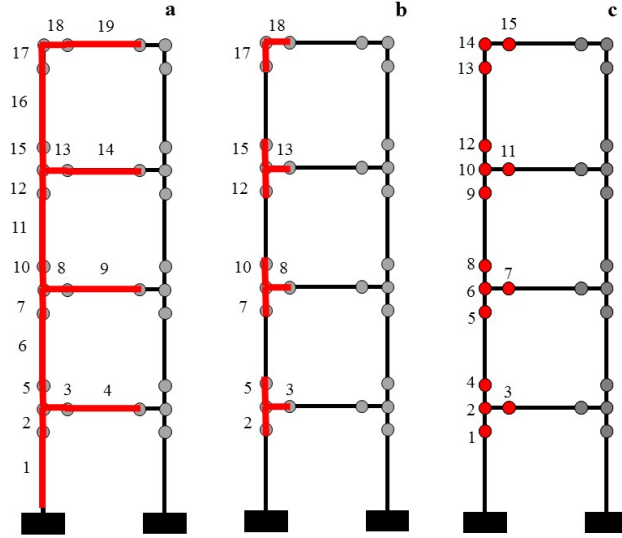
Figure 4.6: Parameter subset selections highlighted in red: a) the stiffness elements associated with beams, posts, and connections, b) the stiffness elements associated with connections only, and c) the mass nodes

derived from the baseline model, computed as

$$\mathbf{C}_{i,j} = \frac{|\mathbf{S}_i \cdot \mathbf{S}_j|}{||\mathbf{S}_i||_2 ||\mathbf{S}_j||_2}, \; i, j = 1...p_k \tag{4.13}$$

where i and j respectively indicate the row and column of $\mathbf{C}$. If $\mathbf{C}_{i,j} = 1$ then the ith and j^{th} elements are colinear, and if $\mathbf{C}_{i,j} = 0$ then the ith and j^{th} elements are orthogonal. The white colored blocks represent values of $\mathbf{C}_{i,j} \geq 0.99$. The clusters of $\mathbf{C}_{i,j} \geq 0.99$ indicate that the parameters representing the connections and the parameters defining the adjacent beams or posts (e.g. El.1 and El.2; El.3 and El.4) are nearly colinear and indistinguishable. The model discretization created additional complications because of the disproportionate scaling of the colinear adjacent parameters. Fig. 4.7b presents the normalized euclidean magnitudes of the columns of the sensitivity matrix indicating the disproportionate scaling. It is clear from Fig. 4.7b

that the beams and posts are more sensitive to damage than the connections. The proposed method, like any inverse based approach, cannot distinguish parameters among a colinear cluster. Instead inverse algorithms have a strong tendency to identify the most sensitive parameter among a colinear cluster which in this case are the beams and posts.
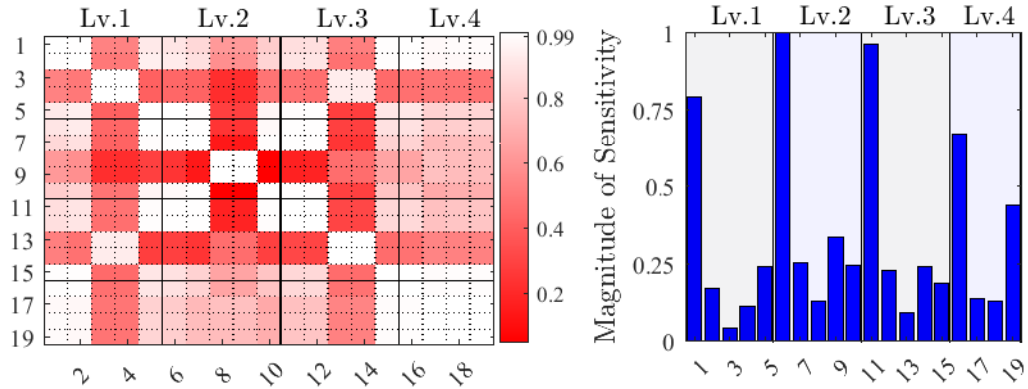
Figure 4.7: Left hand side figure depicts the cosine angles between each column of the stiffness sensitivity matrix normalized between zero and one where zero indicates orthogonality. The right hand side figure presents the normalized Euclidean magnitude of each column of the stiffness sensitivity matrix

Since the inverse method cannot distinguish damage between the connections and the beams and posts, only the stiffness parameters associated with the connections are included in the columns of the stiffness sensitivity matrix in addition to the mass parameters for the remainder of this paper. The 11 stiffness parameters associated with connections are demarcated in Fig. 4.6b.

4.6 NUMERICAL VERIFICATION: FRAME STRUCTURE

This section presents numerical simulations representative of the experiment to follow intended to verify the proposed methods and observations. Only the first damage case is simulated in this section. The removed third level steel angle was modelled as an equivalent reduction in bending stiffness through the change in its inertial term by reducing the thickness of El.13 and El.15 by one-third and one-half respectively. The damage was implemented in the model by reducing the elastic modulus of El.13 and El.15 to respectively 29.6% and 12.5% their original values, and reducing the mass at nodes 10, 11, and 12 to respectively 83.3%, 71.4%, and 85.7% their original values. The solutions are presented as estimated changes in stiffness δk and changes in mass δm where $+1$ indicates a 100% reduction. The parameter setup is comprised of the 15 mass parameters and the 11 stiffness parameters associated with the connections rendering the sensitivity matrix as $\mathbf{S} \in \Re^{4x26}$.

The following simulation again suggests that sparsity alone may be too weak a prior to differentiate between changes in mass from changes in stiffness using measured natural frequencies. The basis pursuit denoising (eq. 4.8) and the nonlinear LASSO (eq. 4.10) are investigated. Fig. 4.8a and Fig. 4.8b present the solution paths to respectively the basis pursuit denoising and the nonlinear LASSO as functions of the regularization parameter (α). Consider Fig. 4.8a. If an over-fit solution is selected, indicated by the dashed (1) line, 100% and 45% mass increases are incorrectly estimated at the first level. The sparsest solution, indicated by the dashed (2) line,

provides no information on stiffness and incorrectly identifies the mass reduction location. Note that some solutions overestimate the damage magnitudes predicting over 100% reductions in stiffness and increases in mass. This phenomenon is a result of the linear truncation error and the underlying monotonic properties of the nonlinear operator. Fig. 4.8b indicates that the nonlinear LASSO performs in a similar manner with the exception that the estimated magnitudes are more accurate. The stiffness reduction at El.13 is correctly identified, however significant mass increases are falsely detected at the first level. Note that the solution path to the nonlinear LASSO lacks relative smoothness because the optimization program is non-convex and hence lacks guarantees on convergence or global optimality.

The next simulation verifies the performance of the proposed non-negative inverse method. Since the magnitude of the stiffness and mass reduction is substantial, the solution to the non-negative basis pursuit requires updating to account for the linear truncation error. As described in section three, the method entails solving the non-negative basis pursuit (eq. 4.11) and then updating the parameters associated with the nonzero elements of the solution using the non-negative nonlinear least squares (eq. 4.12). Fig. 4.9a presents the final solution as the estimated change in stiffness δk and change in mass δm. Alongside the optimal solution, Fig. 4.9b presents the values of the simulated damage. By observation, it is clear that the proposed non-negative method correctly quantifies and locates the stiffness reductions. The method identifies a mass reduction at the correct level, however only one damaged node was located. In terms of quantification, the contribution of all three mass reductions accumulate at the single node, and hence appears as an overestimation in mass reduction.

The final simulation investigates the effects of measurement error. A vector of
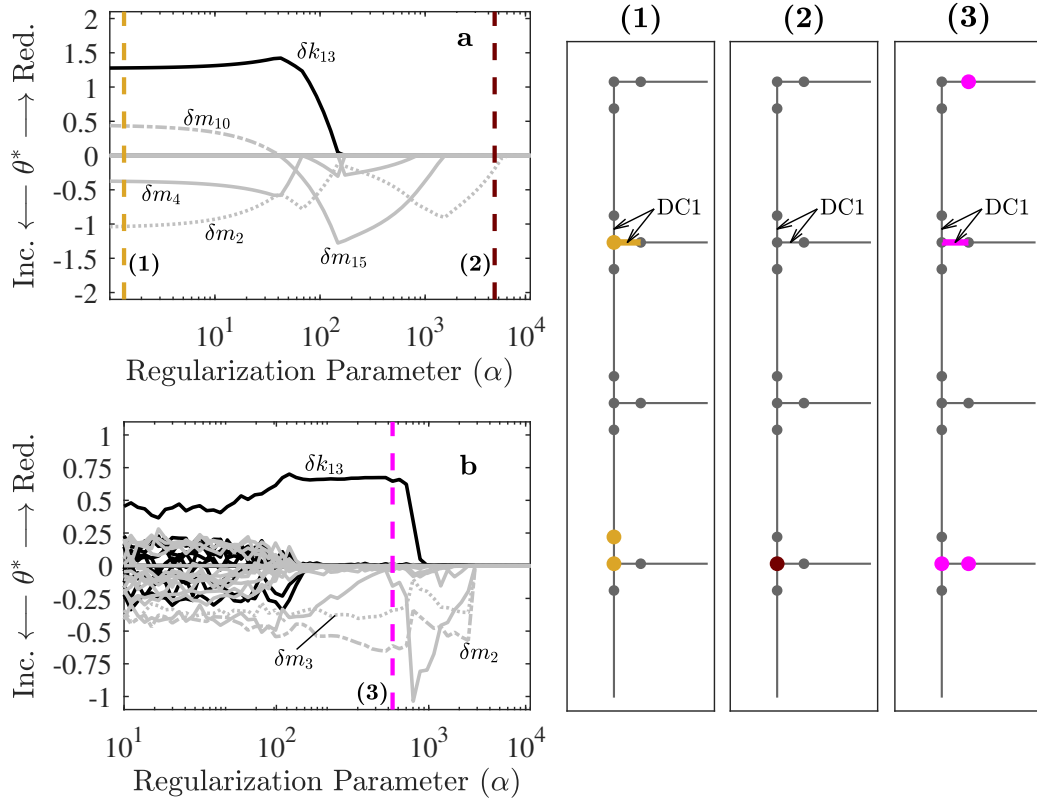
Figure 4.8: a) The solution path to the basis pursuit denoising, and b) the nonlinear LASSO as functions of the regularization parameters. Black and grey lines indicate stiffness and mass parameters respectively. Solutions selected at (1), (2), and (3) are superimposed over the frame in the right hand figures. Solid circles indicate estimated changes in mass and thick colored lines indicate estimated changes in stiffness

simulated measurement noise ϵ is added to both the damaged and undamaged eigenvalues. The measurement error contained in ϵ is defined as the realization of a q-dimensional Gaussian random vector with zero mean and standard deviation of each component ϵ_i proportional to the specified coefficient of variation (cv). Two tests comprised of random noise defined by $cv = 0.001$ and 0.002 were performed. 0.002 was equal to the maximum coefficient of variation obtained from uncertainty quantification studies in system identification using ambient vibrations [32]. For each test, the algorithm was implemented on 1,000 realizations of ϵ.
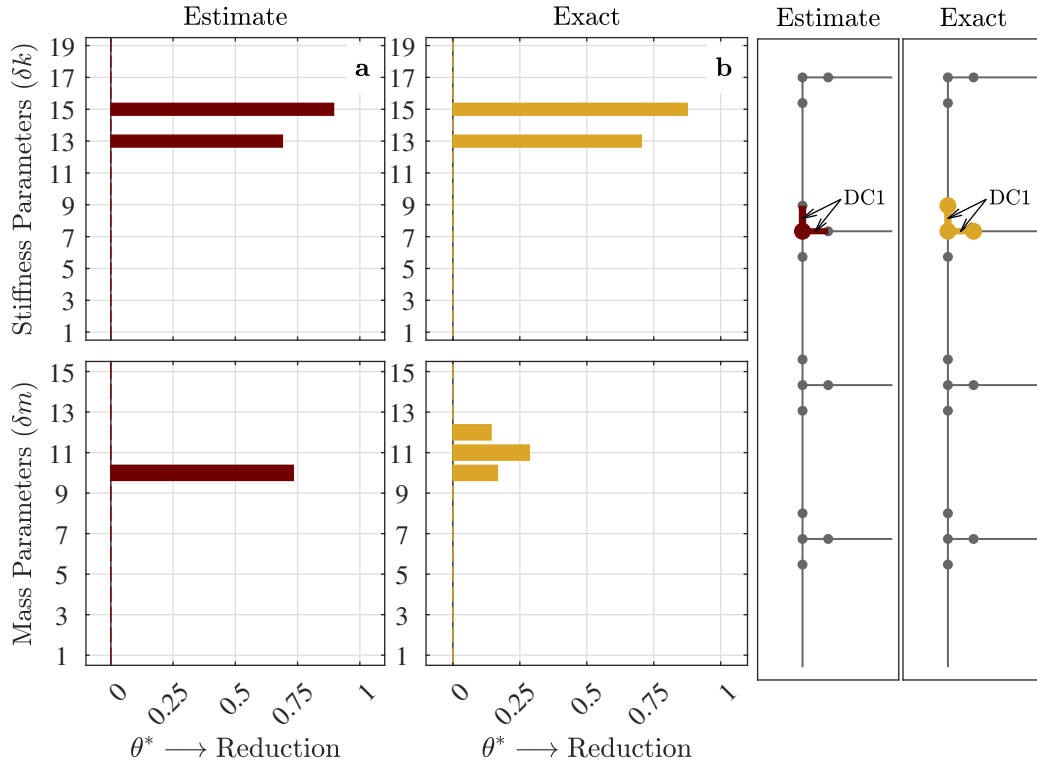
Figure 4.9: Proposed non-negative method applied to simulated damage case 1 (DC1). The results presented as a) the estimated change in stiffness (δk) and the estimated change in mass (δm), alongside b) the exact change in stiffness and mass. The locations of the estimated and exact damage locations are shown in the right hand figures

Fig. 4.10a and Fig. 4.10b presents the estimated changes in stiffness and mass for all 1,000 realizations of the Gaussian random variable with respectively $cv = 0.001$ and $cv = 0.002$. The results are compiled into box plots, where the central hash denotes the median, and the bottom and top edges of the box denote the 25th and 75th percentiles. The whiskers extend to the most extreme data points not considered outliers, where the extreme data is within $+/-$ 2.7 standard deviations from the mean assuming a normal distribution [31]. For both levels of measurement noise, the variance of the estimated stiffness reductions is small at the true damaged locations. The estimated mass reduction appears to be more sensitive to measurement error

than the estimated changes in stiffness. The location of the damage in terms of mass and stiffness is still apparent despite the measurement error.
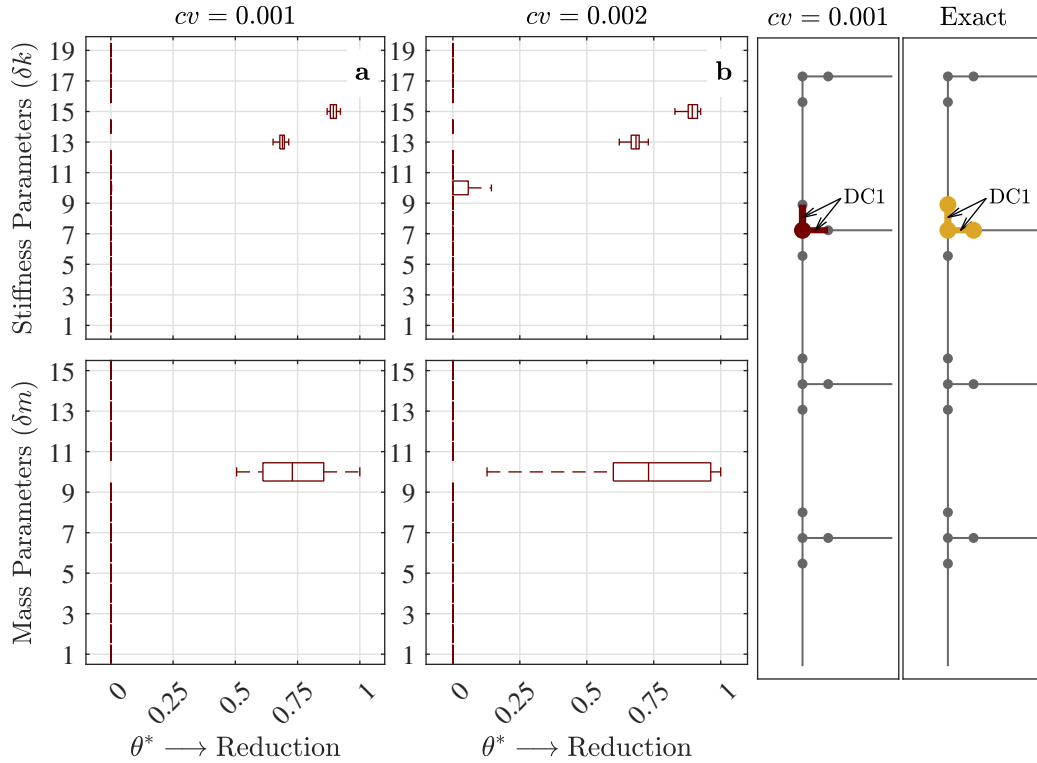
Figure 4.10: Box plots of estimated change in stiffness δk and mass δm using proposed non-negative method on simulated damage case 1 (DC1) perturbed by white noise with a) cv = 0.001 and b) cv = 0.002. Estimated solution and exact damage locations superimposed over the frame in right hand side figures. Solid circles indicate changes in mass and thick colored lines indicate changes in stiffness

4.7   EXPERIMENTAL VALIDATION RESULTS

This section presents a summary of the experimental results aimed at validating the proposed methodology using the physical system. The proposed non-negative inverse method is used to quantify and locate the missing steel connections using the

changes in the four natural frequencies identified from the vibration data measured from the damaged and undamaged frame. Both damage scenarios are considered. The parameter setup is again comprised of the mass parameters and the stiffness parameters associated with the connections totalling 26 parameters rendering $\mathbf{S} \in \Re^{4x26}$.

Fig. 4.11 presents the estimated changes in stiffness and in mass for damage case 1 alongside the modelled damage location and magnitude. The algorithm identifies approximately 50% reductions in mass and stiffness at the third level of the frame, and a false positive at the fourth level. The false positive is not detrimental as it is in close proximity to the true damage. Overall, the algorithm successfully identifies both the change in mass and in stiffness. Fig. 4.12 presents the estimated changes in stiffness and in mass for damage case 2 alongside the modelled damage location and magnitude. The algorithm identifies approximately 60% reduction in stiffness at the first level of the frame, and a small false positive at third level. The estimated changes in mass are also located at first and second level, however it is unclear if changes in mass are present or if these are spurious results given the small estimated magnitude.

4.8 CONCLUSION

This paper suggests and demonstrates that sparse vector recovery is too weak a prior to simultaneously identify changes in stiffness and mass from a subset of identified natural frequencies. However, in cases where damage is defined by strict reductions in stiffness and mass, the associated underdetermined inverse eigenvalue problem can
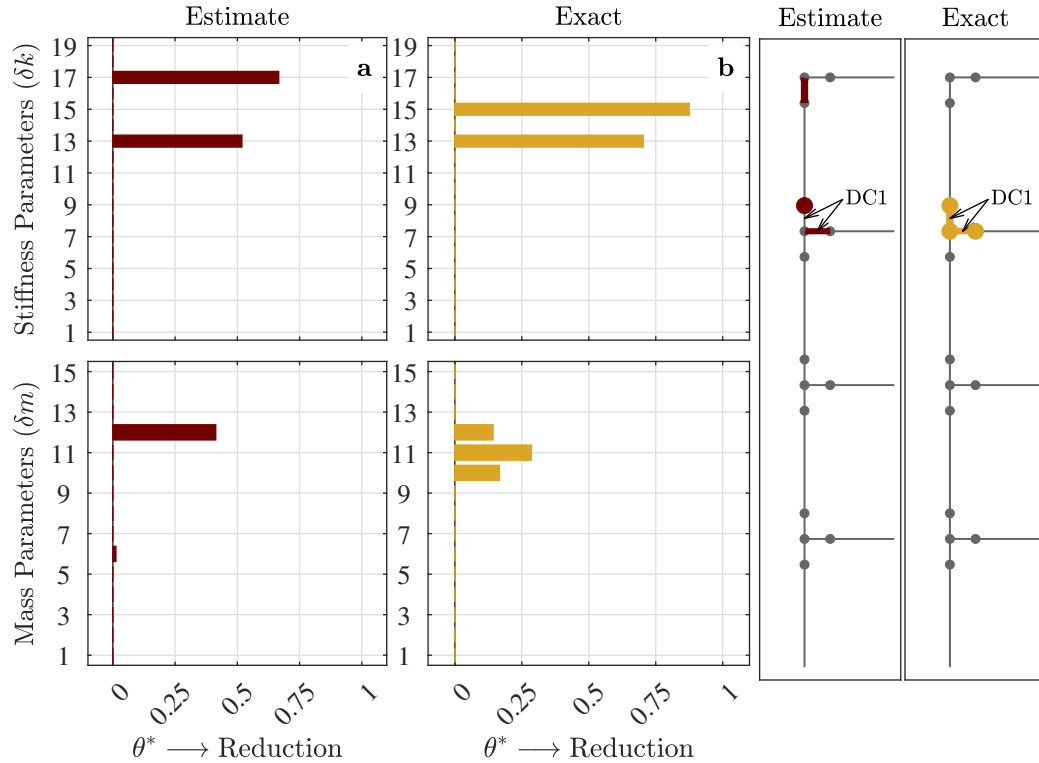
Figure 4.11: a) Estimated change in stiffness δk and change in mass δm using proposed method on simulated damage case 1 using the vibration data. b) The modelled changes in stiffness and mass due to the damage

be uniquely solved when non-negativity is imposed on the solution space. This claim is substantiated using a numerically simulated ten degree of freedom shear beam and a four-level frame. Simulations regarding the shear beam indicate that it is impossible to quantify and locate both the mass and stiffness parameters for most sparse damages located along the beam's length unless a non-negative constraint was included. A multi-damage location scenario using the simulated frame also indicated the same finding; a non-negative constraint is needed to identify changes in mass and stiffness.

In addition to these observations, this paper proposed a two-step model updat-
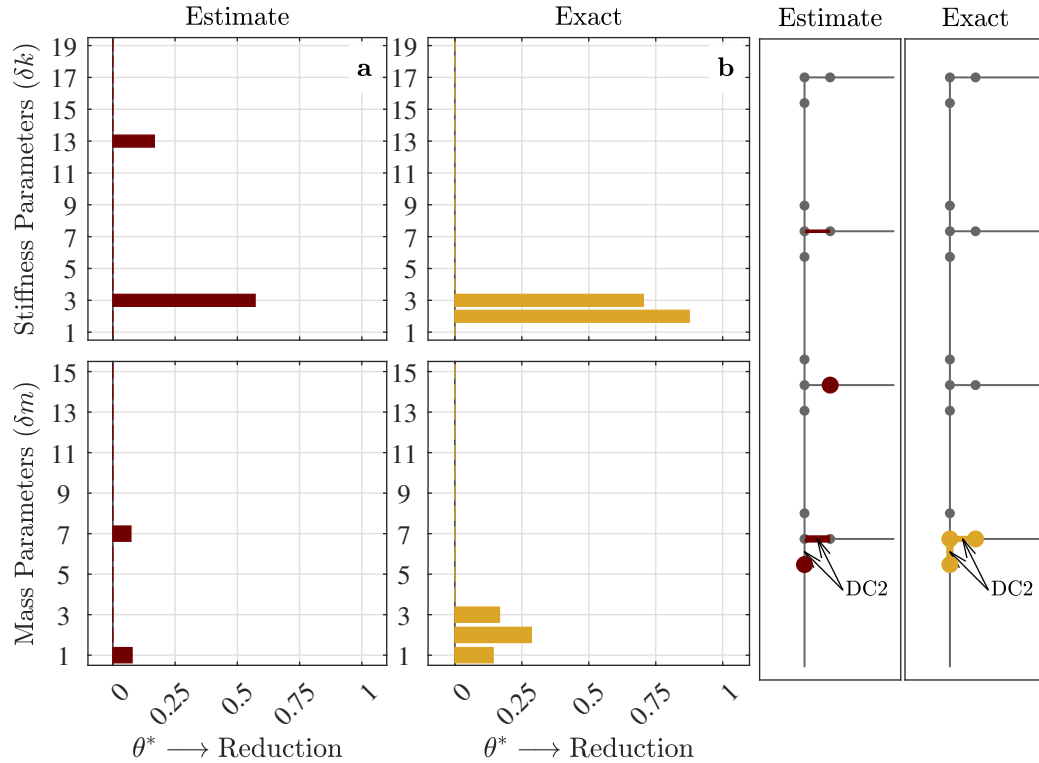
Figure 4.12: a) Estimated change in stiffness δk and change in mass δm using proposed method on simulated damage case 2 using the vibration data. b) The modelled changes in stiffness and mass due to the damage

ing method to solve the nonlinear inverse problem, which combined the non-negative constraint, l_1-norm optimization, and the nonlinear least squares. The method was verified on the frame model in the presence of measurement error, and then validated using vibration data measured from a four-level bolted steel frame subjected to damage. Two damage cases were investigated. In each case, a steel connection angle was removed which significantly reduced the stiffness and mass of the associated damaged element. Using four identified natural frequencies, the proposed non-negative inverse method successfully quantified and located the local reductions to mass and stiffness for the first tested damage case. In the second damage case, the method

correctly identified stiffness reductions but underestimated the true quantity of the mass reductions.

For future work, the authors wish to determine if the sparse and non-negative constraints are sufficient to differentiating local damage in global vibrations from changes in environmental features such as temperature. In addition to environmental impacts, the scalability of the method needs further investigation in the context of larger experiments.

Acknowledgements

Bibliography

[1] E. M. Hernandez, Identification of isolated structural damage from incomplete spectrum information using l1-norm minimization, Mech. Syst. Signal Process. 46 (1) (2014) 59–69.

[2] X. Q. Zhou, Y. Xia, S. Weng, L1 regularization approach to structural damage detection using frequency data, Struct. Heal. Monit. An Int. J. 14 (6) (2015) 571–582.

[3] G. M. Gladwell, Inverse problems in vibration, Appl. Mech. Rev. 39 (7) (1986) 1013–1018.

[4] M. T. Chu, Inverse eigenvalue problems, SIAM Rev. 40 (1) (1998) 1–39.

[5] S. W. Doebling, C. R. Farrar, M. B. Prime, D. W. Shevitz, Damage identification and health monitoring of structural and mechanical systems from changes in their vibration characteristics: A literature review, Tech. rep. (1996).

[6] O. S. Salawu, Detection of structural damage through changes in frequency: A review, Eng. Struct. 19 (9) (1997) 718–723.

[7] C. R. Farrar, S. W. Doebling, D. A. Nix, Vibration-based structural damage identification, Philos. Trans. R. Soc. London. Ser. A Math. Phys. Eng. Sci. 359 (1778) (2001) 131–149.

[8] D. L. Donoho, Compressed sensing, IEEE Trans. Inf. Theory 52 (4) (2006) 1289–1306.

[9] A. M. Bruckstein, D. L. Donoho, M. Elad, From sparse solutions of systems of equations to sparse modeling of signals and images, SIAM Rev. 51 (1) (2009) 34–81.

[10] T. Hastie, R. Tibshirani, M. Wainwright, Statistical Learning with Sparsity: The Lasso and Generalizations, Chapman & Hall/CRC Monographs on Statistics & Applied Probability, CRC Press, 2015.

[11] E. J. Candes, J. Romberg, T. Tao, Robust uncertainty principles: exact signal reconstruction from highly incomplete frequency information, IEEE Trans. Inf. Theory 52 (2) (2006) 489–509.

[12] M. I. Friswell, Damage identification using inverse methods, Philos. Trans. R. Soc. A Math. Phys. Eng. Sci. 365 (2007) 393–410.

[13] J. E. Mottershead, M. I. Friswell, Model updating in structural dynamics: A survey, J. Sound Vib. 167 (2) (1993) 347–375.

[14] E. M. Hernandez, Identification of localized structural damage from highly incomplete modal information : theory and experiments, J. Eng. Mech. 142 (2) (2016) 1–9.

[15] S. Zhou, Y. Bao, H. Li, Structural damage identification based on substructure sensitivity and l1 sparse regularization, in: Proc. SPIE - Int. Soc. Opt. Eng., 2013.

[16] R. Hou, Y. Xia, X. Zhou, Structural damage detection based on l1 regularization using natural frequencies and mode shapes, Struct. Control Heal. Monit. 25 (3).

[17] N. Grip, N. Sabourova, Y. Tu, Sensitivity-based model updating for structural damage identification using total variation regularization, Mech. Syst. Signal Process. 84 (2017) 365–383.

[18] R. J. Link, D. C. Zimmerman, Structural damage diagnosis using frequency response functions and orthogonal matching pursuit: theoretical development, Struct. Control Heal. Monit. 22 (6) (2015) 889–902.

[19] C. B. Smith, E. M. Hernandez, Detection of spatially sparse damage using impulse response sensitivity and LASSO regularization, Inverse Probl. Sci. Eng. 27 (1) (2019) 1–16.

[20] D. Sen, A. Aghazadeh, A. Mousavi, S. Nagarajaiah, R. Baraniuk, Sparsity-based approaches for damage detection in plates, Mech. Syst. Signal Process. 117 (2019) 333–346.

[21] C. Farrar, K. Worden, Structural Health Monitoring: A Machine Learning Perspective, John Wiley & Sons Ltd., 2013.

[22] A. M. Bruckstein, M. Elad, M. Zibulevsky, On the uniqueness of nonnegative sparse solutions to underdetermined systems of equations, IEEE Trans. Inf. Theory 54 (11) (2008) 4813–4820.

[23] M. Wang, W. Xu, A. Tang, Conditions for a unique non-negative solution to an underdetermined system: from vectors to matrices, IEEE Trans. Signal Process. 3 (59) (2011) 1007–1016.

[24] S. Hassiostis, G. Jeong, Identification of stiffness reductions using natural frequencies, J. Eng. Mech. 121 (10) (1995) 1106–1113.

[25] X. Y. Li, S. S. Law, Adaptive Tikhonov regularization for damage detection based on nonlinear model updating, Mech. Syst. Signal Process. 24 (6) (2010) 1646–1664.

[26] W. Ren, G. De Roeck, Structural damage identification using modal data. I: Simulation verification, J. Struct. Eng. 128 (1) (2002) 87–95.

[27] J. E. Mottershead, M. Link, M. I. Friswell, The sensitivity method in finite element model updating: A tutorial, Mech. Syst. Signal Process. 25 (7) (2011) 2275–2296.

[28] R. Fox, M. Kapoor, Rates of change of eigenvalues and eigenvectors., AIAA J. 6 (12) (1968) 2426–2429.

[29] S. Boyd, L. Vandenberghe, Convex optimization, Cambridge university press, 2004.

[30] M. Grant, S. Boyd, {CVX}: Matlab Software for Disciplined Convex Programming, version 2.1, \url{http://cvxr.com/cvx} (mar 2014).

[31] MATLAB, version 7.4.0 (R2018a), The MathWorks Inc., Natick, Massachusetts, 2018.

[32] E. Reynders, R. Pintelon, G. De Roeck, Uncertainty bounds on modal parameters obtained from stochastic subspace identification, Mech. Syst. Signal Process. 22 (4) (2008) 948–969.

Chapter 5

Non-negative and Sparsity Constrained Inverse Problems in Damage Identification - Application to a Full-scale 3D Truss

Abstract

Non-negative constrained least squares and l_1-norm optimization are sometimes viable inverse-based methods used to quantify and locate damage described by local stiffness reductions using measured changes in natural frequencies. Although the two methods provide meaningful solutions to the associated underdetermined inverse problem when

94

the physically correct solution is sufficiently sparse, each method is disadvantaged in terms of either solution uniqueness, regularization, or forced sparsity. This paper addresses these challenges and argues that combining the non-negative constraint and l_1-norm optimization improves performance and abates or improves upon the deficiencies of the standalone methods. This paper demonstrates that the optimal set of solutions satisfying the non-negative least squares is bounded and that estimating these bounds provides a novel measure for interpreting the validity of the sparse solution recovered from the proposed non-negative constrained l_1-norm optimization method. The proposed method is numerically verified and experimentally tested on vibration data taken from a 17.24 m long full-scale three-dimensional truss subjected to three progressive local damage cases.

5.1 INTRODUCTION

Damage identification is often contextualized as a parameter estimation inverse problem where the parameters of a finite element (FE) model are periodically calibrated to the physical system in order to deduce the physical cause of any measured shifts in dynamic behavior [1]. When measured dynamic features are restricted to the natural frequencies, calibration (FE model updating) requires solving a severely ill-posed inverse problem described by an underdetermined system of equations given that the number of parameters defining the spatial domain greatly outnumbers the identifiable modes of vibration. Conventional regularized least squares methods that may improve ill-conditioning are insufficient to determine physically meaningful solutions to underdetermined inverse problems [2].

Sparsity, the characteristic describing vectors with few nonzero elements, can be one necessary condition for obtaining meaningful solutions to underdetermined inverse problems [3]. Damage defined by reductions in stiffness at local regions of the spatial domain are represented by sparse vectors. Hence damage sufficiently restricted in space, i.e. sufficiently sparse, may be identifiable from changes in natural frequencies using the inverse method [4].

If the local characteristics of damage are known apriori, one approach to solving the inverse problem is to directly impose locality on the solution space in the form of sparsity. The first attempts at imposing locality, thus indirectly imposing sparsity, were through minimum rank perturbation theory [5,6]. Since that time, convex optimization theory matured and efficient convex methods that target sparse solutions to inverse problems were introduced [3, 7, 8]. The most popular methods minimize the l_1-norm - the convex surrogate to counting a vector's nonzero elements [9]. In structural health monitoring (SHM), l_1-norm optimization has applications in force localization [10], data compression [11], and notably local damage identification. In damage identification, Hernandez proposed l_1-norm optimization to identify small changes in stiffness from natural frequencies [4] and validated the method on a cantilever beam [12]. The authors in [13] presented an l_1-norm regularized nonlinear least squares approach to account for the eigenvalues' nonlinear dependence on stiffness. The application of the l_1-norm has been extended to other damage features as well such as: the combination of natural frequencies and mode shapes [14, 15], the time-domain impulse response [16], and measured response signals [17]. Other notable sparse vector recovery approaches are based on orthogonal matching pursuit [18] and total variation regularization [19].

Although l_1-norm regularization has facilitated using natural frequencies for damage identification, the sparsity prior is not without its limitations. l_1-norm optimization forces a sparse solution with at most k nonzero elements where k is the number of unique measurements [20]. Forced sparsity is problematic to solution interpretation since not all changes in frequencies are due to local damage and hence not all solutions should be sparse [21]. Furthermore, the solution to l_1-norm optimization may not be unique [4,13]. These characteristics are unsatisfactory in terms of interpreting the validity of the solution, since the solution is always sparse yet may be physically meaningless and(or) non-unique.

When defined in terms of stiffness, damage has another important property - non-negativity. Physically, non-negativity reflects the property that damage tends to strictly reduce the stiffness of the damaged element [22,23]. Methods that target sparse solutions such as l_1-norm optimization are not necessary to the recovery of sparse and non-negative solutions [24]. If a sufficiently sparse non-negative solution exists, then it may be the only non-negative solution to satisfy the underdetermined linear system [25, 26]. This implies that the non-negative constraint can induce a unique and sparse solution without explicitly imposing sparsity. Hassiotis and Jeong first demonstrated that local damage identification could be performed with a subset of natural frequencies by using non-negative constraints [27]. Later Smith and Hernandez bridged the gap between sparse damage and non-negativity, and found that the eigenvalue sensitivity matrix satisfies the necessary conditions to induce unique non-negative solutions [21]. The necessary condition is that the span of rows of the matrix must intersect the non-negative orthant [7, 26]. In [21], a measure for determining whether the system of equations possesses a nontrivial unique non-negative

solution was presented based on work by [28]. Despite the appeal in using non-negative least squares, the method also has its disadvantages. Specifically, there is no mechanism to penalize the magnitude of the estimated stiffness reduction in order to regularize the solution.

This paper leverages the concepts of non-negativity, uniqueness, and sparsity to improve and build upon the l_1-norm optimization and the non-negative least squares. The objective of this paper is to illustrate that the linearized damage identification inverse problem using natural frequencies: (i) is among a special class of underdetermined inverse problems with a bounded set of solutions satisfying the non-negative least squares, (ii) that finding the sparsest solution within this non-negative set improves the inverse method's performance over the standalone application of l_1-norm optimization or the non-negative least squares, and (iii) that measuring the bounds of the non-negative least squares solution space can aid in interpreting the validity of the recovered sparse solution. Using the sensitivity-based inverse method, this papers proposes a non-negative constrained l_1-norm optimization program to identify local stiffness reductions from a subset of natural frequencies. This paper provides a method to measure the bounds on the optimal set to the non-negative least squares in order to aid in interpreting the validity of the sparse prior. The proposed methods are first verified numerically, and then tested using vibration data measured from a 17.24m long aluminum 3D truss subjected to three local damage scenarios. Only 6 modes of vibration were identified and the spatial domain is defined by 144 stiffness parameters. In this experiment, the derived natural frequencies from the finite element (FE) model do not match the natural frequencies identified from the healthy structure. In order to discern damage from model error, the proposed method min-

imizes the residual between the natural frequencies identified from the undamaged and damaged structure.

The outline of the paper is as follows. Section 5.2 develops the damage identification inverse problem using the sensitivity method in structural dynamics. Section 5.3 develops the theory of the unique sparse and non-negative solution to the underdetermined inverse problem, and details the proposed methodologies: the non-negative constrained l_1-norm optimization method, and the measure of solution space bounds. All of the convex optimization programs were implemented using the CVX package in MATLAB using the Gurobi solver [29]. Section 5.4 introduces the model of the truss, which is then used to illustrate the proposed methods. Section 5.5 compares the proposed method to the standalone applications of the l_1-norm optimization and the non-negative least squares. Section 5.6 details how solutions can be interpreted from the solution set bounds, also referred to as the measure of uniqueness. The remaining paper is devoted to experimental validation. Section 5.7 provides a detailed summary of the physical structure and additional details on the FE model. Section 5.8 summarizes the vibration modal tests conducted on the truss, the process used to identify the natural frequencies, and the sources of uncertainty in the identified modes. In section 5.9, the results of the proposed method using the vibration data are summarized.

5.2   Method of approach

From the sensitivity-based inverse method to structural dynamics [2], this paper relates changes in the stiffness parameters defining a model to changes in the identified

eigenvalues (natural frequencies squared) between the undamaged and potentially damaged structure through an approximate system of linear equations:

$$\mathbf{S}\Delta\theta = \Delta\lambda \tag{5.1}$$

where $\Delta\lambda \in \Re^q$ is the change in the eigenvalues identified from the undamaged and potentially damaged physical system, $\mathbf{S} \in \Re^{qxp}$ is the sensitivity matrix, and $\Delta\theta \in \Re^p$ is the unknown change in the parameters defining the stiffness matrix.

This paper is restricted to cases where changes to the mass matrix $\mathbf{M} = \mathbf{M}^T \in \Re^{nxn}$ due to damage are negligible, and the stiffness matrix $\mathbf{K} = \mathbf{K}^T \in \Re^{nxn}$ can be written as a linear combination of the candidate parameters:

$$\mathbf{K} = \mathbf{K}_0 - \sum_{i=1}^{p} \mathbf{K}_i \Delta\theta_i \tag{5.2}$$

where $\Delta\theta_i \in \Re$ is the change in the ith parameter contributing to the change in the stiffness and $\mathbf{K}_i$ is an elementary influence matrix. $\mathbf{K}_0$ is the stiffness matrix defining the model of the baseline structure. The linear decomposition is valid when damage affects material properties such as elastic modulus, shear modulus, cross-sectional area, and other linear multipliers of stiffness.

From the rate of change of the eigenvalues [30] and the sensitivity method [2], the sensitivity matrix $\mathbf{S} \in \Re^{qxp}$ is

$$\mathbf{S}_{j,i} = \frac{\partial\lambda_j}{\partial\Delta\theta_i} = \phi_j^T \left(\frac{\partial\mathbf{K}}{\partial\Delta\theta_i} - \lambda_j \frac{\partial\mathbf{M}}{\partial\Delta\theta_i} \right) \phi_j \tag{5.3}$$

100

Combining eq. 5.2 and eq. 5.3,

$$\mathbf{S}_{j,i} = -\phi_j^T \mathbf{K}_i \phi_j \tag{5.4}$$

where $\phi_j \in \Re^n$ is the mode shape corresponding to the jth eigenvalue $\lambda_j \in \Re$ which satisfy

$$\mathbf{K}\phi_j = \mathbf{M}\phi_j \lambda_j \tag{5.5}$$

and

$$\phi_j^T \mathbf{M}\phi_j = 1 \tag{5.6}$$

In practice, the number of identifiable eigenvalues q is far less than the number of parameters defining the stiffness matrix p, hence eq. 5.1 is an underdetermined system of linear equations. The sensitivity matrix is derived from an imperfect model of the physical system and the identified eigenvalues contain measurement error.

5.3 Non-negative sparse

vector recovery

5.3.1 l_1-norm optimization

The intuition behind sparse vector recovery is to minimize the number of nonzero elements of a feasible vector which fits the system of equations to a specified degree of satisfaction. The following convex optimization program, known as the basis pursuit

denoising, targets sparse solutions to eq. 5.1:

$$\min_{\Delta\theta} \quad ||\Delta\theta||_1$$
$$\text{s.t.} \quad ||\mathbf{S}\Delta\theta - \Delta\lambda||_2 \leq \alpha \tag{5.7}$$

where $\{\alpha \in \Re \mid \alpha \geq 0\}$ is the regularization parameter; a predefined scalar acting as a weight between the solution fit in terms of the Euclidean norm ($||.||_2$) and sparsity in terms of the vector l_1-norm ($||.||_1$). As $\alpha \to ||\Delta\lambda||_2$, one obtains the sparsest solution $\Delta\theta^* = \mathbf{0}$, i.e. the optimal point with the fewest nonzero elements. As $\alpha \to 0$, one obtains the least sparse solution, which typically is comprised of at most q nonzero elements, the row rank of $\mathbf{S}$ [20]. If we consider a sparse solution as having at most q-nonzero elements, it is clear that eq. 5.7 must force a sparse solution for all α.

Note that issues regarding uniqueness of solutions are expected and that reductions in stiffness from different elements are indistinguishable if they generate the same changes in the subset of the spectrum being used. Even if every element is distinguishable, the underdetermined system of equations may have two satisfactory and different sparse solution both with the same number of nonzero elements.

5.3.2   NON-NEGATIVE CONSTRAINED

l_1-NORM OPTIMIZATION

The stiffness reduction prior can be imposed on the solution space as a non-negative constraint, that is $\Delta\theta \geq 0$, in accordance with eq. 5.2. This paper proposes the non-negative constrained basis pursuit (NNL1) to estimate the spatially sparsest reduction

in stiffness. The NNL1 convex optimization program is written as

$$\min_{\Delta\theta} \quad ||\Delta\theta||_1$$

$$\text{s.t.} \quad ||\mathbf{S}\Delta\theta - \Delta\lambda||_2 \leq \alpha \tag{5.8}$$

$$\Delta\theta \geq 0$$

The trade-off between sparsity and fit using α as defined for eq. 5.7 is also valid for the NNL1. The exception is α can be bounded by a value greater than zero below which the problem is infeasible. The smallest feasible α is unique and can be obtained from the optimal solution to the non-negative least squares (NNLS). The NNLS is a constrained convex optimization program taken as

$$\min_{\Delta\theta, \epsilon_0} \quad ||\epsilon_0||_2$$

$$\text{subject to} \quad \mathbf{S}\Delta\theta = \Delta\lambda + \epsilon_0 \tag{5.9}$$

$$\Delta\theta \geq 0$$

where $\epsilon_0 \in \Re^q$ is an optimization variable. Since the NNLS is strictly convex in ϵ_0, then an optimal point minimizing the NNLS (ϵ_0^*) is unique by definition [20]. Since $||\epsilon_0^*||_2$ is the unique global minimum to the NNLS, then the NNL1 is only feasible if $\alpha \geq ||\epsilon_0^*||_2$.

By considering the trade-off between the degree of sparsity and fit, we expect that if $\alpha = ||\epsilon_0^*||_2$, then the NNL1 yields the best fit solution and one that is sparse containing at most q-nonzero elements. The set of vectors satisfying the infimum of the NNL1 when $\alpha = ||\epsilon_0^*||_2$ is of primary importance in this paper since it shares information with the non-negative least squares solution while also being sparse enough

for physical interpretation.

5.3.3 Measure of uniqueness

The set of all possible vectors satisfying the infimum to the specified optimization program is defined as its optimal set. We define the optimal set of the NNLS with

$$S_{NN} = \{\Delta\theta^* | \; \mathbf{S}\Delta\theta^* = \widetilde{\Delta\lambda}, \; \Delta\theta^* \geq 0\}$$

where for convenience $\widetilde{\Delta\lambda} = \Delta\lambda + \epsilon_0^*$. Note that the optimal set to the NNL1 evaluated at $\alpha = ||\epsilon_0^*||_2$ is a subset of S_{NN}. We are interested in quantifying bounds on S_{NN} as an aid for interpreting the legitimacy of the sparse solution resulting from the NNL1. Consider the following argument. In addition to the system of equations, $\mathbf{S}\Delta\theta = \widetilde{\Delta\lambda}$, additional equations may arise when the non-negative constraint is active on elements of the optimal point $\Delta\theta_i^* = 0$. Hence, sparse solutions tend to induce additional equations through the non-negative constraint thus improving the proximity to a unique solution. From optimization theory, this phenomenon can be attributed to the complementary slackness condition [20]. If a total of $p - q$ non-negative constraints are active on $\Delta\theta_i^* = 0$, then S_{NN} is a singleton set. This phenomenon was frequently observed for a variety of damage cases using a numerically simulated shear beam, 2D truss, and 3D truss [21]. In the case the S_{NN} is a singleton, then the optimal set has one unique point and that optimal point simultaneously satisfies the infimum of the NNL1 and the NNLS. If the optimal point is not unique, we can quantify bounds on S_{NN} to determine a metric for the optimal set's size, or in other words, its proximity to a unique solution.

An intuitive approach to determining bounds on S_{NN} was provided in [28] based on similar techniques developed in [31]. We may interpret bounds on S_{NN} as the worst-case distance between any two members of the solution set satisfying the NNLS for each vector coordinate. This is equivalent to solving the following convex optimization program for all p coordinates:

$$
\begin{aligned}
d_k = \max_{\Delta\theta' \geq 0,\, \Delta\theta \geq 0} \quad & \Delta\theta_k - \Delta\theta'_k \\
\text{subject to} \quad & \mathbf{S}\Delta\theta = \widetilde{\Delta\lambda} \\
& \mathbf{S}\Delta\theta' = \widetilde{\Delta\lambda}
\end{aligned}
\tag{5.10}
$$

For intuition, d_k for $k = 1 \cdots p$ is the length of the kth side of the smallest hyper-cube containing S_{NN}. Eq. 5.10 can be reformulated using duality theory to obtain a single convex optimization program

$$
\begin{aligned}
\min_{\mathbf{Y},\mathbf{Y}',\tilde{d}} \quad & ||\tilde{d}||_1 \\
\text{subject to} \quad & (\mathbf{Y} - \mathbf{Y}')^T(\widetilde{\Delta\lambda}) = \tilde{d} \\
& \mathbf{Y}^T\mathbf{S} \geq \mathbf{I} \\
& \mathbf{Y}'^T\mathbf{S} \leq \mathbf{I}
\end{aligned}
\tag{5.11}
$$

where $\mathbf{Y}, \mathbf{Y}' \in \Re^{pxq}$ are optimization variables.

Since each coordinate $\tilde{d}_k$ is an upper bound on d_k and strong duality holds, then $||\tilde{d}^*||_1$ provides a metric on the bounds of S_{NN}. In [32], it was proven that if $||\tilde{d}^*||_1 = 0$ then S_{NN} was a singleton. It follows from $||\tilde{d}^*||_1 = 0$ that $\Delta\theta^*$ is the unique optimal point to both the NNLS and the NNL1 evaluated at $\alpha = ||\epsilon_0^*||_2$. Hence we refer to $||\tilde{d}^*||_1$ as the measure of uniqueness.

Although eq. 5.11 has a clear interpretation when $||\tilde{d}||_1 = 0$, the implications of $||\tilde{d}^*||_1 > 0$ are unclear. In order to interpret a non-zero measure of uniqueness, this paper derives an upper bound on $||\tilde{d}||_1$ to normalize about. For convenience, let $\mathbf{M} = (\mathbf{Y} - \mathbf{Y}')^T$. The optimal point $\tilde{d}^*$ of eq. 5.11 remains unchanged if the objective function is substituted with $||\mathbf{M}\widetilde{\Delta\lambda}||/||\widetilde{\Delta\lambda}||$. By definition of an induced matrix norm, $||\mathbf{M}\widetilde{\Delta\lambda}||/||\widetilde{\Delta\lambda}|| \leq ||\mathbf{M}||$. Hence, if we normalize $||\tilde{d}||_1$ with $||\widetilde{\Delta\lambda}||_1$, then an upper bound on the uniqueness measure can be determined by the following convex optimization program

$$\delta_{ub} = \min_{\mathbf{Y},\mathbf{Y}'} \quad ||\mathbf{Y} - \mathbf{Y}'||_1$$

$$\text{subject to} \quad \mathbf{Y}^T\mathbf{S} \geq \mathbf{I} \tag{5.12}$$

$$\mathbf{Y}'^T\mathbf{S} \leq \mathbf{I}$$

Using the upper bound, we implement the measure of uniqueness as

$$\delta = \frac{||\tilde{d}||_1}{\delta_{ub}||\Delta\lambda + \epsilon_0^*||_1} \ , \ 0 \leq \delta \leq 1 \tag{5.13}$$

Note that if eq. 5.12 is feasible then S_{NN} must be bounded. This program is always feasible since the sensitivity matrix has all non-positive entries.

5.4   TRUSS MODEL

This section provides a description of the FE model of the experimental truss and the three damage scenarios. Ideal numerical simulations based on the truss model are used in the following sections to verify and illustrate the methodologies. A more detailed

description of the physical truss and damage cases are provided in the experimental validation section.

The simulated 3D truss is a beam element model based on the physical description of the 17.24m long aluminum truss. Fig. 5.1 presents a plan view of the truss with overall dimensions and descriptive labels. The truss is comprised of aluminum cylindrical tubes each having modulus of elasticity of 69.64 GPa, density of 2714.5 kg/m^3, and Poisson's ratio equal to 0.33. Fig. 5.2a presents the beam element model demarcated by the 11 bays. The FE model is comprised of 144 beam elements. The boundary conditions were pinned in all three directions at the end of bay 1, and pinned in the y and z directions at the end of bay 11. The stiffness matrix was condensed to the translation degrees of freedom associated with the z and y coordinates. The first six natural frequencies of the condensed FE model are presented in Table 5.1. Their associated mode shapes are presented in Fig. 5.13. Fig. 5.2b-e presents the naming convention for each cluster of elements defining a section of the truss. The element groups are intended to help convey the results of the simulations to the reader.

Three damage cases are studied. Each of the three damage cases was modelled as an approximate reduction in the damaged element's elastic modulus proportional to the reduction in axial stiffness expected in the physical experiments. The three damage cases are in shown in Fig. 5.3. DC1 consists of a 30% reduction in the elastic modulus at bay 9, DC2 consists of an 82% reduction in elastic modulus at the same element in bay 9, and DC3 consists of 82% reductions in stiffness at bay 5 and bay 9. For clarity, note that the damaged element in Bay 9 is parallel to the $x - y$ plane, and the damage element in Bay 5 is parallel to the $x - z$ plane.
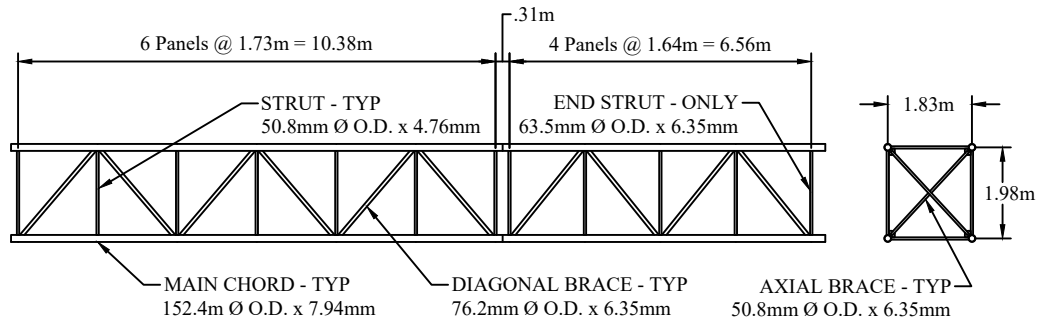
Figure 5.1: Plan view of the truss with dimensions and nomenclature
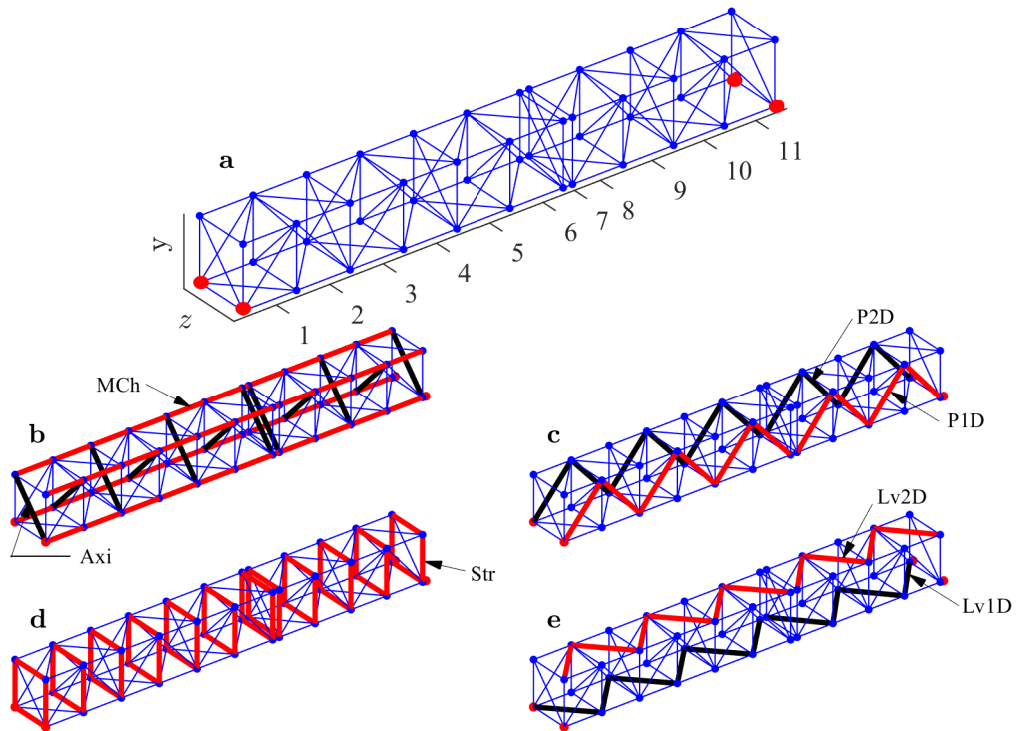
Figure 5.2: a) 3D truss model with bays numbered 1-11. Red nodes indicate locations of boundary conditions. Clusters of elements defining the truss sections use the following naming conventions: b) main chords in red (MCh) and axial diagonals (Axi) in black, c) diagonal braces at plane 1 (P1D) in red and diagonal braces in plane 2 (P2D) in black, d) struts (Str) in red, and e) diagonal braces at level 1 (Lv1D) in black and diagonal braces at level 2 (Lv2D) in red
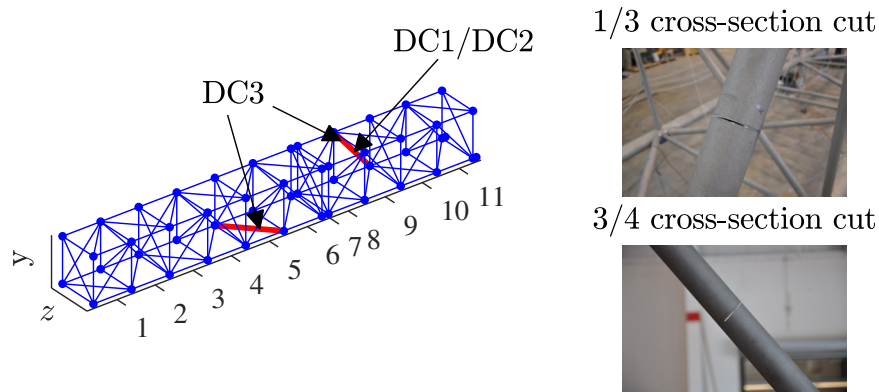
Figure 5.3: Damage locations indicated in red accompanied by photos of the true damage. Damage Case 1 (DC1): 1/3rd cut located at bay 9. Damage Case 2 (DC2): 3/4th cut located at Bay 9. Damage Case 3 (DC3): 3/4th cut located at bay 5 and bay 9

5.5 NUMERICAL SIMULATIONS

This section presents a series of ideal numerical simulations representative of the experiment to follow. The purpose of the numerical simulations is to compare l_1-norm optimization and non-negative least squares as standalone programs while verifying the non-negative constrained basis pursuit and the measure of uniqueness. The simulations are ideal because the model used to derive the algorithms is also the one used to generate the data.

Fig. 5.4 presents the solution path for the basis pursuit denoising as a function of the regularization parameter (eq. 5.7) for the three damage cases. Each line color represents a different section of the truss denoted by the legend. Superimposed over the truss is the solution when $\alpha = 0$ (the basis pursuit). From Fig. 5.4, l_1-norm optimization fails to deliver meaningful solutions in all three damage cases. In contrast, the non-negative constraint forces additional equations from which a solution that is sparse and meaningful is obtained. Fig. 5.5 presents the estimated
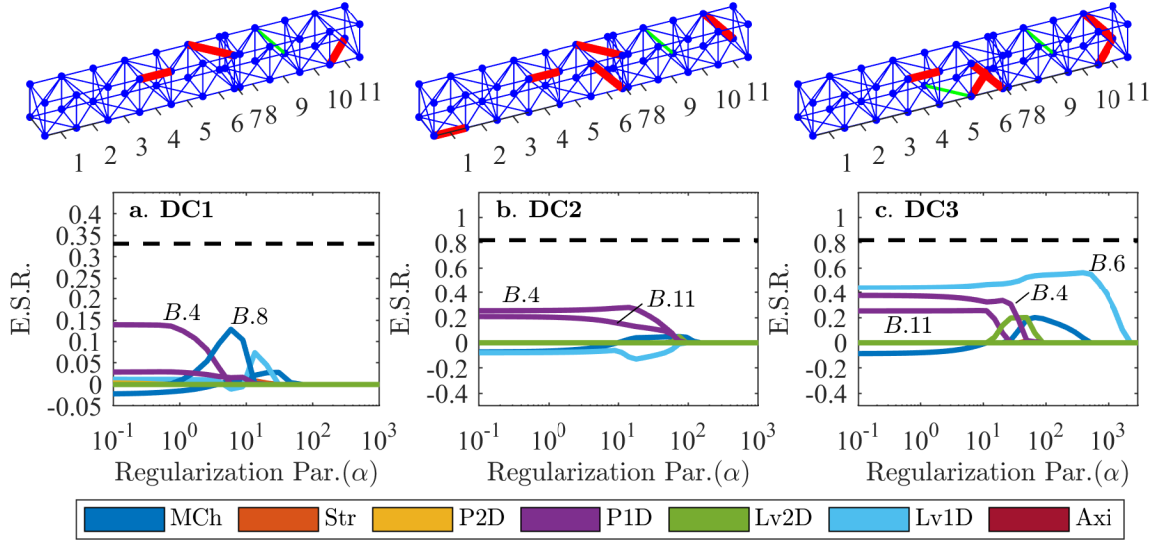
Figure 5.4: Estimated stiffness reduction (E.S.R.) using the basis pursuit denoising and 6 natural frequencies plotted as a function of the regularization parameter (α) for a) damage case 1, b) damage case 2, and c) damage case 3

stiffness reductions for the three damage cases using the non-negative least squares (eq. 5.9). In DC1, the optimal point to the NNLS identifies the damage exactly. As the damage severity increases to DC2, noting Fig. 5.6b, the NNLS preserves the correct damage location and provides an acceptable approximation of magnitude albeit overestimated. As the linear truncation error increases, so does the optimal solution $||\epsilon_0^*||_2$. In DC3, the NNLS fails to identify the damaged elements. The optimal point to the NNLS, although displaying apparent peaks, is not sparse.

Fig. 5.6 presents the estimated stiffness reduction using the NNL1 (eq. 5.8) for the three damage cases along with the measure of uniqueness (δ). In DC1 and DC2, $\delta = 0$ indicates that the optimal points for the NNLS and the NNL1 are identical. As the number of damage locations increase to DC3, the uniqueness measure results in $\delta > 0$, which indicates that the optimal point is not unique. Where the NNLS
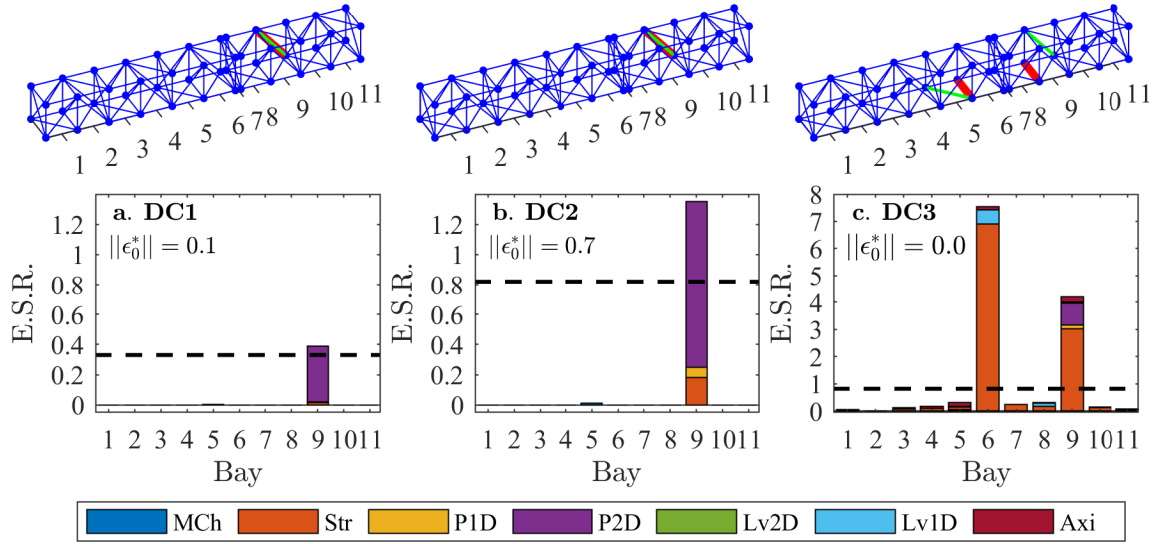
Figure 5.5: Estimated stiffness reduction (E.S.R.) using the non-negative least squares and 6 eigenvalues for a) damage case 1, b) damage case 2, and c) damage case 3

failed to deliver an interpretable solution, the non-negative basis pursuit provides a reasonable estimation in term of quantity, sparsity, and location. Note that the stiffness parameters at Lv1D bays 5 and 6 are nearly inseparable given that a small perturbation in each induces nearly identical changes in the 6 eigenvalues.

5.6 Uniqueness measure investigation

5.6.1 Interpretation

As indicated in the previous example, the measure of uniqueness provides information to interpret the characteristics of the solution to the NNL1 and the NNLS. If S_{NN} is not a singleton (i.e. $\delta > 0$) then the NNLS fails to deliver a sparse and meaningful solution. On the contrary, the NNL1 is expected to always yield a sparse and non-
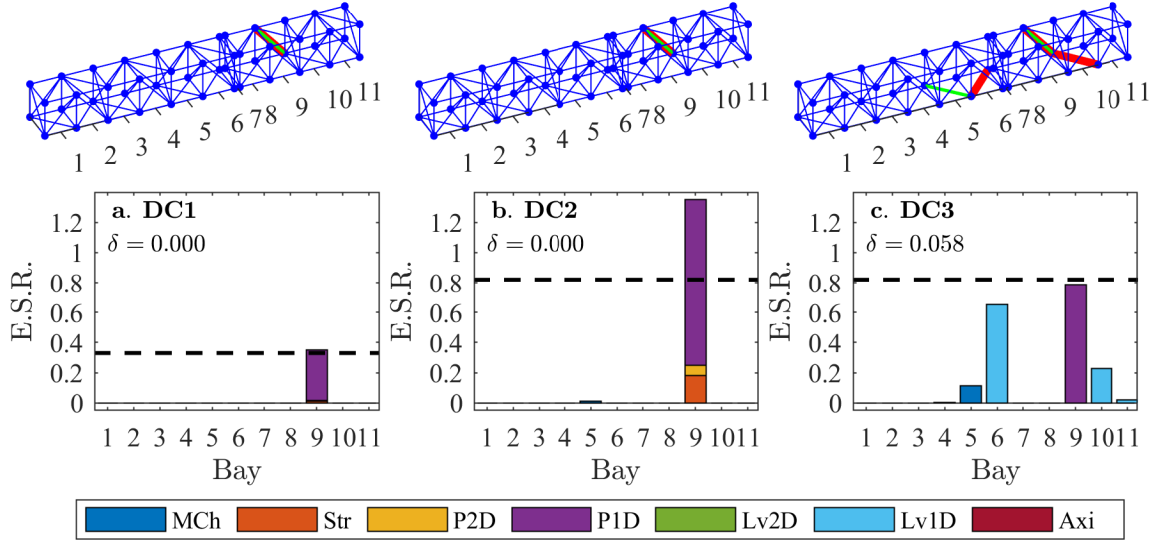
Figure 5.6: Estimated stiffness reduction (E.S.R) using the non-negative basis pursuit with 6 eigenvalues for a) damage case 1, b) damage case 2, and c) damage case 3. δ is the measure of uniqueness

negative solution. Although the NNL1 provides an opportunity to identify the damage where the NNLS fails (see DC3), the lack of uniqueness implies that the optimal point to the NNL1 is one sparse solution among other satisfactory solutions. How then can we decide if the sparse solution to the NNL1 is physically meaningful in the case where the solution is not unique? This paper suggests when the measure of uniqueness is large, the optimal point to the NNL1 is more likely meaningless since the non-negative constraints are not providing additional equations. Since the non-negative constraints only act as equations where $\Delta\theta_i = 0$, then we can deduce that the underlying solution has too many non-zero elements relative to available equations to solve the underdetermined system of equations. We now proceed to substantiate this claim with the following numerical simulations.

We first quantify the normalization term δ_{ub} as a function of the total identified

natural frequencies, evaluating δ_{ub} between 2 and 8 natural frequencies (see Fig. 5.7a). Consider the normalized measure of uniqueness δ as a function of the number of identified frequencies and the number of damage locations. Beginning with DC2 as the single damage location case, then DC3 as the two location case, we iteratively produce 82% reductions at other arbitrarily selected beam elements until 9 elements have been damaged. Fig. 5.7b presents δ as a function of damage location and total number of identified natural frequencies. Observe from Fig. 5.7b that as the total number of damage locations increases, δ increases consistently across every tested natural frequency case. This trend clearly indicates that as the solution becomes less sparse (i.e. more damage locations) the measure of uniqueness increases. Also observe that as the number of identified natural frequencies increases, δ tends to decrease. Finally, consider that the number of damage locations must be less than the number of identified frequencies to obtain a meaningful solution. With that consideration, we observe that large values of δ consistently indicate a failed attempt at identifying a physically meaningful solution.
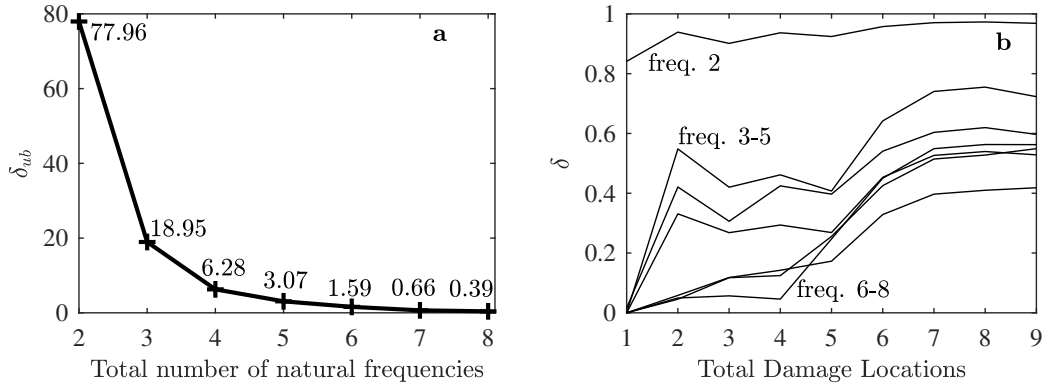
Figure 5.7: a) Estimated upper bound on the uniqueness measure as a function of total identified natural frequencies. b) Normalized measure of uniqueness as a function of total identified frequencies and total number of damage locations

113

5.6.2 REGULARIZATION

The measure of uniqueness can also help interpret the need for regularization. Consider the following. Again, the optimal points for the NNL1 and the NNLS are identical when $\delta = 0$ and $\alpha = ||\epsilon_0^*||_2$. Since these solutions are identical, we can infer that the l_1-norm was not active in the NNL1 and therefore no regularization took place in the traditional sense of penalizing the magnitude of the solution. In the presence of measurement error, it may be necessary to maintain a small solution norm if the sensitivity matrix is ill-conditioned. Therefore, when the solution is unique, we suggest to perturb the regularization parameter by a small amount in order to activate the l_1-norm if necessary. From observation of testing these methods, if a small change in $||\mathbf{S}\Delta\theta - \Delta\lambda||_2$ results in a significant decrease in $||\Delta\theta||_1$, then the regularization parameter should be incrementally relaxed until the optimal solution to the non-negative basis pursuit becomes stable. This process is akin to regularization parameter selection using the L-curve method.

To illustrate this phenomenon, consider as an example the optimal solution trade-off curves shown in Fig. 5.8 for two different realizations of DC2 with an arbitrary level of measurement error added to $\Delta\lambda$. In both cases, the solution to the NNLS is unique. However, in case (a), if the estimated stiffness reduction is based on the optimal point at $\alpha = ||\epsilon_0^*||_2$, we obtain an incorrect solution with an unrealistically large l_1-norm ($||\Delta\theta^*||_1 = 10$). However by perturbing the regularization parameter, the optimal point rapidly moves to a more reasonable solution occurring at the L-curve criterion. Notice that Fig. 5.8a exhibits the classic shape of the L-curve with a well defined corner, while Fig. 5.8b does not. The L-curve phenomenon is a result of ill-

conditioning. The underdetermined matrix cannot be defined as ill-conditioned since the matrix is already rank deficient. Instead, we can treat the sensitivity matrix as an overdetermined (or exact) system of equations by forming a new matrix comprised of the columns of the sensitivity matrix associated with the non-zero elements of the optimal point to the NNLS. Then calculating the condition of the reduced sensitivity matrix, measured by the ratio of its smallest and largest singular values, we find an indicative discrepancy in conditioning between the two examples. In Fig. 5.8a the condition of the reduced sensitivity matrix is approximately 500, while the condition of the reduced sensitivity matrix in Fig. 5.8b is only 54.8. Since case (a) is poorly conditioned, it is necessary to regularize in the traditional sense, hence the need for the L-curve criteria. On the other hand, case (b) is well conditioned and hence lacks the sharp corner. These results are consistent with the examples provided in [2].
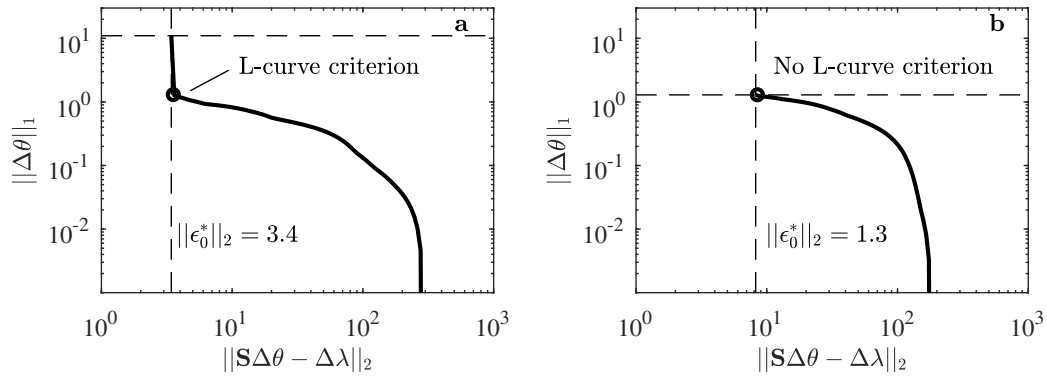
Figure 5.8: Optimal solution trade-off curves for DC2 with measurement error in the case a) exhibiting the L-curve criterion, and b) not exhibiting L-curve criterion

5.6.3 NUMERICAL VERIFICATION IN THE PRESENCE OF MEASUREMENT ERROR

The performance of the proposed NNL1 with the combined interpretation from the uniqueness measure is investigated in the presence of measurement error. Measurement noise is defined by the vector $\epsilon \in \Re^q$ and is added to both the eigenvalues associated with the undamaged and damaged structure. ϵ is defined as a realization of a q-dimensional Gaussian random vector with zero mean and standard deviation of component ϵ_i proportional to the specified coefficient of variation. Four tests with coefficients of variation (CoV) equal to 0.0005, 0.001, 0.0015, and 0.002 were performed. The range of values selected for the CoV were obtained from uncertainty quantification studies in system identification [33]. DC3 is investigated. In quantifying the probability of detection, a successful detection occurred when the maximum values of $\Delta\theta^*$ contained the correct damage locations and their values were 50% larger than any other element. For DC3, we allowed Lv1D bay 5 and 6 to both indicate a correct damage location given that these elements are inseparable in terms of their associated eigenvalue sensitivity.

Fig. 5.9 presents the probability of detection (PoD) and the statistics of δ: the median value, and the 25th and 75th percentiles as functions of the total number of identified frequencies. The method was performed on 500 realizations of ϵ for each test. Each sub-figure corresponds to one of the four CoV values. Consider first the difference between the solid and dashed black lines. The dashed is the PoD if the regularization parameter perturbation addressed in the previous subsection is not considered. Notice that this PoD is significantly lower than when the perturbation is

116

used (solid line). Consider the uniqueness measure. From Fig. 5.9a-d, there is clear indication in the PoD and the uniqueness measure that the NNL1 requires at least 6 natural frequencies to successfully identify DC3. Two important observations are made: i) independent of noise, large values of uniqueness indicate that the number of frequencies is insufficient to identify the correct solution and ii) a low-value or a unique solution does not aid in discerning successful detection in the presence of measurement error.
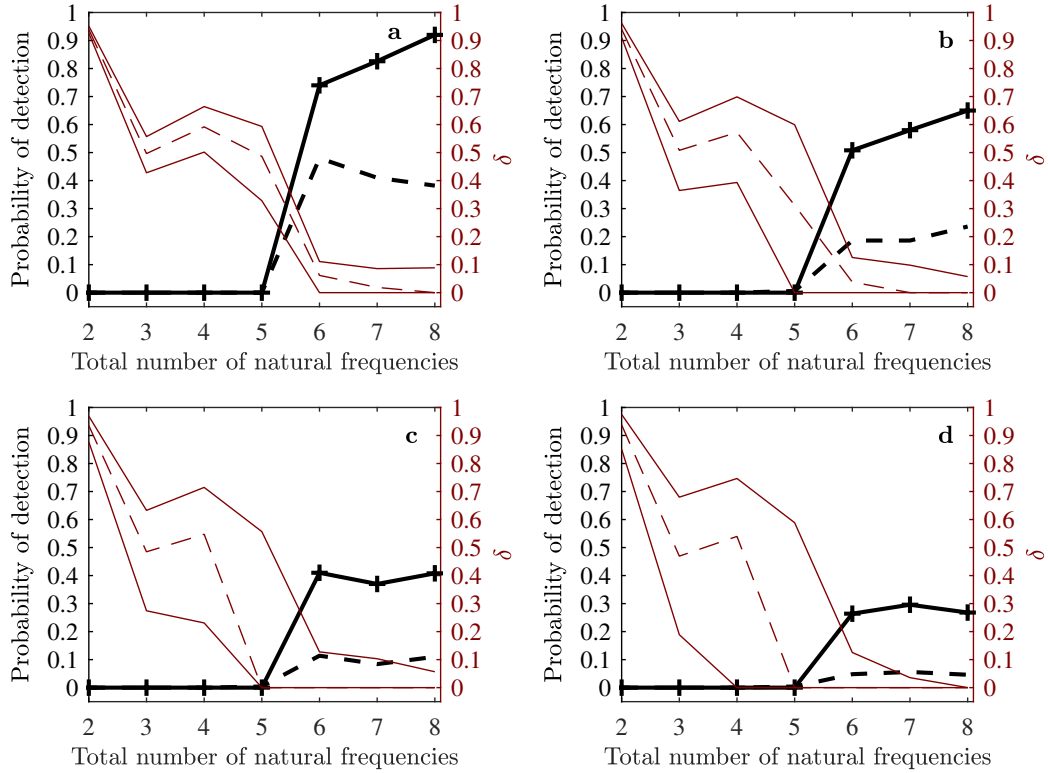
Figure 5.9: Probability of detection for DC3 with regularization perturbation (thick black line) and without perturbation (dashed black line) presented as functions of the number of natural frequencies for the coefficients of variation: a) 0.0005, b) 0.001, c) 0.0015, and d) 0.002. The median (dashed) and 25th and 75th percentiles (solid) for the measure of uniqueness shown with thin red lines.

5.7 Experiment physical description

The experimental structure used to validate the proposed methods is a highway sign support truss tested at Purdue University [34]. A series of modal tests were conducted on the truss in various damage states. The vibration data and all the necessary experiment details were originally made publicly available through the Network for Earthquake Engineering Simulations and is now available in [34]. Fig. 5.10a presents a photo of the truss taken during the time of testing. The three-dimensional structure is comprised of two truss sections bolted together at 10.38m from the left-hand side (Fig. 5.10b) with each section constructed entirely by welded 6061-T6 aluminum pipes. The axial braces were welded to aluminum stiffener plates that offset the ends of each axial brace from the outer diameter of the main chord by approximately 7.5cm (Fig. 5.10c). Fig. 5.1 presents the plan view of the truss with additional details.
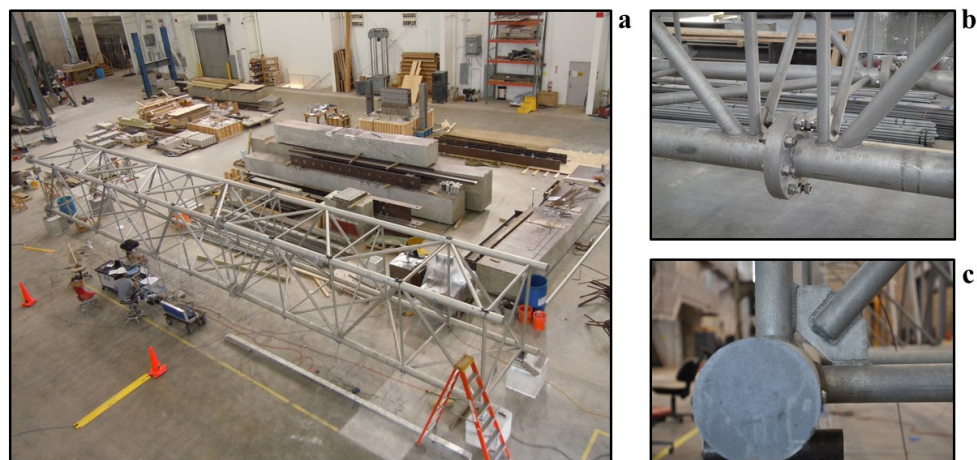
Figure 5.10: Photos of a) the experimental truss taken during the time of testing, b) one of the four bolted splines at bay 7, and c) a typical axial brace-stiffener assembly [34]

Three successive damage cases were introduced to the truss, each damage state a progression from the previous damage state. The first damage state, damage case 1 (DC1), consists of a 0.3cm thick saw-cut driven $1/3^{rd}$ the pipe's diameter deep located at the center of a vertically oriented diagonal brace at bay 9. After the DC1 vibration tests were performed, additional material was removed from the existing saw-cut increasing the cut depth to approximately $3/4^{th}$ the pipe's diameter. This saw-cut constitutes damage case 2 (DC2). For the third damage state, damage case 3 (DC3), a second saw-cut $3/4^{th}$ the pipe's diameter deep was introduced to a transverse oriented diagonal brace at bay 5. Photos of the $1/3^{rd}$ and $3/4^{th}$ thick saw-cuts are presented in Fig. 5.3 along with the locations of the damage superimposed over the truss model. Since the baseline structure was established and tested prior to introducing the damage, any unintended damage accumulation or changes in environmental conditions between tests would not be normalized for. Hence, this experiment emulates the properties inherent to the field application of an SHM system.

5.7.1 FINITE ELEMENT MODEL

The FE model used to verify the methodologies is also the model used to derive the sensitivity matrix for the physical system. Additional details on the model updating are provided for completeness. The FE model was constructed in the software ANSYS using a physical description of the truss. After initial model construction, the primary beam elements associated with the diagonal and axial braces were discretized again at each end to provide a mechanism to perform model updating as shown in Fig. 5.11. The connection elements were then updated to account for the increased flexibility of the welds and the offset of the connections. The axial stiffness of the updating

parameters associated with the vertically oriented and transverse oriented diagonals were all assigned the same stiffness reduction based on the results from a high fidelity model of the connections. After the initial updating, a single parameter defining all axial brace connections (elements labelled (1) in Fig. 5.11) was updated to improve the modal match with those identified from the vibration data taken from the baseline structure. The model was calibrated using only the three mentioned parameters.
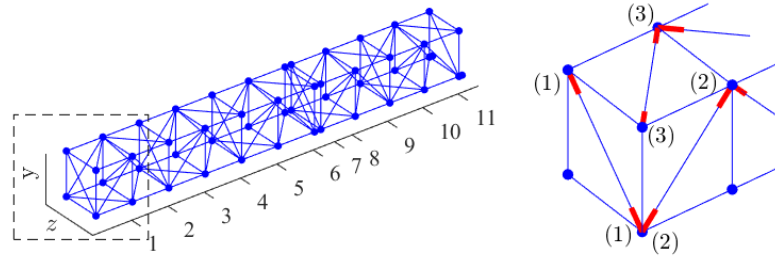
Figure 5.11: Locations of the three model updating parameters: (1) axial braces, (2) vertically oriented diagonals, and (3) transverse oriented diagonals

5.8 MODAL TESTS AND ANALYSIS

This section provides details on the physical test setup. The vibration data acquisition system consisted of 22 uni-directional (PCB 333B40) accelerometers. In order to maximize the number of observable modes, the data acquisition system was assembled into four various output configurations each comprised of the 22 sensors. Fig. 5.12 presents the locations and orientations of the sensors comprising each output configuration as well as the nomenclature used to reference each test setup i.e. $y1$, $y2$, $z1$, $z2$. For each output configuration,the dynamic response was induced using two types of vertically oriented forced oscillation: the electro-dynamic shaker (VG-100

from Vibration Test Systems), and the modal sledge hammer (PCB 086D50). The shaker input consisted of band limited white noise at 0 - 200 Hz. For each hammer test, between 14 and 17 hammer strikes were delivered. Measurements were taken for 320 seconds at a 512 Hz sampling frequency for both experiments.
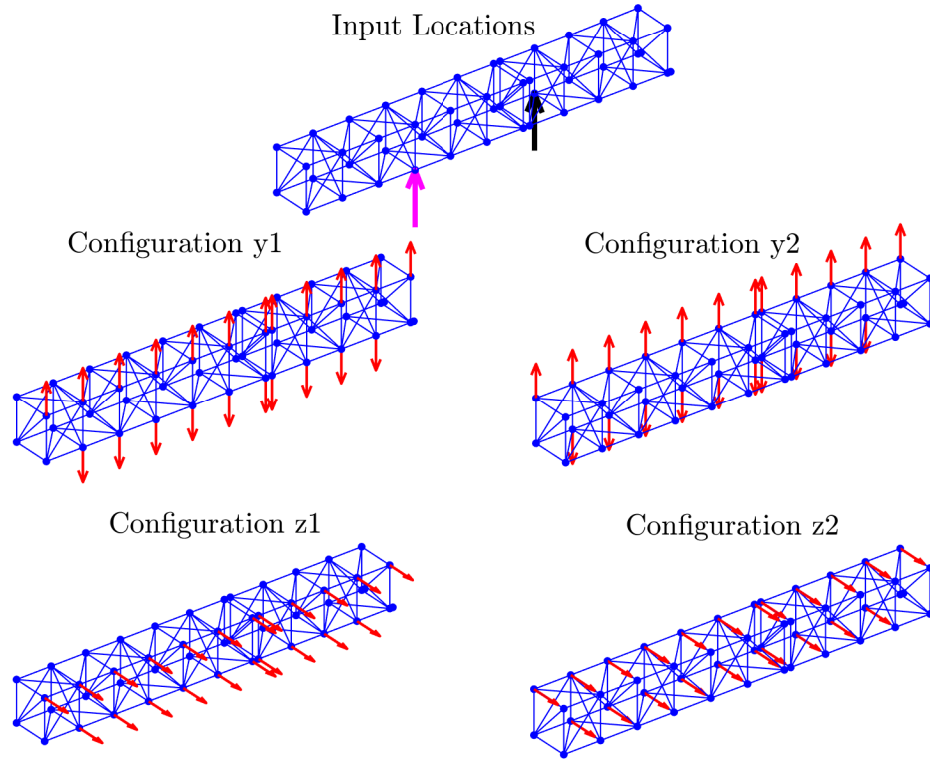
Figure 5.12: Excitation-input locations and sensor-output configurations

5.8.1 SYSTEM IDENTIFICATION

Modal analysis was performed in two parts: first the extraction of the mode shapes necessary for matching the modes from the model to the physical system, followed by the extraction of natural frequencies used to implement the damage identification algorithms. For each of the 8 possible single-input multi-output test setups, the sub-

space identification algorithm was used to extract the mode shapes. The mode shapes obtained were stitched together using the coincident nodes shared with an additional triaxial sensor configuration not shown. At 6 samples per cycle, 40 Hz was considered a reasonable upper bound on the largest identifiable natural frequency. After identifying the mode shapes, six modes that also could be produced by the FE model were selected for damage identification implementation. Fig. 5.13 presents the mode shapes produced by the FE model shown in blue superimposed over those identified and averaged in red. Note strong agreement with modes exhibiting uni-directional motion, such as 1st transverse bending, 1st vertical bending, and 2nd vertical bending, and weaker agreement with modes exhibiting bi-planar motion. For the purposes of modal matching, the observed agreement was sufficient.

One simple yet effective method for identifying natural frequencies is to calculate the frequency response function (FRF) for each single-input single-output sensor combination and select the peaks. By identifying modes from each sensor, the contribution to uncertainty from the sensor noise could be estimated. Regarding the shaker excitation, the FRF, being the ratio of the power spectral densities of the measured input and output, was obtained using Welch's method with a Hamming window segmented into seven sections. The power spectral densities of the hammer tests were obtained using the same method, except the window spanned each hammer strike. The power spectral densities were then averaged. Fig. 5.14 presents a sample FRF calculated from the shaker test and the y_1 and z_1 sensor at bay 6. The example highlights that the obsevability of the modes dependend on sensor orientation. In the example presented in Fig. 5.14, the 2nd transverse mode at 21.3 Hz was only observable in the z-oriented sensor, while the 2nd vertical mode at 32.6 Hz was only
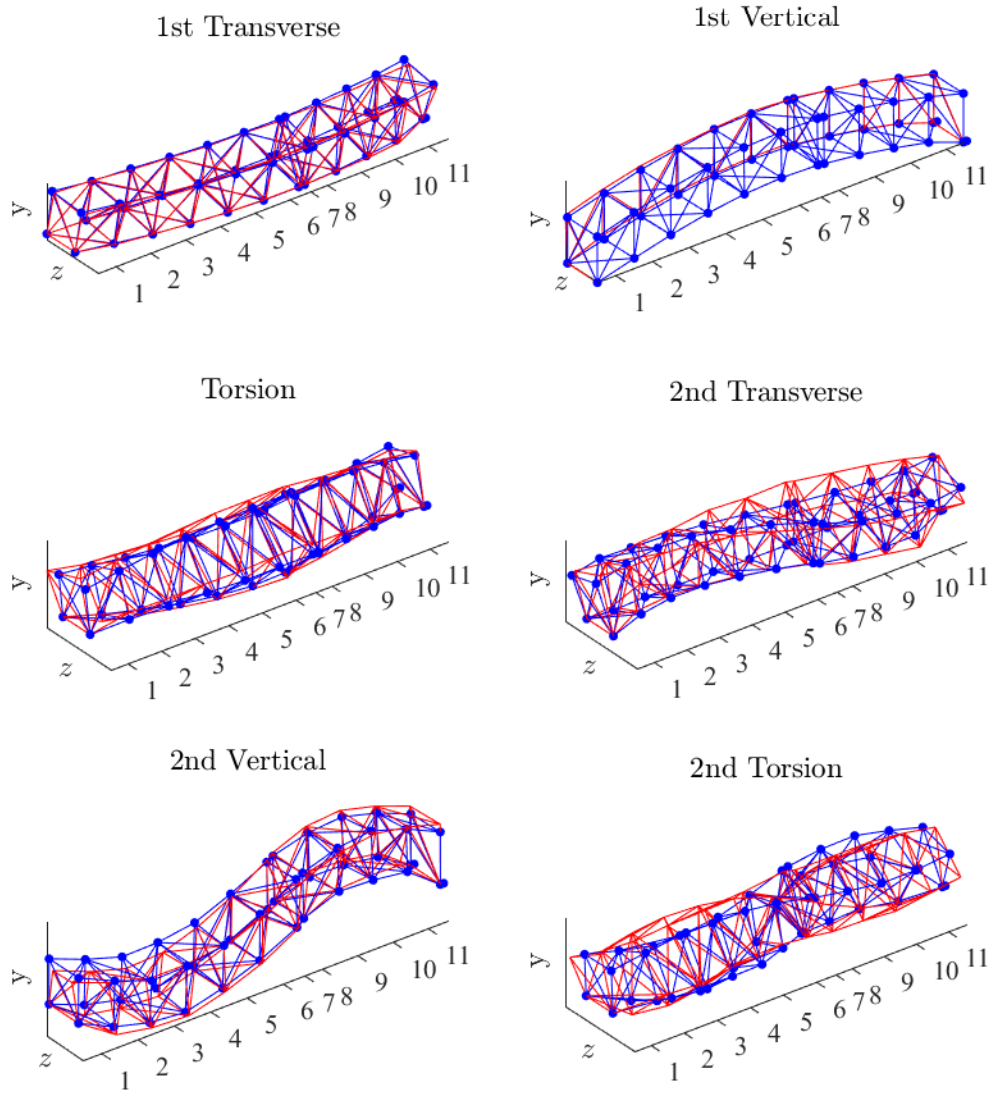
Figure 5.13: The six mode shapes selected for implementation. The averaged identified mode shape presented in red superimposed over the modes produced by the FE model in blue

observable in the *y*-oriented sensor. There were 9 observable modes in the 40 Hz range, however, only 6 were produced by the FE model. The 6 labeled modes in Fig. 5.14 are those that were selected and implemented for damage identification.
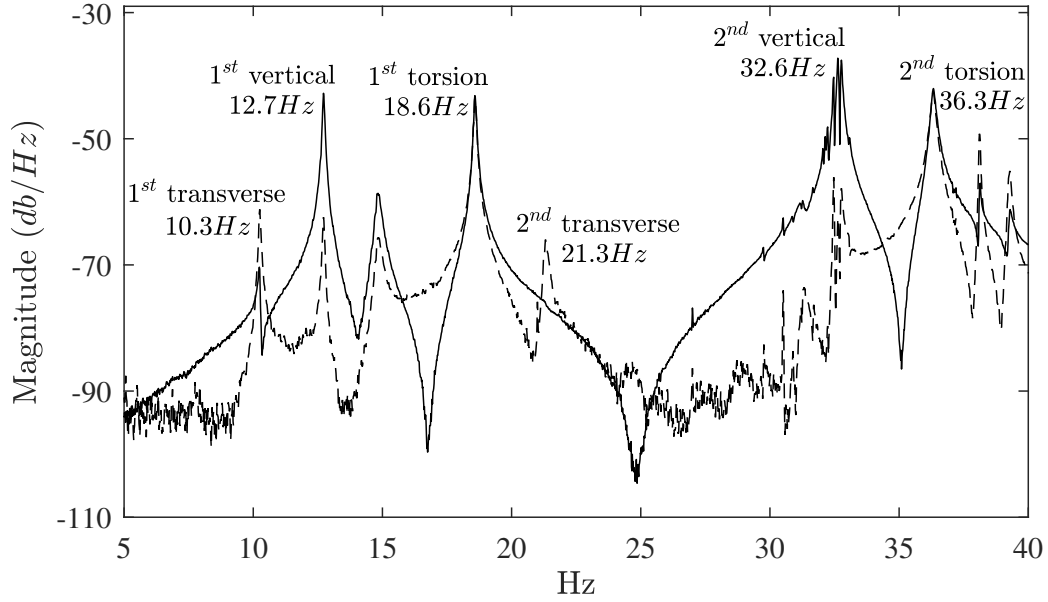
Figure 5.14: Sample FRF evaluated from the shaker input using outputs $y1$ (solid line) and $z1$ (dashed line) at bay 6. Labelled modes are those selected for damage identification implementation

5.8.2 SUMMARY OF IDENTIFIED NATURAL FREQUENCIES AND SOURCES OF UNCERTAINTY

Table 5.1 provides a summary of the average identified natural frequencies for each of the four tested structural states. The average percent deviation of the listed natural frequencies are compared to those identified from the undamaged structure. The error between the natural frequencies produced by the updated FE model and those identified from the undamaged structure was large ($\approx 6\%$). This relative error is significant because the change in natural frequencies induced by damage ($< 2\%$) is overshadowed by the model uncertainty. Hence, it would be impossible to identify damage without comparing relative shifts in the identified natural frequencies between the undamaged and damaged structure.

124

To convey the sources of uncertainty in the modal tests, Table 5.2 provides the coefficient of variation for each mode measured across all possible single-input single-output sensor combinations for all 8 test setups. Juxtaposed is the average coefficient of variation for each mode identified from the 22 sensors comprising a single test setup then averaged across all 8 test setups. The first statistic estimates the variance of the natural frequencies identified from every test, while the second statistic estimates the variance corresponding to an individual sensor. A comparison of the two statistics reveals that the contribution to uncertainty from the test setup far outweighed the contribution from measurement noise and system identification error. The uncertainty due to measurement noise was reasonably low ($< .001$). The variation between tests were orders of magnitude larger than values indicated in literature relating to uncertainty quantification of identified natural frequencies [33]. Since the authors were not present during the time of testing, they cannot provide an adequate physical explanation for the source of this significant error.

Table 5.1: Comparison of Average Modal Frequencies (Hz)

	FE Model-undamaged	Undamaged	DC I	DC II	DC III
$1^{st}\ Trans.$	11.46	10.23	10.09	10.23	10.19
$1^{st}\ Vert.$	13.65	12.72	12.64	12.54	12.56
$1^{st}\ Tors.$	17.35	18.61	18.43	18.50	18.48
$2^{nd}\ Trans.$	22.74	21.34	20.98	21.22	20.45
$2^{nd}\ Vert.$	33.93	32.63	32.62	32.58	32.53
$2^{nd}\ Tors.$	36.01	36.20	35.97	35.86	35.11
Av. Deviate	**6.07%**	-	**0.88%**	**0.61%**	**1.64%**

Table 5.2: Average Coefficient of Variation (σ/μ)

	1st Trans.	1st Vert.	1st Tors.	2nd Trans.	2nd Vert.	2nd Tors.
All Tests	.014	.0047	.0065	.0140	.0005	.0039
Sensor Noise	.0008	.0006	.0001	.0008	.0001	.0009

5.9 Experimental validation results

This section summarizes the results of the proposed non-negative constrained basis pursuit in identifying damage on the 3D truss using changes in the natural frequencies identified from the vibration measurements. The proposed method was implemented on the average of all the test setups shown in Fig. 5.12; their average values summarized in Table 5.1. In considering the probability of detection in the previous measurement error investigations presented in Fig. 5.9, it was unlikely that successful damage identification was possible using a single realization of the natural frequencies given how large the variance in the identified frequencies were. By averaging, we minimized the intolerable level of uncertainty in the test setups. Despite using all of the sensors for the presentation of these results, we could also have used data from 1 sensor from each test configuration and ended up with similar results since the variance between sensors was reasonably low.

Fig. 5.15 presents the estimated stiffness reduction using the NNL1 along with the measure of uniqueness for DC1, DC2, and DC3. In DC1, shown in Fig. 5.15a, the NNL1 algorithm fails to locate the 1/3rd saw-cut at bay 9. However, the measure of uniqueness ($\delta = 0.409$) reflects the lack of a unique solution indicating that the obtained sparse solution is not physically meaningful. This result may be reasonable

given that the 1/3rd saw-cut most likely did not produce a statistically significant change in the natural frequencies. In DC2, shown in Fig. 5.15b, the NNL1 accurately identifies the damage at bay 9 though overestimates the magnitude of the damage. The measure of uniqueness ($\delta = 0.075$) satisfies the condition that the optimal set of the NNLS should be tightly bounded for a meaningful solution. Finally in DC3, shown in Fig. 5.15c, the estimated stiffness reduction is a unique solution ($\delta = 0$). The algorithm predicts damage at bay 6 adjacent to the true damage and indicates the second damage location at bay 9. The bay 6 estimation, though adjacent to the true damage, is consistent with the numerical simulations. Although the predicted damage at Bay 9 is located at the P1D member, this is a good result given that P1D and P2D are nearly colinear due to the local symmetry between between the two vertically oriented planes. Other indications that the damage is detected is that the identified damage locations are oriented in the same direction as the true damaged elements, and that the estimated stiffness reduction at bay 9 is approximately equal in both DC2 and DC3. Despite these positives, the algorithm does significantly overestimate the stiffness reduction at bay 5.

5.10 CONCLUSION

Although natural frequencies extracted from global vibrations lack sufficient information to uniquely estimate unknown model parameters for the purposes of model updating or other general applications, they can be sufficient to uniquely identify damage described by sparse reductions in stiffness. Previous research suggests imposing sparsity on the solution space with l_1-norm optimization or non-negative least
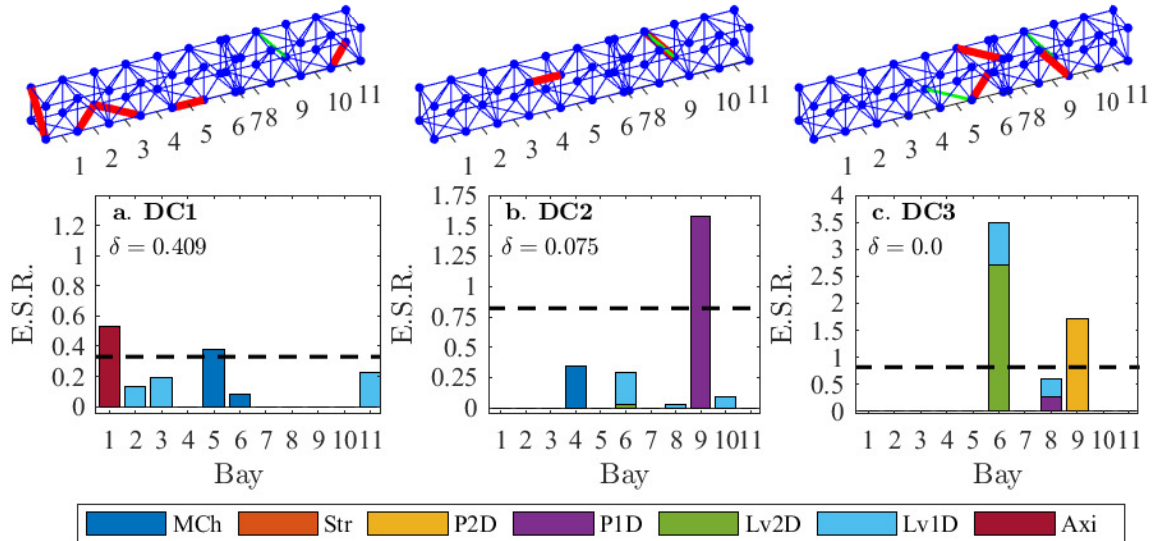
Figure 5.15: Estimated stiffness reduction and measure of uniqueness using the non-negative constrained basis pursuit implemented on vibration data taken from DC1, DC2, and DC3

squares in order to obtain meaningful solutions. This paper argues as standalone applications, they exhibit clear disadvantages: (i) the lack of regularization using the non-negative least squares, and (ii) forced sparse solutions using l_1-norm optimization. However by determining the intersection of their optimal set of solutions using the non-negative constrained l_1-norm optimization (NNL1), these deficiencies are abated or improved upon.

This paper shows that the optimal set of solutions for the NNL1 is contained in the optimal set of the non-negative least squares. This paper verifies using measurement noise, that if the non-negative least squares has a unique solution, i.e. its optimal set is a singleton, then the regularization parameter should be relaxed to check for ill-conditioning. In cases where the optimal set to the non-negative least squares is not unique and hence fails to deliver a sparse and meaningful solution, the non-negative constrained l_1-norm optimization can provide improvement by enforcing

128

sparsity. However, if the bounds on the optimal set to the NNL1 are large than this implies that the forced sparse solution of the NNL1 is likely physically meaningless.

The proposed NNL1 method is validated using vibration data measured from a full-scale 17.24 m long aluminum 3D truss subjected to three progressive damage cases. The truss model contains 144 possible damage locations and only 6 natural frequencies were identified from the vibration data. Despite significant model error and a severely underdetermined inverse problem, we considered the results of all three damage cases successful validations.

For future work, the authors wish to improve the tightness of the measured bounds on the optimal set to the non-negative least squares, and verify and validate the concepts provided in this work on a wider range of structures and in more severe environments. In addition, only the linearized inverse problem is solved and hence estimated solutions needs improvement in terms of quantification. In future work, we will address how to update the solution in order to more accurately quantify the magnitude of the damage.

ACKNOWLEDGEMENTS

Bibliography

[1] M. I. Friswell, J. E. Mottershead, H. Ahmadian, Finite-element model updating using experimental test data: parametrization and regularization, Philos. Trans. R. Soc. A Math. Phys. Eng. Sci. 359 (2001) 169–186.

[2] J. E. Mottershead, M. Link, M. I. Friswell, The sensitivity method in finite element model updating: A tutorial, Mech. Syst. Signal Process. 25 (7) (2011) 2275–2296.

[3] D. L. Donoho, Compressed sensing, IEEE Trans. Inf. Theory 52 (4) (2006) 1289–1306.

[4] E. M. Hernandez, Identification of isolated structural damage from incomplete spectrum information using l1-norm minimization, Mech. Syst. Signal Process. 46 (1) (2014) 59–69.

[5] M. Kaouk, D. C. Zimmerman, Structural damage assessment using a generalized minimum rank perturbation theory, AIAA J. 32 (4) (1994) 836–842.

[6] S. W. Doebling, Minimum-rank optimal update of elemental stiffness parameters for structural damage identification, AIAA J. 34 (12) (1996) 2615–2621.

[7] A. M. Bruckstein, D. L. Donoho, M. Elad, From sparse solutions of systems of equations to sparse modeling of signals and images, SIAM Rev. 51 (1) (2009) 34–81.

[8] T. Hastie, R. Tibshirani, M. Wainwright, Statistical Learning with Sparsity: The Lasso and Generalizations, Chapman & Hall/CRC Monographs on Statistics & Applied Probability, CRC Press, 2015.

[9] E. J. Candes, J. Romberg, T. Tao, Robust uncertainty principles: exact signal reconstruction from highly incomplete frequency information, IEEE Trans. Inf. Theory 52 (2) (2006) 489–509.

[10] B. Qiao, X. Zhang, J. Gao, R. Liu, X. Chen, Sparse deconvolution for the large-scale ill-posed inverse problem of impact force reconstruction, Mech. Syst. Signal Process. 83 (2017) 93–115.

[11] Y. Bao, J. L. Beck, H. Li, Compressive sampling for accelerometer signals in structural health monitoring, Struct. Heal. Monit. 10 (3) (2011) 235–246.

[12] E. M. Hernandez, Identification of localized structural damage from highly incomplete modal information : theory and experiments, J. Eng. Mech. 142 (2) (2016) 1–9.

[13] X. Q. Zhou, Y. Xia, S. Weng, L1 regularization approach to structural damage detection using frequency data, Struct. Heal. Monit. An Int. J. 14 (6) (2015) 571–582.

[14] S. Zhou, Y. Bao, H. Li, Structural damage identification based on substructure sensitivity and l1 sparse regularization, in: Proc. SPIE - Int. Soc. Opt. Eng., 2013.

[15] R. Hou, Y. Xia, X. Zhou, Structural damage detection based on l1 regularization using natural frequencies and mode shapes, Struct. Control Heal. Monit. 25 (3).

[16] C. B. Smith, E. M. Hernandez, Detection of spatially sparse damage using impulse response sensitivity and LASSO regularization, Inverse Probl. Sci. Eng. 27 (1) (2019) 1–16.

[17] D. Sen, A. Aghazadeh, A. Mousavi, S. Nagarajaiah, R. Baraniuk, Sparsity-based approaches for damage detection in plates, Mech. Syst. Signal Process. 117 (2019) 333–346.

[18] R. J. Link, D. C. Zimmerman, Structural damage diagnosis using frequency response functions and orthogonal matching pursuit: theoretical development, Struct. Control Heal. Monit. 22 (6) (2015) 889–902.

[19] N. Grip, N. Sabourova, Y. Tu, Sensitivity-based model updating for structural damage identification using total variation regularization, Mech. Syst. Signal Process. 84 (2017) 365–383.

[20] S. Boyd, L. Vandenberghe, Convex optimization, Cambridge university press, 2004.

[21] C. B. Smith, E. M. Hernandez, Non-negative constrained inverse eigenvalue problems - Application to damage identification, Mech. Syst. Signal Process. 129 (2019) 629–644.

[22] C. R. Farrar, S. W. Doebling, D. A. Nix, Vibration-based structural damage identification, Philos. Trans. R. Soc. London. Ser. A Math. Phys. Eng. Sci. 359 (1778) (2001) 131–149.

[23] X. Y. Li, S. S. Law, Adaptive Tikhonov regularization for damage detection based on nonlinear model updating, Mech. Syst. Signal Process. 24 (6) (2010) 1646–1664.

[24] D. L. Donoho, J. Tanner, Sparse nonnegative solution of underdetermined linear equations by linear programming, Proc. Natl. Acad. Sci. 102 (27) (2005) 9446–9451.

[25] A. M. Bruckstein, M. Elad, M. Zibulevsky, On the uniqueness of nonnegative sparse solutions to underdetermined systems of equations, IEEE Trans. Inf. Theory 54 (11) (2008) 4813–4820.

[26] M. Wang, W. Xu, A. Tang, A unique "nonnegative" solution to an underdetermined system: From vectors to matrices, IEEE Trans. Signal Process. 59 (3) (2011) 1007–1016.

[27] S. Hassiostis, G. Jeong, Identification of stiffness reductions using natural frequencies, J. Eng. Mech. 121 (10) (1995) 1106–1113.

[28] K. Dillon, Y. P. Wang, Imposing uniqueness to achieve sparsity, Signal Processing 123 (2016) 1–8.

[29] M. Grant, S. Boyd, {CVX}: Matlab Software for Disciplined Convex Programming, version 2.1, \url{http://cvxr.com/cvx} (2014).

[30] R. Fox, M. Kapoor, Rates of change of eigenvalues and eigenvectors., AIAA J. 6 (12) (1968) 2426–2429.

[31] R. J. Tibshirani, The lasso problem and uniqueness, Electron. J. Stat. 7 (2013) 1456–1490.

[32] K. Dillon, Y. Fainman, Bounding pixels in computational imaging., Appl. Opt. 52 (10) (2013) 55–63.

[33] E. Reynders, R. Pintelon, G. De Roeck, Uncertainty bounds on modal parameters obtained from stochastic subspace identification, Mech. Syst. Signal Process. 22 (4) (2008) 948–969.

[34] S. Dyke, S. Krishnan, Z. Sun, 144 DOF Dynamic Measurement from a 50' Full Scale Highway Sign Support Truss (NEES-2011-1013), \url{https://datacenterhub.org/resources/14462} (2017).

CHAPTER 6

CONCLUSION

This research concludes that the inverse problem in vibration-based structural health monitoring aimed at damage identification requires significantly less measurements to solve than what is needed to ensure uniqueness provided: (i) damage produces a sufficiently sparse reduction in the stiffness and(or) mass parameters, and (ii) sparsity and(or) non-negativity are imposed on the solution space.

The findings of this research suggest that for severely underdetermined inverse problems, such as the ones exhibited by strictly using eigenvalues, l_1-norm optimization may not be sufficient for practical application since (i) it does not recover unique solutions, (ii) it forces sparsity which is not necessarily desirable since the solution may in fact be the realization of uncertainty unrelated to damage, and (iii) may be too weak in applications to full-scale structures. However, if the damage strictly reduces stiffness and(or) mass, these issues are clearly improved upon or abated by imposing both non-negativity and sparsity on the solution space. These conclusions are evidenced by successful attempts at identifying damage on a four-story lab-scale frame and a 17 m long 3D truss using the proposed non-negative constrained l_1-norm

optimization method while the standalone application of l_1-norm optimization failed. The specific conclusions of each chapter are as follows:

- Chapter 4 finds that the linearized underdetermined inverse problem is uniquely solvable with respect to the optimal set satisfying the non-negative constrained least squares only if there exists a solution that is sufficiently sparse. The optimal solution is only unique and meaningful if a sufficiently sparse solution exists. We prove that the linearized inverse eigenvalue problem satisfies the necessary conditions to obtain a unique solution if the sensitivity matrix is defined by changes in stiffness only. The non-negative constrained nonlinear least squares also shows a similar tendency to a unique solution. In the presence of measurement error, the non-negative constrained method performs adequately, however its robustness to measurement error may be problematic if the changes in stiffness induced by damage are insignificant in size.

- In chapter 5, this work finds that when the sensitivity matrix is defined by stiffness and mass, it violates the necessary conditions for the non-negative least squares to induce a unique solution. In addition, the l_1-norm optimization as a standalone program performs poorly in identifying both stiffness and mass. The proposed combined method, the non-negative constrained l_1-norm optimization, does however recover meaningful solutions to both the linear and nonlinear inverse problem. The method is experimentally validated using vibration data measured from a four-story lab-scale steel frame. The frame highlights an important challenge in using eigenvalues. Since unique measurements are limited, it is common to have quasi-dependent parameters due to global and local geometric symmetries. These quasi-dependent parameters should be identified

134

prior to solving the inverse problem in order to determine possible uniqueness issues with the obtained solution.

- In chapter 6, we show that the optimal solution sets to the non-negative constrained l_1 norm optimization and the non-negative least squares intersect. We find that measuring the bounds on the optimal set satisfying the non-negative least squares provides a meaningful interpretation to the non-negative l_1-norm optimization method. The proposed method and our interpretation to the measure on solution bounds are validated using vibration data measured from a 17 m long aluminum 3D truss subject to three damage cases. The results of this experiment demonstrate the method's robustness to significant model error. However, since only the linear inverse problem was solved, only the location of damage was determined. Quantification necessitates further solution updating to account for non-linearity in the inverse problem.

Although the proposed methods were tested on a variety of structures including a full-scale experiment, the performance of the proposed methods in operational environments are unknown and require further investigation. We suggest for future work to determine tight bounds on the maximum number of identifiable damage locations given a specified number of eigenvalues. In terms of broader future studies, we suggest investigating how sparsity can be leveraged to detect the presence of local damage and discern true damage from signal noise or changes in environment. One potential damage indicator appears with the proposed measure of uniqueness, where the existence of a sparse solution due to damage induced solution uniqueness. However, the damage detection application requires further investigation.

Bibliography

[Abdel Wahab et al., 1999] Abdel Wahab, M., De Roeck, G., and Peeters, B. (1999). Parameterization of damage in reinforced concrete structures using model updating. *J. Sound Vib.*, 228(4):717–730.

[Ahmadian et al., 1998] Ahmadian, H., Mottershead, J., and Friswell, M. (1998). Regularization methods for finite element model updating. *Mech. Syst. Signal Process.*, 12(1):47–64.

[Bao et al., 2011] Bao, Y., Beck, J. L., and Li, H. (2011). Compressive sampling for accelerometer signals in structural health monitoring. *Struct. Heal. Monit.*, 10(3):235–246.

[Berman, 1984] Berman, A. (1984). System identification of structural dynamic models - Theoretical and practical bounds. In *AIAA Conf. Pap. 84-0929*.

[Berman and Flannelly, 1971] Berman, A. and Flannelly, W. G. (1971). Theory of incomplete models of dynamic structures. 9(8):1481–1486.

[Boyd and Vandenberghe, 2004] Boyd, S. and Vandenberghe, L. (2004). *Convex optimization*. Cambridge university press.

[Brewer, 1977] Brewer, J. W. (1977). The derivative of the exponential matrix with respect to a matrix. *IEEE Trans. Automat. Contr.*, 22(4):656–657.

[Brownjohn, 2007] Brownjohn, J. M. (2007). Structural health monitoring of civil infrastructure. *Philos. Trans. R. Soc. A Math. Phys. Eng. Sci.*, 365(1851):589–622.

[Bruckstein et al., 2009] Bruckstein, A. M., Donoho, D. L., and Elad, M. (2009). From sparse solutions of systems of equations to sparse modeling of signals and images. *SIAM Rev.*, 51(1):34–81.

[Bruckstein et al., 2008] Bruckstein, A. M., Elad, M., and Zibulevsky, M. (2008). On the uniqueness of nonnegative sparse solutions to underdetermined systems of equations. *IEEE Trans. Inf. Theory*, 54(11):4813–4820.

[Candes et al., 2006] Candes, E. J., Romberg, J., and Tao, T. (2006). Robust uncertainty principles: exact signal reconstruction from highly incomplete frequency information. *IEEE Trans. Inf. Theory*, 52(2):489–509.

[Cattaneo et al., 2013] Cattaneo, A., Theiler, J., and Farrar, C. (2013). Compressed sensing techniques for detecting damage in structures. *Struct. Heal. Monit.*, 4(12):325–338.

[Cawley and Adams, 1979] Cawley, P. and Adams, R. D. (1979). The location of defects in structures from measurements of natural frequencies. *J. Strain Anal. Eng. Des.*, 14(2):49–57.

[Chellini et al., 2010] Chellini, G., De Roeck, G., Nardini, L., and Salvatore, W. (2010). Damage analysis of a steel-concrete composite frame by finite element model updating. *J. Constr. Steel Res.*, 66(3):398–411.

[Choi and Stubbs, 2004] Choi, S. and Stubbs, N. (2004). Damage identification in structures using the time-domain response. *J. Sound Vib.*, 275(3-5):577–590.

[Chu, 1998] Chu, M. T. (1998). Inverse eigenvalue problems. *SIAM Rev.*, 40(1):1–39.

[Dillon and Fainman, 2013] Dillon, K. and Fainman, Y. (2013). Bounding pixels in computational imaging. *Appl. Opt.*, 52(10):55–63.

[Dillon and Wang, 2016] Dillon, K. and Wang, Y. P. (2016). Imposing uniqueness to achieve sparsity. *Signal Processing*, 123:1–8.

[Doebling, 1996] Doebling, S. W. (1996). Minimum-rank optimal update of elemental stiffness parameters for structural damage identification. *AIAA J.*, 34(12):2615–2621.

[Doebling et al., 1997] Doebling, S. W., Farrar, C. R., and Goodman, R. S. (1997). Effects Of measurement statistics on the detection of damage in the Alamosa Canyon Bridge. In *Proc. 15th Int. Modal Anal. Conf.*, volume 1, pages 919–929.

[Doebling et al., 1996] Doebling, S. W., Farrar, C. R., Prime, M. B., and Shevitz, D. W. (1996). Damage identification and health monitoring of structural and mechanical systems from changes in their vibration characteristics: A literature review. Technical report.

[Döhler et al., 2013] Döhler, M., Lam, X. B., and Mevel, L. (2013). Uncertainty quantification for modal parameters from stochastic subspace identification on multi-setup measurements. *Mech. Syst. Signal Process.*, 36(2):562–581.

[Donoho, 2006] Donoho, D. L. (2006). Compressed sensing. *IEEE Trans. Inf. Theory*, 52(4):1289–1306.

[Donoho and Tanner, 2005] Donoho, D. L. and Tanner, J. (2005). Sparse nonnegative solution of underdetermined linear equations by linear programming. *Proc. Natl. Acad. Sci.*, 102(27):9446–9451.

[Dyke et al., 2017] Dyke, S., Krishnan, S., and Sun, Z. (2017). 144 DOF Dynamic Measurement from a 50' Full Scale Highway Sign Support Truss (NEES-2011-1013). \url{https://datacenterhub.org/resources/14462}.

[Engl et al., 2000] Engl, H., Hanke, M., and Neubauer, A. (2000). *Regularization of Inverse Problems*. Kluwer Academic Publishers, The Netherlands.

[Farrar and Worden, 2013a] Farrar, C. and Worden, K. (2013a). *Structural Health Monitoring: A Machine Learning Perspective*. John Wiley & Sons Ltd.

[Farrar and Worden, 2013b] Farrar, C. and Worden, K. (2013b). Structural Health Monitoring: A Machine Learning Perspective. chapter Damage-Sen, pages 234–237. John Wiley & Sons Ltd.

[Farrar et al., 2001] Farrar, C. R., Doebling, S. W., and Nix, D. A. (2001). Vibration-based structural damage identification. *Philos. Trans. R. Soc. London. Ser. A Math. Phys. Eng. Sci.*, 359(1778):131–149.

[Figueiredo et al., 2011] Figueiredo, E., Figueiras, J., and Park, G. (2011). Influence of autoregressive model order on damage detection. *Int. J. Comput. Civ. Infrastruct. Eng.*, 26(3):225–238.

[Fox and Kapoor, 1968] Fox, R. and Kapoor, M. (1968). Rates of change of eigenvalues and eigenvectors. *AIAA J.*, 6(12):2426–2429.

[Friswell, 2007] Friswell, M. I. (2007). Damage identification using inverse methods. *Philos. Trans. R. Soc. A Math. Phys. Eng. Sci.*, 365:393–410.

[Friswell and Mottershead, 1995] Friswell, M. I. and Mottershead, J. (1995). *Finite element model updating in structural dynamics*. Springer Science & Business Media Dordrecht.

[Friswell et al., 1998] Friswell, M. I., Mottershead, J. E., and Ahmadian, H. (1998). Combining subset selection and parameter constraints in model updating. *J. Vib. Acoust.*, 120(4):854.

[Friswell et al., 2001] Friswell, M. I., Mottershead, J. E., and Ahmadian, H. (2001). Finite-element model updating using experimental test data: parametrization and regularization. *Philos. Trans. R. Soc. A Math. Phys. Eng. Sci.*, 359:169–186.

[Fritzen et al., 1998] Fritzen, C., Jennewein, D., and Kiefer, T. (1998). Damage detection based on model updating methods. *Mech. Syst. Signal Process.*, 12(1):163–186.

[Gladwell, 1986] Gladwell, G. M. (1986). Inverse problems in vibration. *Appl. Mech. Rev.*, 39(7):1013–1018.

[Gladwell and Ahmadian, 1995] Gladwell, G. M. and Ahmadian, H. (1995). Generic element matrices suitable for finite element model updating. *Mech. Syst. Signal Process.*, 9(6):601–614.

[Görl and Link, 2003] Görl, E. and Link, M. (2003). Damage identification using changes of eigenfrequencies and mode shapes. *Mech. Syst. Signal Process.*, 17(1):103–110.

[Grant and Boyd, 2014] Grant, M. and Boyd, S. (2014). {CVX}: Matlab Software for Disciplined Convex Programming, version 2.1. \url{http://cvxr.com/cvx}.

[Grip et al., 2017] Grip, N., Sabourova, N., and Tu, Y. (2017). Sensitivity-based model updating for structural damage identification using total variation regularization. *Mech. Syst. Signal Process.*, 84:365–383.

[Hassiostis and Jeong, 1995] Hassiostis, S. and Jeong, G. (1995). Identification of stiffness reductions using natural frequencies. *J. Eng. Mech.*, 121(10):1106–1113.

[Hassiotis, 2000] Hassiotis, S. (2000). Identification of damage using natural frequencies and Markov parameters. *Comput. Struct.*, 74(3):365–373.

[Hastie et al., 2015] Hastie, T., Tibshirani, R., and Wainwright, M. (2015). *Statistical Learning with Sparsity: The Lasso and Generalizations.* Chapman & Hall/CRC Monographs on Statistics & Applied Probability. CRC Press.

[Hearn and Testa, 1991] Hearn, G. and Testa, R. B. (1991). Modal analysis for damage detection in structures. *J. Struct. Eng.*, 117(10):3042–3063.

[Hernandez, 2014] Hernandez, E. M. (2014). Identification of isolated structural damage from incomplete spectrum information using l1-norm minimization. *Mech. Syst. Signal Process.*, 46(1):59–69.

[Hernandez, 2016] Hernandez, E. M. (2016). Identification of localized structural damage from highly incomplete modal information : theory and experiments. *J. Eng. Mech.*, 142(2):1–9.

[Hou et al., 2018a] Hou, R., Xia, Y., Bao, Y., and Zhou, X. (2018a). Selection of regularization parameter for l1-regularized damage detection. *J. Sound Vib.*, 423:141–160.

[Hou et al., 2018b] Hou, R., Xia, Y., and Zhou, X. (2018b). Structural damage detection based on l1 regularization using natural frequencies and mode shapes. *Struct. Control Heal. Monit.*, 25(3).

[Imregun et al., 1995] Imregun, M., Sanliturk, K. Y., and Ewins, D. J. (1995). Finite element model updating using frequency response function data - II. Case study on a medium-size finite element model. *Mech. Syst. Signal Process.*, 9(2):203–213.

[Jang and Smyth, 2017] Jang, J. and Smyth, A. W. (2017). Model updating of a full-scale FE model with nonlinear constraint equations and sensitivity-based cluster analysis for updating parameters. *Mech. Syst. Signal Process.*, 83:337–355.

[Juang, 2002] Juang, J. (2002). *Applied System Identification*. Prentice Hall, Upper Saddle River, NJ.

[Kaltenbacher, 1997] Kaltenbacher, B. (1997). Some Newton-type methods for the regularization of nonlinear ill-posed problems. *Inverse Probl.*, 13(3):729–753.

[Kaouk and Zimmerman, 1994] Kaouk, M. and Zimmerman, D. C. (1994). Structural damage assessment using a generalized minimum rank perturbation theory. *AIAA J.*, 32(4):836–842.

[Law and Li, 2006] Law, S. S. and Li, X. Y. (2006). Wavelet-based sensitivity analysis of the impulse response function for damage detection. *J. Appl. Mech.*, 74(2):375–377.

[Li and Law, 2010] Li, X. Y. and Law, S. S. (2010). Adaptive Tikhonov regularization for damage detection based on nonlinear model updating. *Mech. Syst. Signal Process.*, 24(6):1646–1664.

[Link and Weiland, 2009] Link, M. and Weiland, M. (2009). Damage identification by multi-model updating in the modal and in the time domain. *Mech. Syst. Signal Process.*, 23(6):1734–1746.

[Link and Zimmerman, 2015] Link, R. J. and Zimmerman, D. C. (2015). Structural damage diagnosis using frequency response functions and orthogonal matching pursuit: theoretical development. *Struct. Control Heal. Monit.*, 22(6):889–902.

[MATLAB, 2018] MATLAB (2018). *version 7.4.0 (R2018a)*. The MathWorks Inc., Natick, Massachusetts.

[Moaveni et al., 2013] Moaveni, B., Stavridis, A., Lombaert, G., Conte, J. P., and Shing, P. B. (2013). Finite-element model updating for assessment of progressive damage in a 3-story infilled RC frame. *J. Struct. Eng.*, 139(10):1665–1674.

[Moser and Moaveni, 2011] Moser, P. and Moaveni, B. (2011). Environmental effects on the identified natural frequencies of the Dowling Hall Footbridge. *Mech. Syst. Signal Process.*, 25(7):2336–2357.

[Mottershead and Foster, 1991] Mottershead, J. E. and Foster, C. D. (1991). On the treatment of ill-conditioning in spatial parameter estimation from measured vibration data. *Mech. Syst. Signal Process.*, 5(2):139–154.

[Mottershead and Friswell, 1993] Mottershead, J. E. and Friswell, M. I. (1993). Model updating in structural dynamics: A survey. *J. Sound Vib.*, 167(2):347–375.

[Mottershead et al., 2011] Mottershead, J. E., Link, M., and Friswell, M. I. (2011). The sensitivity method in finite element model updating: A tutorial. *Mech. Syst. Signal Process.*, 25(7):2275–2296.

[Natke, 1988] Natke, H. G. (1988). Updating computational models in the frequency domain based on measured data: a survey. *Probabilistic Eng. Mech.*, 3(1):28–35.

[Neubauer, 1989] Neubauer, A. (1989). Tikhonov regularisation for non-linear ill-posed problems: Optimal convergence rates and finite-dimensional approximation. *Inverse Probl.*, 5(4):541–557.

[Pintelon et al., 2007] Pintelon, R., Guillaume, P., and Schoukens, J. (2007). Uncertainty calculation in (operational) modal analysis. *Mech. Syst. Signal Process.*, 21(6):2359–2373.

[Pothisiri and Hjelmstad, 2003] Pothisiri, T. and Hjelmstad, K. (2003). Structural damage detection and assessment from modal response. *J. Eng. Mech.*, 129(2):135–145.

[Qiao et al., 2017] Qiao, B., Zhang, X., Gao, J., Liu, R., and Chen, X. (2017). Sparse deconvolution for the large-scale ill-posed inverse problem of impact force reconstruction. *Mech. Syst. Signal Process.*, 83:93–115.

[Ren and De Roeck, 2002] Ren, W. and De Roeck, G. (2002). Structural damage identification using modal data. I: Simulation verification. *J. Struct. Eng.*, 128(1):87–95.

[Reynders et al., 2008] Reynders, E., Pintelon, R., and De Roeck, G. (2008). Uncertainty bounds on modal parameters obtained from stochastic subspace identification. *Mech. Syst. Signal Process.*, 22(4):948–969.

[Richardson, 1980] Richardson, M. (1980). Detection of damage in structures from changes in their dynamic (modal) propertie- A survey.

[Rytter, 1993] Rytter, A. (1993). *Vibrational based inspection of civil engineering structures.* Phd thesis, University of Aalborg.

[Salawu, 1997] Salawu, O. S. (1997). Detection of structural damage through changes in frequency: A review. *Eng. Struct.*, 19(9):718–723.

[Sen et al., 2019] Sen, D., Aghazadeh, A., Mousavi, A., Nagarajaiah, S., and Baraniuk, R. (2019). Sparsity-based approaches for damage detection in plates. *Mech. Syst. Signal Process.*, 117:333–346.

[Shahverdi et al., 2009] Shahverdi, H., Mares, C., Wang, W., and Mottershead, J. E. (2009). Clustering of parameter sensitivities: Examples from a helicopter airframe model updating exercise. *Shock Vib.*, 16(1):75–87.

[Silva et al., 2016] Silva, T. A., Maia, N. M., Link, M., and Mottershead, J. E. (2016). Parameter selection and covariance updating. *Mech. Syst. Signal Process.*, 70-71:269–283.

[Simoen et al., 2015] Simoen, E., De Roeck, G., and Lombaert, G. (2015). Dealing with uncertainty in model updating for damage assessment: A review. *Mech. Syst. Signal Process.*, 56:123–149.

[Smith and Hernandez, 2018] Smith, C. B. and Hernandez, E. M. (2018). Detection of spatially sparse damage using impulse response sensitivity and LASSO regularization. *Inverse Probl. Sci. Eng.*, 27(1):1–16.

[Smith and Hernandez, 2019] Smith, C. B. and Hernandez, E. M. (2019). Non-negative constrained inverse eigenvalue problems - Application to damage identification. *Mech. Syst. Signal Process.*, 129:629–644.

[Teughels and De Roeck, 2004] Teughels, A. and De Roeck, G. (2004). Structural damage identification of the highway bridge Z24 by FE model updating. *J. Sound Vib.*, 278(3):589–610.

[Teughels et al., 2002] Teughels, A., Maeck, J., and De Roeck, G. (2002). Damage assessment by FE model updating using damage functions. *Comput. Struct.*, 80(25):1869–1879.

[Tibshirani, 1996] Tibshirani, R. J. (1996). Regression shrinkage and selection via the lasso. *J. R. Stat. Soceity B*, 58(1):267–288.

[Tibshirani, 2013] Tibshirani, R. J. (2013). The lasso problem and uniqueness. *Electron. J. Stat.*, 7:1456–1490.

[Tikhonov, 1963] Tikhonov, A. (1963). The solution of incorrectly formulated problems and the regularization method. *Dokl. Akad. Nauk. SSSR*, 151(3):501–504.

[Titurus and Friswell, 2008] Titurus, B. and Friswell, M. I. (2008). Regularization in model updating. *Int. J. Numer. Methods Eng.*, 75(4):440–478.

[Tropp, 2004] Tropp, J. A. (2004). Greed is good: Algorithmic results for sparse approximation. *IEEE Trans. Inf. Theory*, 50(10):2231–2242.

[Vandiver, 1975] Vandiver, J. (1975). Detection of structural failure on fixed platforms by measurement of dynamic response. In *7th Annu. Offshore Technol. Conf.*, pages 243–252.

[Vogel, 2002] Vogel, C. (2002). *Computational Methods for Inverse Problems.* S.I.A.M.

[Wang et al., 2011] Wang, M., Xu, W., and Tang, A. (2011). A unique "nonnegative" solution to an underdetermined system: From vectors to matrices. *IEEE Trans. Signal Process.*, 59(3):1007–1016.

[Weber et al., 2009] Weber, B., Paultre, P., and Proulx, J. (2009). Consistent regularization of nonlinear model updating for damage identification. *Mech. Syst. Signal Process.*, 23(6):1965–1985.

[Wu and Law, 2004] Wu, D. and Law, S. S. (2004). Model error correction from truncated modal flexibility sensitivity and generic parameters: Part Iâsimulation. *Mech. Syst. Signal Process.*, 18(6):1381–1399.

[Yan et al., 2012] Yan, G., Dyke, S. J., and Irfanoglu, A. (2012). Experimental validation of a damage detection approach on a full-scale highway sign support truss. *Mech. Syst. Signal Process.*, 28:195–211.

[Yang and Nagarajaiah, 2014] Yang, Y. and Nagarajaiah, S. (2014). Structural damage identification via a combination of blind feature extraction and sparse representation classification. *Mech. Syst. Signal Process.*, 45(1):1–23.

[Zhou et al., 2013] Zhou, S., Bao, Y., and Li, H. (2013). Structural damage identification based on substructure sensitivity and l1 sparse regularization. In *Proc. SPIE - Int. Soc. Opt. Eng.*

[Zhou et al., 2015] Zhou, X. Q., Xia, Y., and Weng, S. (2015). L1 regularization approach to structural damage detection using frequency data. *Struct. Heal. Monit. An Int. J.*, 14(6):571–582.

Appendix A

Detection of Spatially Sparse Damage Using Impulse Response Sensitivity and LASSO Regularization

Abstract

This paper presents an impulse response sensitivity approach enhanced with a least absolute shrinkage and selection operator (LASSO) regularization in order to detect spatially sparse (localized) damage. The analytical expression for impulse response sensitivity was derived using Vetter calculus. The proposed algorithm exploits the fact that when damage is sparse, an l_1-norm regularization is more suitable than the common least squares (l_2-norm) minimization. The proposed methodology is

145

successfully applied in the context of a simulated 21 degree of freedom non-uniform shear beam with noise-contaminated measurements, limited modal parameters, and limited sensor locations. Single input-single output and single input-two output cases are investigated.

A.1 INTRODUCTION

Damage is generally defined as any change that adversely affects the system's current or future performance. In some cases, such as corrosion, damage takes place over a large portion of the structural domain. However, in other cases, such as perforations, dents or cracks, damage takes place in a small region of the domain. Detecting localized damage from global vibration measurements is an appealing but challenging proposition of structural health monitoring (SHM). The appeal comes from the efficiency and cost effectiveness of monitoring large domains with a small number of sensors. The difficulties stem from a combinations of factors: (i) local damage has a limited effect on global vibrations, (ii) analytical damage sensitivity is affected by modeling errors and (iii) measurement noise can overshadow response changes due to damage. These effects combined conspire to make the problem ill-posed (non-unique solutions) and ill-conditioned (high sensitivity to measurement noise and model perturbations).

When a finite element model (FEM) is used to represent the structure of interest, localized damage can be modeled as a change in the corresponding stiffness and(or) damping of a small subset of elements (Fig. A.1). The change in stiffness and(or) damping manifests itself as changes in the structure's dynamic properties. In this

paper, we focus on changes in the impulse response. More specifically, this paper aims to use inverse sensitivity to map temporal changes in the impulse response to changes in the vector that describes the elastic properties of each element in the model.
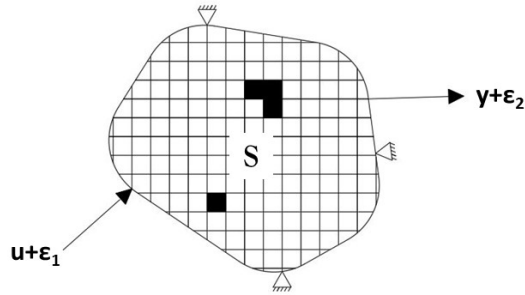
Figure A.1: Example k-sparse damages located on finite element mesh where $k = 4$. The impulse response of the system is evaluated using noisy single input-single output system

Searching through all possible combinations of damaged elements in order to find which one better represents the observed changes is clearly impractical, and not very elegant. Therefore it is necessary to simultaneously find effective algorithms and impose realistic constraints that eliminate the need to resort to the combinatorial approach. This paper imposes a constrain on the solution that promotes sparsity. Physically, sparsity means that the number of damaged elements is small with respect to the total number of elements that describes the domain.

By definition k-sparse vector is one that contains k non-zero elements in which k is

significantly less than the dimension of the vector. Imposing sparsity on the optimal solution, while simultaneously satisfying the linear system of equations can be done via a variety of optimization algorithms [1–3]. Though differing in form, each of these methodologies promotes sparsity by minimizing the l_1-norm.

Recognizing sparsity in structural dynamic inverse problems has provided advantages to other applications outside of damage detection, particularly in force identification. In [4, 5], impact force location and time histories were successfully identified using sparse reconstruction techniques. In [6], the weighted l_1-norm regularization was used to determine the time histories of moving forces, an important inverse problem in bridge structural health monitoring.

Sparsity constraints have been indirectly used by Kaouk and Zimmerman [7] to detect damage using a minimum rank perturbation criteria. Although low rank perturbation of the stiffness matrix does not necessarily imply spatial sparsity, their work represents one of the first contributions that use sparsity as a constraint in structural dynamics. It was not until the benefits of sparsity constraints were realized in signal processing fields, such as compressed sensing [1, 2, 8] that any direct connection was made between localized damage and sparsity in SHM.

The most notable uses of spatial sparsity in localized damage detection are found in [9–12]. Link and Zimmerman [9] used greedy matching pursuit methods to detect spatially sparse damage using frequency response functions. However, more effective and efficient sparse recovery algorithms such as the Basis Pursuit are now commonly used. In [10], eigenvalue and eigenvector sensitivities were employed to detect localized damage in a simulated truss. One experimentally validated example of exploiting spatial sparsity in SHM can be found in work by Hernandez [11,12], which strictly uti-

lizes eigenvalue shifts and l_1 minimization to locate sparse damages. This FEM based work completely undermined the traditional requirements on modal information for local damage recovery in a global setting.

Results from [11] indicate that the increase in modal information improves the effectiveness of the l_1 optimization, and that additional modal information allows each perturbed element a more unique effect on the global response; an important characteristic for successful inversion in convex optimization theory. In this paper, the framework in [11] is reformulated such that modal information and uniqueness are improved, while at the least preserving the level of modal spectrum incompleteness conducted in [11]. The impulse response is the natural choice for satisfying the above criteria because it contains information on mode shapes, natural frequencies, and damping.

This paper uses impulse response sensitivity to locate and quantify spatially sparse damage with respect to a finite element model. Using empirical changes in the impulse response as a damage sensitive feature has been used by other researchers [13, 14], however without imposing the spatial sparsity constraint explicitly. Using Vetter calculus, an analytical expression for the sensitivity of the impulse response is derived and used to setup the inverse problem of detecting reductions in model parameters based on identified changes in impulse response. The inverse problem is effectively solved using least absolute shrinkage and selection operator (LASSO) regularization, an efficient l_1-based optimization scheme.

The paper begins by presenting the systems of interest and the method of approach. This is followed by a brief section on LASSO regularization, then a section on implementation and verification. The numerical implementation is carried out using

a shear-beam structure with 21 degrees of freedom. The impulse response sensitivity is defined by single input-single output (SISO), and single input-two output (SITO) systems. In all cases, limited spectral data and noise-contamination are considered.

A.2   Method of approach

The sensitivity approach is a popular and practical framework for finite model updating in structural dynamics [15]. The sensitivity matrix maps changes in element stiffness and(or) damping to associated changes in system response characteristics. In this paper, we seek a relationship between small changes in the impulse response to small changes in the parameters that define the stiffness matrix. The impulse response of a linear system is described by [16]

$$h(t, \theta) = \int_0^t \mathbf{C}(\theta) e^{\mathbf{A}(\theta)(t-\tau)} \mathbf{B} \delta(\tau) d\tau + \mathbf{D}\delta(t) = \mathbf{C}(\theta) e^{\mathbf{A}(\theta)t} \mathbf{B} + \mathbf{D}\delta(t) \qquad \text{(A.1)}$$

where $\mathbf{A}$, $\mathbf{B}$, $\mathbf{C}$, and $\mathbf{D}$ are the matrices that define the state-space model of the system. We seek to find

$$\Delta h(t) = \mathbf{S}(t)\Delta(\theta) \qquad \text{(A.2)}$$

where $\Delta\theta \in \Re^{px1}$ is a vector of changes in the parameters that define the stiffness and(or) damping matrix of the structure, $\mathbf{S} \in \Re^{rmxp}$ is the impulse response sensitivity matrix, and $\Delta h(t) \in \Re^{rmx1}$ is the corresponding change in the impulse response between damaged and undamaged state. r is the number of output sensors, p is the total number of damage sensitive parameters, and m is length of the impulse response i.e. the sampling frequency times the total time of the impulse response.

In the case of multiple outputs, the impulse response and the sensitivity matrix for each input-output combination are concatenated. Unless the domain of possible damage locations is larger than the time domain of the impulse response, eq. A.2 is overdetermined. In this paper, eq. A.2 is highly overdetermined.

The sparse nature of the inverse problem is revealed in $\Delta\theta$ with respect to localized damage. In the case of localized damage, only a few parameters that define the stiffness and damping matrix are affected. Therefore only a few elements of the vector $\Delta\theta$ will be nonzero indicating damaged parameters, and the elements unaffected by damage will be zero. This implies that the optimal solution $\Delta\theta$ is sparse.

We restrict our attention to the case where the stiffness $\mathbf{K}$ and damping $\mathbf{C}_d$ matrices may be expressed as

$$\mathbf{K}(\theta) = \sum_{i=1}^{p_k} \mathbf{E}_{i,K} f_i(\theta) \text{ and } \mathbf{C_d}(\theta) = \sum_{j=1}^{p_d} \mathbf{E}_{j,C_d} g_j(\theta) \tag{A.3}$$

where $\mathbf{E}_{.,.}$ is an elementary influence matrix and $f_i(\theta)$ and $g_j(\theta)$ are differentiable functions. By taking the first term of the Taylor series expansion around the parameter of interest, the stiffness and damping matrices may be approximated as

$$\mathbf{K}(\theta) = \sum_{i=1}^{p_k} \mathbf{E}_{i,K} \theta_i \text{ and } \mathbf{C_d}(\theta) = \sum_{j=1}^{p_d} \mathbf{E}_{j,C_d} \theta_j \tag{A.4}$$

where $p = p_k + p_d$. In this paper, the sensitivity matrix is defined as the derivative of the impulse response with respect to a change in parameter θ, written as

$$\mathbf{S}(t,\theta) = \frac{\partial h(t,\theta)}{\partial\theta} = \frac{\partial}{\partial\theta} \left(\mathbf{C}(\theta) e^{\mathbf{A}(\theta)t} \mathbf{B} + \mathbf{D}\delta(t) \right) \tag{A.5}$$

151

Where $\mathbf{A}$, $\mathbf{B}$, $\mathbf{C}$, and $\mathbf{D}$ are written as (for acceleration measurements)

$$\mathbf{A} = \begin{bmatrix} \mathbf{0} & \mathbf{I} \\ -\mathbf{M}^{-1}\mathbf{K}(\theta) & -\mathbf{M}^{-1}\mathbf{C_d}(\theta) \end{bmatrix}, \ \mathbf{B} = \begin{bmatrix} 0 \\ -\mathbf{M}^{-1}b_2 \end{bmatrix} \tag{A.6}$$

$$\mathbf{C} = c_2 \begin{bmatrix} -\mathbf{M}^{-1}\mathbf{K}(\theta) & -\mathbf{M}^{-1}\mathbf{C_d}(\theta) \end{bmatrix}, \ \mathbf{D} = c_2 \mathbf{M}^{-1}b_2$$

b_2 and c_2 are respectively the input and output influence matrices, and $\mathbf{M} = \mathbf{M}^T \in \Re^{nxn}$ is the mass matrix [16]. The derivative of an exponential mapping can be obtained using results from Vetter [17] and Brewer [18]. Applying the chain rule from Vetter's calculus [17] the sensitivity is written as

$$\frac{\partial h(t,\theta)}{\partial \theta} = \frac{\partial \mathbf{C}}{\partial \theta} e^{\mathbf{A}t} \mathbf{B} + (\mathbf{I}_p \otimes \mathbf{C}) \frac{\partial e^{\mathbf{A}t}}{\partial \theta} \mathbf{B} + (\mathbf{I}_p \otimes (\mathbf{C}e^{\mathbf{A}t})) \frac{\partial \mathbf{B}}{\partial \theta} + \frac{\partial \mathbf{D}}{\partial \theta} \delta(t) \tag{A.7}$$

Such that $\otimes$ is the Kronecker product, and $\mathbf{I}_p$ is a p x p identity matrix. Because $\mathbf{B}$ and $\mathbf{D}$ are not dependent on θ, $\partial \mathbf{B}/\partial \theta = \mathbf{0}$ and $\partial \mathbf{D}/\partial \theta = \mathbf{0}$. Thus eq. A.7 is reduced to

$$\frac{\partial h(t,\theta)}{\partial \theta} = \frac{\partial \mathbf{C}}{\partial \theta} e^{\mathbf{A}t} \mathbf{B} + (\mathbf{I}_p \otimes \mathbf{C}) \frac{\partial e^{\mathbf{A}t}}{\partial \theta} \mathbf{B} \tag{A.8}$$

where

$$\frac{\partial \mathbf{C}}{\partial \theta_i} = \begin{bmatrix} -\mathbf{M}^{-1}\mathbf{E}_{i,K} & -\mathbf{M}^{-1}\mathbf{E}_{i,C_d} \end{bmatrix} \tag{A.9}$$

and

$$\frac{\partial \mathbf{C}}{\partial \theta} = \begin{bmatrix} \frac{\partial \mathbf{C}}{\partial \theta_1} & \frac{\partial \mathbf{C}}{\partial \theta_2} & \cdots & \frac{\partial \mathbf{C}}{\partial \theta_p} \end{bmatrix}^T \tag{A.10}$$

Using Brewer's derivation [18], the derivative of the matrix exponential can be ex-

pressed in terms of complex eigenvalues and mode shapes as

$$\frac{\partial e^{\mathbf{A}t}}{\partial \theta} = \sum_k^{2n} \sum_l^{2n} (\alpha_k \gamma_k^*) \frac{\partial \mathbf{A}}{\partial \theta} (\mathbf{I}_p \otimes \alpha_l \gamma_l^*) f_{kl}(t), \; f_{kl}(t) = \left\{ \begin{array}{ll} t e^{\lambda_k t} & , \lambda_k = \lambda_l \\ \frac{e^{\lambda_l t} - e^{\lambda_k t}}{\lambda_l - \lambda_k} & , \lambda_k \neq \lambda_l \end{array} \right\} \quad (A.11)$$

where

$$\frac{\partial \mathbf{A}}{\partial \theta_i} = \begin{bmatrix} \mathbf{0} & \mathbf{0} \\ -\mathbf{M}^{-1}\mathbf{E}_{i,K} & -\mathbf{M}^{-1}\mathbf{E}_{i,C_d} \end{bmatrix}, \; \frac{\partial \mathbf{A}}{\partial \theta} = \begin{bmatrix} \frac{\partial \mathbf{A}}{\partial \theta_1} & \frac{\partial \mathbf{A}}{\partial \theta_2} & \cdots & \frac{\partial \mathbf{A}}{\partial \theta_p} \end{bmatrix}^T \quad (A.12)$$

λ_k is the kth eigenvalue of $\mathbf{A}$, α_k is the kth eigenvector of $\mathbf{A}$, and γ_k is the kth eigenvectors of $\mathbf{A}^T$ which are normalized such that

$$\gamma_k^* \alpha_k = 1 \quad (A.13)$$

In order to be consistent with the spectral bandwidth of the identified impulse response used to compute $\Delta h(t)$, the sensitivity matrix is truncated at the specified number of identified frequencies (m). Using the spectral representation of an exponential mapping, the truncation at the specified eigenvalue λ_m is defined as

$$e^{\mathbf{A}t} = \sum_{k=1}^{2m} \alpha_k \gamma_k^* e^{\lambda_k t} \quad (A.14)$$

where α and γ are normalized according to eq. A.13.

A.3 LASSO REGULARIZATION

In 1996, R. Tibshirani [3] proposed LASSO regression for estimating linear models which seeks to minimize the following residual function (in reference to eq. A.2)

$$\min_{\Delta\theta \in \Re^p} \frac{1}{2}||\Delta h - \mathbf{S}\Delta\theta||_2^2 + \lambda||\Delta\theta||_1 \qquad (A.15)$$

with regularization parameter $\lambda \geq 0$. Note that the regularization parameter (λ) in the context of the LASSO should not be confused with the eigenvalue.

LASSO typically recovers a sparse solution due to the l_1-norm constraint. For implementation purposes, this paper implements LASSO via the MATLAB package, Lasso and Elastic-Net Regularized Generalized Linear Models (glmnet), an efficient procedure for fitting the lasso regularization path for linear regression [19]. The algorithm uses cyclical coordinate descent computed along a regularization path to optimize the objective function over each parameter with others fixed, and cycles repeatedly until convergence.

The choice of the regularization parameter is subject to the user where larger values of λ tend towards sparser solutions at the expense of increased noise sensitivity. To remove user bias to the known solution, we use the glmnet's built in cross validation algorithm to select a value of λ. The cross validation uses 10 folds. An external loop of cross validation is used to avoid selection bias. After cross validation we choose the λ value which gives the most regularized model such that the error is within one standard error of the minimum. We constrain the maximum number of nonzero elements in $\Delta\theta$ to about 20 percent of the total number of elements (p).

A.4 Simulations and verification

This section compares the proposed methodology with that proposed in [11], which uses l_1-norm minimization and frequency sensitivity. Results are presented for both single input-single output systems and single input-two output systems. The simulations are ideal because the model used to generate the simulated data is also the one used to implement the algorithm. For this proof-of-concept paper this might be adequate, however for a complete investigation, the effects of irreducible model error should be included. This aspect will be considered in an upcoming paper by the authors which will also include validation using experimental results.

The simulated model is a 21 degree of freedom, non-uniform shear beam with degrees of freedom enumerated from 1 the first mass closest to the support, to 21 the free end. The spring stiffness are as follows: $k_1 = ... = k_7 = 1000$, $k_8 = ... = k_{14} = 750$, and $k_{15} = ... = k_{21} = 500$, and the masses: $m_1 = ... = m_7 = 1$, $m_8 = ... = m_{14} = 0.75$, and $m_{15} = ... = m_{21} = 0.5$. The structure is classically damped with a damping coefficient of 0.01. The fundamental frequency is 0.436 Hz.

In all simulations to follow, only small stiffness related damage is considered. The proposed method does not hold for larger damages. Large damage cases require updating the sensitivity matrix iteratively to account for the nonlinear relationship between changes in impulse response and changes in stiffness.

The impulse response is measured in units of acceleration. The impulse response sensitivity matrix is defined by eq. A.8. The change in impulse response between the damaged and undamaged system contains only the specified lower natural frequencies, which are typically the only ones that can be identified from structural vibrations.

Localized damage is less prominent in the lowest frequencies. The fewer the number of natural frequencies that are identified in the impulse response, the less likely the proposed methodology can identify damage in the presence of noise.
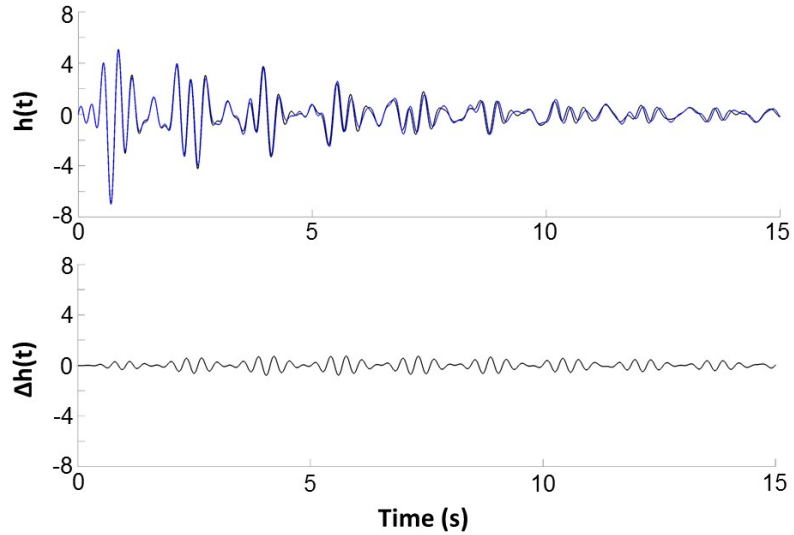
Figure A.2: Above, the undamaged impulse response and the impulse response for a 10% stiffness reduction given 6 identified frequencies. Below, the change in impulse response between the damaged and undamaged system

Fig. A.2 presents the undamaged system impulse response, the impulse response of the system with a 10% stiffness reduction in Element (El.) 6, and the change between the two, given 6 identified frequencies. The following simulations are conducted first for single input-single output (SISO) systems, and then for single input-two output (SITO) systems. The input sensor is fixed at El. 21 for all tests and the output sensor(s) to be specified.

156

A.4.1 SINGLE INPUT-SINGLE OUTPUT

The first simulated case demonstrates the efficacy of the methodology for an ideal simulation without measurement error. The stiffness of element 6 is reduced by 1% and the lowest four frequencies are identified within the impulse responses of the original system and the damaged system. No prior information about the quantity or magnitude of damages are known except that the solution is sparse. The impulse response for the cantilever is defined by a system with a single input and single output, where the output and input are fixed at elements 3 and 21 respectively, and the sensitivity matrix is truncated according to the number of identified frequencies (eq. A.11, A.14).

To demonstrate the preference to the LASSO regularization over the Tikhonov, Fig. A.3 presents the estimated stiffness reduction and its damaged locations using LASSO and the Tikhonov for a range of selected regularization parameters λ. In Fig. A.3a the damage at element 6 is apparent when the LASSO is used , while in Fig. A.3b the Tikhonov provides no information on the damage at element 6. Note that as the regularization parameter is increased the weight on the penalty is increased. In regards to the LASSO, the solution becomes sparser with increasing λ because the weight on the l_1 norm penalty is increased. Clearly an optimal choice of λ is between 0.01 and 0.1. In regards to the Tikhonov, no benefit is gained from increasing the weight on the l_2 norm penalty.

We then select the regularization parameter using cross validation. It is immediately clear from Fig. A.4 that the l_1 constrained solution identifies the true damaged element, and estimates the magnitude of the reduction in stiffness precisely. In stark
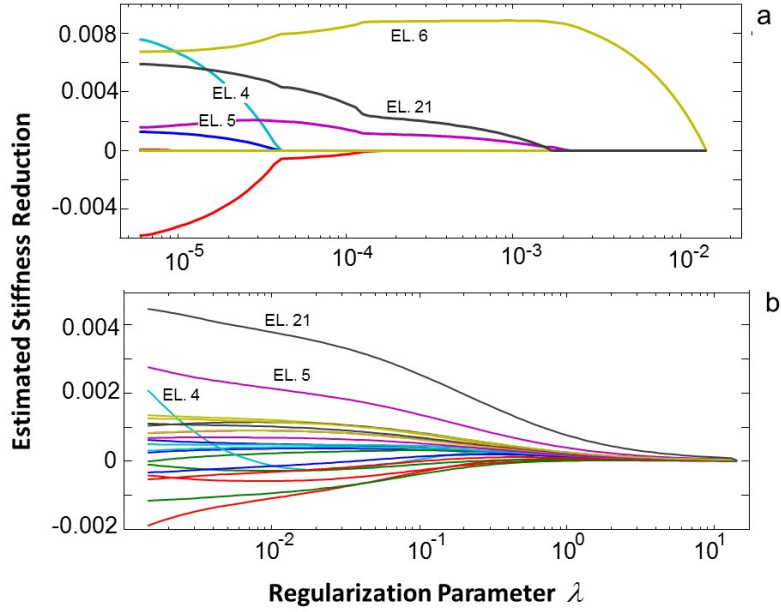
157

Figure A.3: The estimated stiffness reduction for damage at El. 6 as a function of the regularization parameter λ for: a) the LASSO regularization, and b) the Tikhonov regularization

contrast, no information is gained about the damaged element when the regularization is subjected to the l_2 constrained parameter nor is the solution sparse. The solution to the LASSO contains only one non-zero element and hence is sparse.

The performance of the l_1 constrained regularization method in detecting a 1% stiffness reduction in any single element taken separately is considered next. Fig. A.5a presents the minimum number of frequencies required to identify this reduction at any single element. Frequencies are selected sequentially from the lowest in increments of one until a proper detection is obtained. We compare the sparse sensitivity method with frequency shifts from [?] to the proposed sparse sensitivity method with impulse responses. The number of identifiable frequencies required to detect a single damage at any element (exception at El. 15) is less in the impulse response sensitivity method than when using frequency sensitivity. Fig. A.5b presents the estimated stiffness
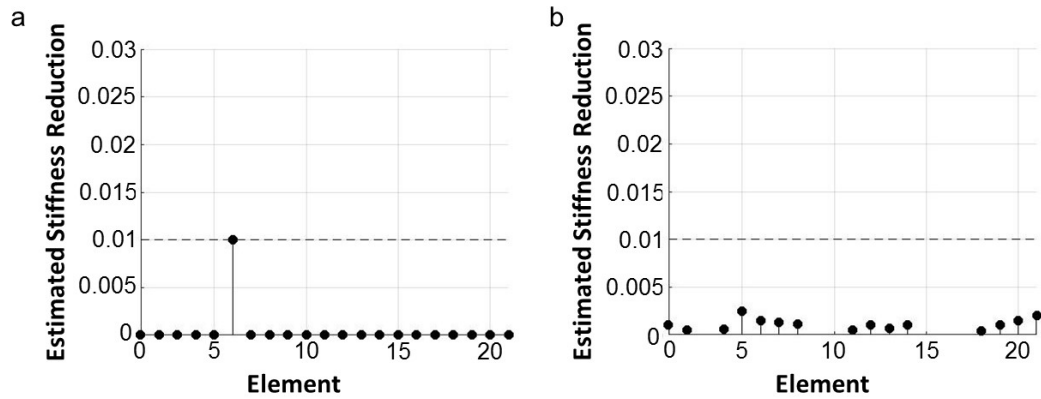
Figure A.4: Estimated stiffness reduction for every element. In this case, only the stiffness of El. 6 was reduced by 1%. (a) The l_1-based solution, and (b) the l_2-based solution

reduction for each damaged element using the impulse response method for the case where only four frequencies were identified.

Sparsity is not necessarily synonymous of a single damage element, thus multiple damage locations and varying percent reductions in stiffness must also be considered. Fig. A.6(a-c) presents the following scenarios:(i) the stiffness of El. 6 reduced by 1% and El. 7 by 1%, (ii) stiffness of El. 6 reduced by 1% and El. 7 by 3%, and (iii) El. 6 reduced by 1% and El. 7 by 5%. Successful damage detection for cases (i-iii) were made despite the proximity of the two damage locations. Fig. A.6(d-f) presents the following scenarios: (iv) the stiffness of El. 6 reduced by 1% and El. 15 by 1%, (v) stiffness of El. 6 reduced by 1% and El. 15 by 3%, and (vi) El. 6 reduced by 1% and El. 15 by 5%. In cases (iv) and (v) damages were correctly located, and their reductions in stiffness accurately estimated. In case (vi) a small false positive
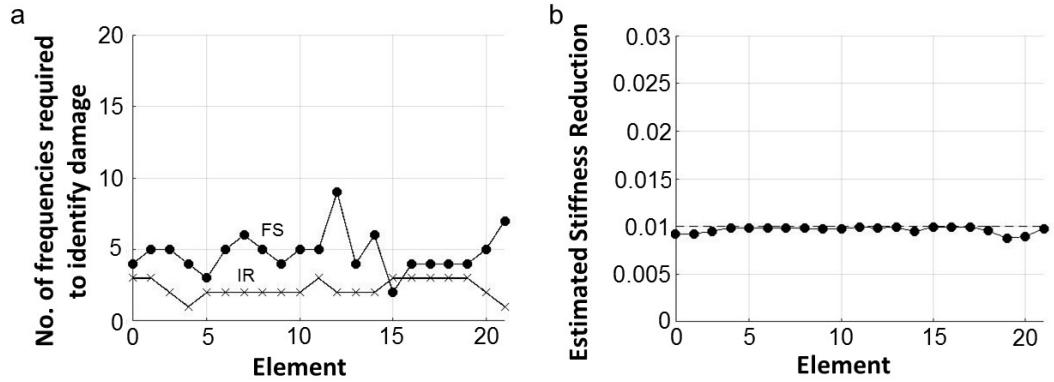
Figure A.5: a) Number of frequencies required in order to identify a single element damage for frequency shift method (FS) and impulse response method (IR). Frequencies selected sequentially from the lowest in increments of one until a proper detection is obtained. (b) Estimated stiffness reduction for every element using the impulse response method and 4 identified frequencies

is obtained at El. 19 and the estimated magnitudes of the stiffness reduction at the true damage locations are underestimated. In all previous cases the impulse response and sensitivity matrix were truncated at the 6$^{\text{th}}$ frequency.

The effect of measurement noise ϵ on eq. A.2 is investigated. Noise is defined as the realization of an n-dimensional Gaussian random vector with zero mean and standard deviation of each component ϵ_i proportional to the corresponding $h(t_i)$, where n is length of the vector in time. The vector of noise is added to the measured output for both damaged and undamaged states. The impulse responses are then identified from the simulated noisy outputs given a white Gaussian input using the Observer/Kalman Filter Identification (OKID). The number of identified frequencies in the spectral bandwidth of the impulse response varied from 4 to 10. The locations of
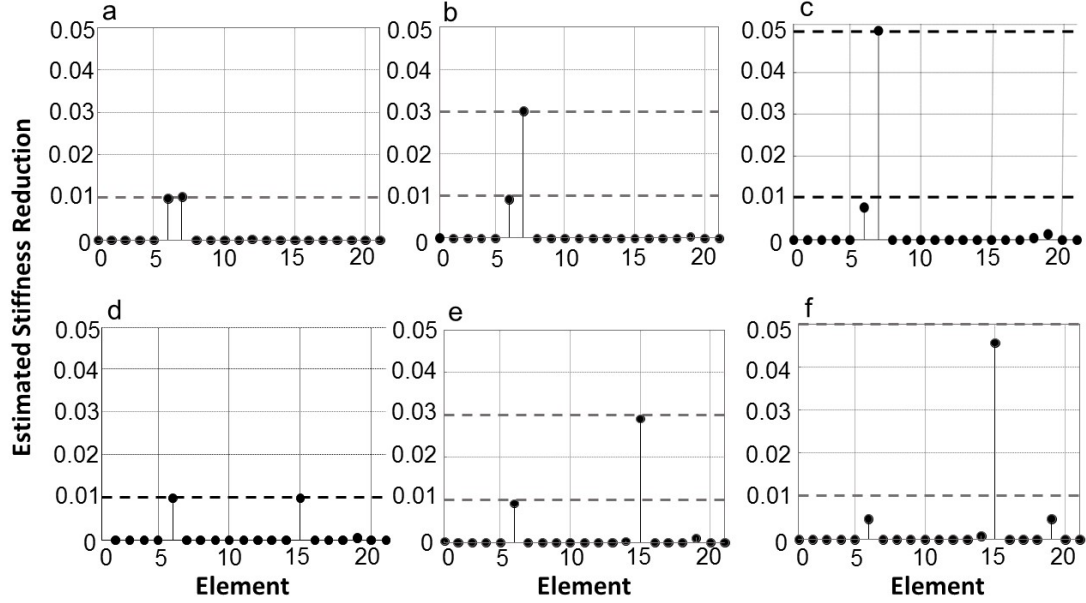
Figure A.6: Estimated stiffness reduction for the following multiple damage cases: a) 1% damage at El. 6 and El. 7, b) 1% damage at El. 6 and 3% at El. 7, c) 1% damage at El. 6 and 5% damage at El. 7, d) 1% damage at El. 6 and El. 15, e) 1% damage at El. 6 and 3% at El. 15, and f) 1% damage at El. 6 and 5% damage at El. 15

the input and output remain the same. In each case, 1000 simulations were performed and a probability of detection (POD) was obtained. The criteria for detection were: (i) the method correctly identifies the damaged element, and (ii) it does not assign a value greater than 20 percent than that of the element of greatest reduction to any other element. The sampling frequency of the impulse response was taken at 20 Hz. To reduce the effects of noise from the identified damping which is often more sensitive to noise than other dynamic features, we consider only the identified impulse response between 2.5 and 27.5 sec. For a single output system with impulse response sampled at a frequency of 20 Hz, the size of the sensitivity matrix is 500 x 21.

The POD is compared to those obtained from [11] for a single 10% stiffness re-duction at El. 2, El. 6, El. 14, and El. 20. Fig. A.7 presents the POD for each case
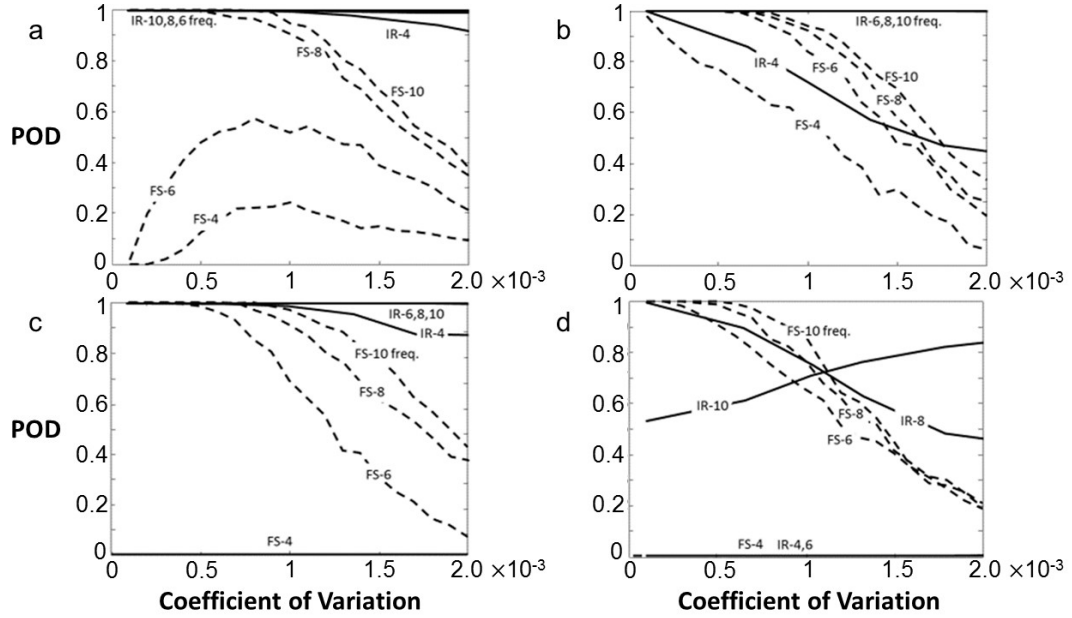
161

Figure A.7: Probability of detection (POD) as a function of the coefficient of variation of the selected frequencies for impulse response (IR) and frequency sensitivity (FS) method [11]. (a) Corresponds to spring 2, (b) to spring 6, (c) to spring 14, and (d) to spring 20

as a function of the maximum coefficient of variation of the identified frequencies. It is clear that the impulse response method results in larger POD values than the frequency sensitivity method for El. 2, 6, and 14. Only for El. 20 are the results comparable. An inverse proportional trend occurs with damage at El. 20 within the specified domain of noise as seen in Fig. A.8d. This trend may be due to collinearity between El. 20 and El. 1, where the method estimates a false positive damage at El. 1 large enough to violate the specified threshold for a correctly identified damage. Fig. A.8a presents the average estimated stiffness reduction for each element for damage at El. 20 with 10 identified frequencies for an increasing fraction of noise (NF) of the standard deviation of ϵ. The small addition of noise is apparently beneficial at first, however an expected depreciation of the POD occurs as the fraction of noise is increased (Fig. A.8b). This effect was not observed in Fig. A.7d due to the realized
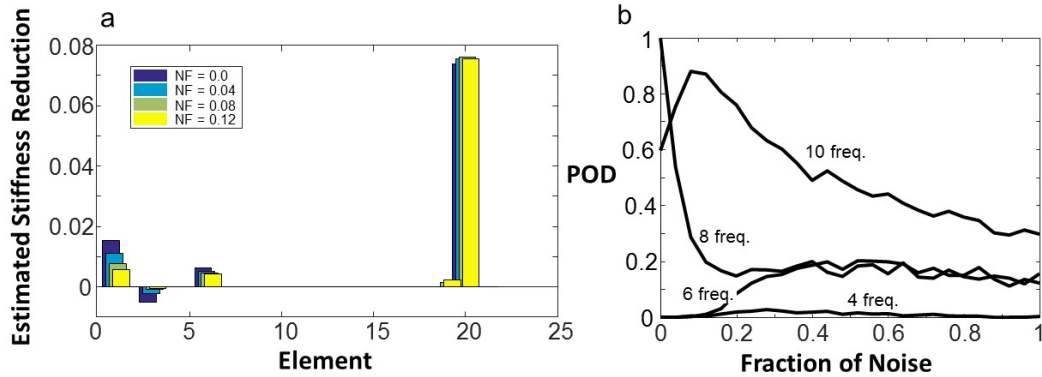
Figure A.8: a) The average estimated stiffness reduction for each element with 10 identified natural frequencies with increasing fraction of noise (NF) for a 10% stiffness reduction at spring 20, and b) the probability of detection (POD) as a function of the fraction of noise for a 10% stiffness reduction at spring 20.

range of noise.

The final SISO simulation is presented in Fig. A.9. The POD is computed as a function of magnitude of stiffness reduction for a fixed level of noise. for each case, 1000 independent simulations are performed for each fraction of stiffness reduction taken at 0.01 to 0.05 in 0.01 increments, and 0.05 to 0.2 in 0.05 increments. In all cases, the maximum coefficient of variation of all frequencies was fixed at 0.001. Again these results are compared to those from [11]. By observation of Fig. A.9, the impulse method detects smaller magnitudes of damage with higher probability than the frequency sensitivity method from [11]. However the maximum fraction of stiffness reduction that the impulse method detects is significantly lower than in [11]. From these simulation results one could hypothesize that linearization errors affect the
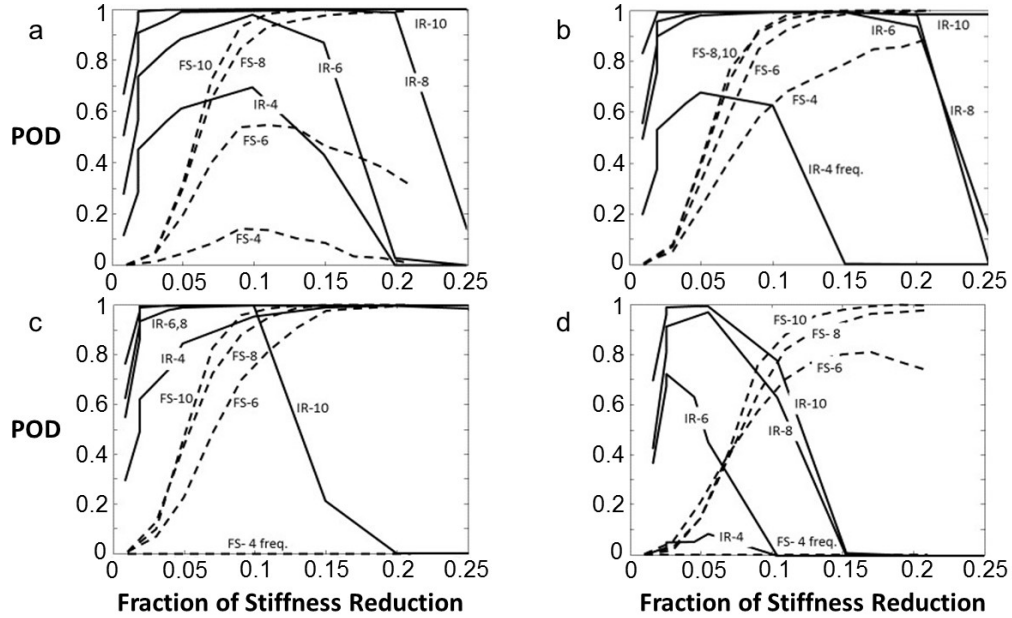
Figure A.9: Probability of detection (POD) as a function of the fraction of stiffness reduction of the selected frequencies for impulse response (IR) and frequency sensitivity (FS) method [11]. The maximum coefficient of variation is 0.001. (a) Corresponds to spring 2, (b) to spring 6, (c) to spring 14, and (d) to spring 20

impulse response sensitivity approach more drastically than the frequency sensitivity approach proposed in [11].

A.4.2 SINGLE INPUT-TWO OUTPUTS

In this section the performance of the proposed methodology is examined in the case of single input and two outputs. For a single input two output system with impulse responses sampled at 20 Hz, the sensitivity matrix is 1000 x 21. In the following simulations, the effects of measurement noise and limited spectral data are considered. The criteria for a sparse damage detection, the LASSO criteria, and the impulse response truncation described in previous sections remain the same. For clarity, output locations are often referred to as outputs, and enumerated from 1 to

164

21 (from top to bottom) based on their associated element locations.

We first examine the efficacy of the single input-two output system with measurement error by estimating the probability of detecting a 10% stiffness reduction at El. 6 as a function of noise. The POD is evaluated at fractions of noise between 0% to 15% the standard deviation of ϵ. The standard deviation of ϵ is proportional to $h(t)$ computed at a single output located at El. 3 with a single input located at El. 21. The vector of noise is added to both outputs. For reference, 4% noise resulted in a 0.001 maximum coefficient of variation in the frequencies in the previous section. Fig. A.10 present the POD for a fixed input at El. 21 and outputs located respectively at i) El. 3, ii) El. 17, and iii) El. 3 and 17.
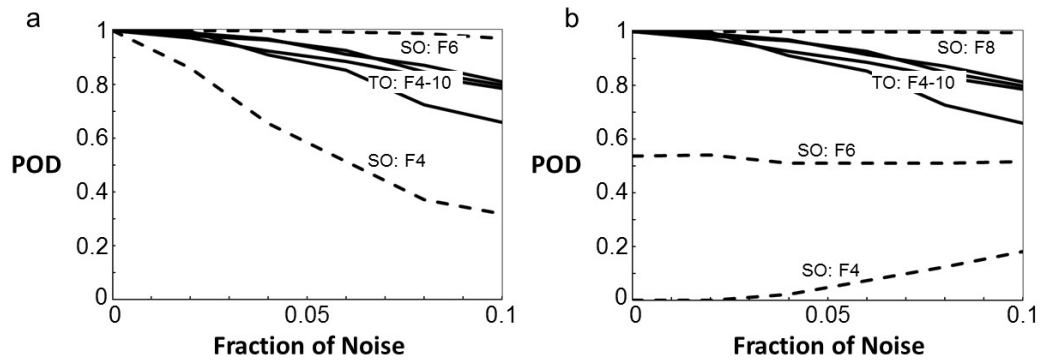

Figure A.10: Probability of detection (POD) as a function of the fraction of noise and identified frequencies (F#) for SISO and SITO systems. Output(s) located at i) El. 3, ii) El. 17, and iii) El. 3 and El. 17 . a) POD of the two output case (TO) and the case with a single output (SO) located at El. 3. b)POD of the two output case (TO) and the the case with a single output (SO) located at El. 17

With 8 and 10 identified frequencies, the POD of the SITO system decays more

rapidly with additional noise than the SISO cases. Perhaps this is a consequence of the addition of noise with additional outputs. With 4 and 6 identified frequencies the SITO outperforms the SISO with output 17. With 4 identified frequencies the SITO outperforms the SISO with output 3.

Next, the performance of both the SISO and SITO systems as a function of all single and two output combinations are investigated. The effects of output location and quantity are isolated by fixing all other variables. We now estimate the probability of detecting a 10% stiffness reduction at El. 6 for a level of noise fixed at 8%. The noise ϵ is the realization of a Gaussian random variable with zero mean, and a fixed standard deviation proportional to $h(t)$ evaluated at outputs located at El. 1 and El. 2 and input located at El. 21. In a two output system, the vector ϵ is added to both outputs, and in the case of a single output only the noise proportional to output 1 is added. The input was fixed at El. 21 for all simulations.

Fig. A.11 presents the POD as a function of all combinations of two outputs located between El. 1 and El. 20. The diagonal of Fig. A.11 depicts the POD of the SISO systems at the specified output locations. The results show a generally high POD for single output systems, and two output systems. 82% of all two output combinations and 65% of the single output possibilities resulted in greater than 90% POD.

Using the data from Fig. A.11, we investigate the maximum and minimum bounds of the POD for SITO systems and compare them to the SISO systems. Fig. A.12 presents the maximum and minimum POD achieved by each output of interest with the addition of the another output. Superimposed is the POD of the SISO system evaluated at the output of interest.
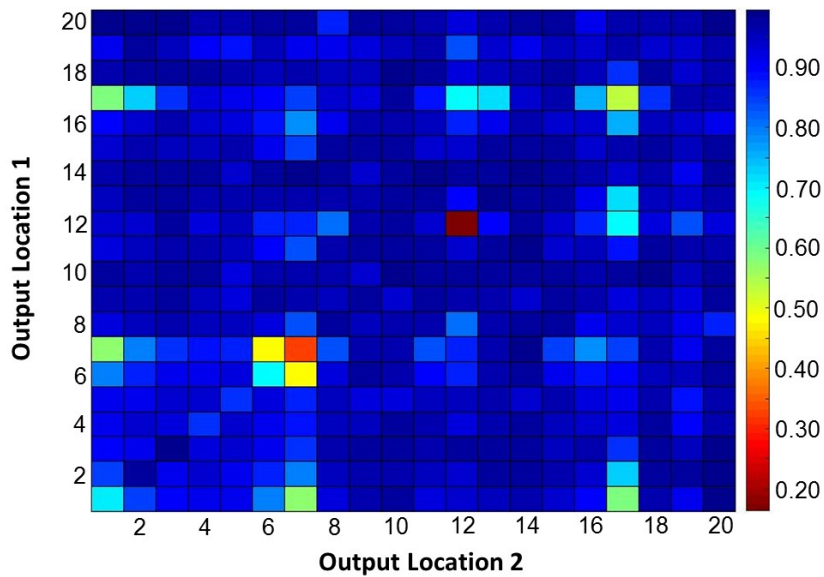
Figure A.11: Probability of detecting a 10% stiffness reduction at El. 6 with 8% noise as a function of all output pairs. The diagonal represents the POD for single output systems

In regards to this damage case, for every output there exists at least one additional output that in combination will yield a POD no worse than that of the output implemented alone. The result of the additional output, and hence the addition of modal information (i.e. mode shapes) is intuitively consistent with observations made in previous simulations where the addition of identified frequencies increased the POD. Despite this intuitive phenomenon, there still exists combinations of outputs that yield a POD that is below that of the single output case as shown by the minimum SITO POD obtained.

Using data from Fig. A.11, we further investigate the POD as a function of output location, and output quantity. Fig. A.13 presents the percent relative difference (PRD) between the POD of the output of interest in combination with all other outputs ($POD_{O^*,O}$), and the POD of all other outputs individually implemented in
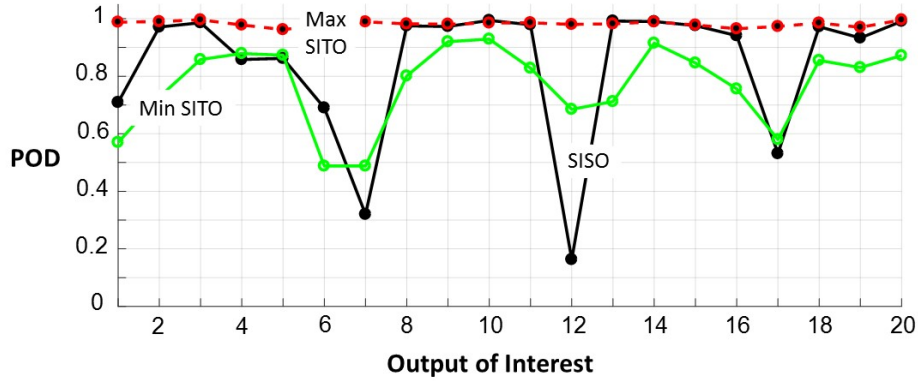
Figure A.12: The maximum (Max SITO) and minimum (Min SITO) achievable POD of each output of interest for a two output system, and the POD for each output of interest for a single output system (SISO)

SISO (POD_O). The PRD is expressed as

$$PRD = \frac{POD_{O^*,O} - POD_O}{POD_O} \tag{A.16}$$

By observation of the PRD in Fig. A.13, the increase in POD with the addition of certain outputs of interest is often disproportionally larger than the decreases in POD that may occur. As an example observe the PRDs of the output of interest located at El. 5. Four individual SISO output cases have a greater than 25% gain in POD when combined with El. 5, while combinations that perform less well than the SISO case only reduce the POD by less than 10%. This phenomenon is typical across all elements, with the exceptions of El. 7, 12, and 17. The majority of SITO combinations that contain outputs located at either 7, 12, and 17 perform less well

than if implemented in a SISO system. This implies that outputs 7, 12, and 17 are poor sensor locations for sparse recovery.
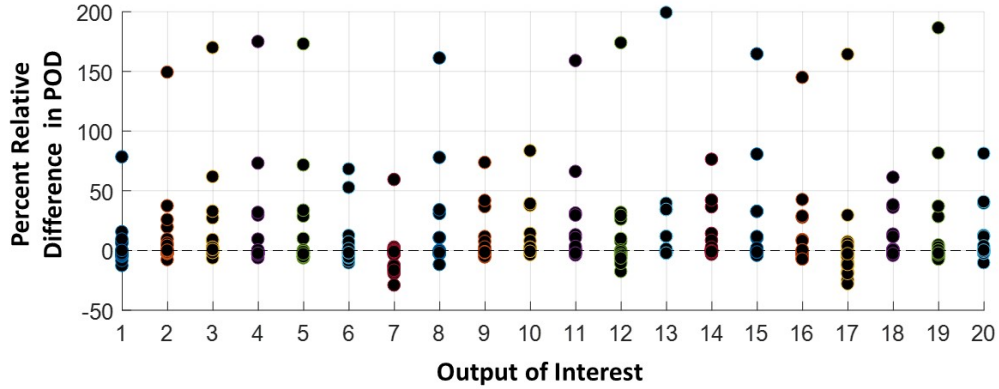

Figure A.13: For each single output of interest, the percent relative difference of the POD between the single input-single output, and the single input-two output case in which the two sensors are the output of interest combined with all other outputs

A.5 CONCLUSION

This paper explores the use of impulse response sensitivity for detecting spatially sparse damage in structural systems. The paper shows that it is possible (at least in simulated systems) to detect spatially sparse stiffness reductions in the presence of noise and limited spectral data by measuring changes in identified impulse response. The sensitivity of the impulse response with respect to changes in stiffness was found using Vetter calculus. The proposed method is compared to the Tikhonov regularization and the frequency sensitivity methods from [11]. It was also found that the

impulse response sensitivity provides better probability of detection results with respect to frequency sensitivity, however it is more sensitive to linearization errors and thus its performance degrades as the size of damage increases.

Within the context of the proposed impulse response sensitivity, the paper investigates the effect of multiple outputs. The results imply that additional output sensors are often better but not always. This paper provides a proof of concept for the impulse response sensitivity using LASSO regularization. In future work the authors plan to expand this study by applying the proposed methodology to experimental data and determining optimal FEM resolution for sparse damage detection. We also seek to bolster the mathematical theory and include large damage extent by formulating the approach to account for the nonlinear sensitivity.

Acknowledgements

Bibliography

[1] Donoho D. L, Elad M. Optimally sparse representation in general (nonorthogonal) dictionaries via l1 minimization. Proc. Natl. Acad. Sci. 2003; 100: 2197-2202.

[2] Tropp J. A. Greed is good: algorithmic results for sparse approximation. IEEE Trans. Inf. Theory. 2004; 50(10): 2231-2242.

[3] Tibshirani, R. Regression shrinkage and selection via the lasso. J. R. Statist. Soc B. 1996; 58(1): 267-288.

[4] Qiao B, Zhang X, Gao J, et al. Sparse deconvolution for the large-scale ill-posed inverse problem of impact force reconstruction. Mech. Syst. Signal Pr. 2017; 83: 93-115.

[5] Qiao B, Zhang X, Gao J, et al. Impact-force sparse reconstruction from highly incomplete and inaccurate measurements. J. Sound Vibration. 2016; 376: 72-94.

[6] Pan C D, Yu L, Liu H L, et al. Moving force identification based on redundant concatenated dictionary and weighted l1-norm regularization. Mech. Syst. Signal Pr. 2018; 98: 32-49.

[7] Kaouk M, Zimmerman D.C. Structural damage assessment using a generalized minimum rank perturbation theory. AIAA J. 1994; 32(4): 836-842.

[8] Candes E, Romberg J. Sparsity and incoherence in compressive sampling. Inverse Probl. 2007;23(1): 969-985.

[9] Link, Ryan J, Zimmerman D.C. Structural damage diagnosis using frequency response functions and orthogonal matching pursuit: theoretical development. Struct. Control Health Monit. 2015; 22: 889-902.

[10] Zhou S, Bao Y, Li H. Structural damage identification based on substructure sensitivity and l1 sparse regularization. Proceedings of the SPIE 8692 Sensors and Smart Structures Technologies for Civil, Mechanical and Aerospace Systems. 2013.

[11] Hernandez, E.M. Identification of isolated structural damage from incomplete spectrum information using l1-norm minimization. Mech. Syst. Signal Pr. 2014; 46(1): 59-69.

[12] Hernandez, E.M. Identification of localized structural damage from highly incomplete modal information: theory and experiments. J. Eng. Mech. ASCE. 2016; 142(2).

[13] Hassiotis, S. Identification of damage using natural frequencies and Markov parameters. Comput. Struct. 2000; 74(3): 365-373.

[14] Law S.S., Li X.Y. Wavelet-based sensitivity analysis of the impulse response function for damage detection. J. Appl. Mech. 2007; 74: 375-377.

[15] Mottershead J.E., Link M, Friswell M. The sensitivity method in finite element model updating: a tutorial. Mech. Syst. Signal Pr. 2011; 25 (7): 2275-2296.

[16] Juang, Jer-Nan. Applied System Identification. Upper Saddle River, NJ: Prentice Hall, 2002. Print.

[17] Vetter W.J. Derivative operations on matrices. IEEE Trans. Autom. Control. 1970; 15(4): 241-244.

[18] Brewer J. The derivative of the exponential matrix with respect to a matrix. IEEE Trans. Inf. Theory. 1997; 22(4): 656-657.

[19] Friedman J, Hastie T, Tibshirani R. Regularization paths for generalized linear models via coordinate descent. J. Stat. Softw. 2010; 33(1): 1-22.